Characterizing Interfacial and Bulk Interactions Between Cellulose Ethers and Bile Salts: Impact on *In Vitro* Lipid Digestion

By

Jennifer Zornjak

Thesis submitted to the faculty of the Virginia Polytechnic Institute and State University in partial fulfillment of the requirements for the degree of

Masters of Life Science

in

Food Science and Technology

Approved by:
Cristina Fernandez-Fraguas
Kevin Edgar
Alan Esker
Andrew Neilson

December 11th, 2018
Blacksburg, Virginia

Keywords: Hydroxypropyl Cellulose, Bile Salts, Lipid Digestion, Quartz Crystal Microbalance with Dissipation Monitoring, Cardiovascular Disease

Characterizing Interfacial and Bulk Interactions Between Cellulose Ethers and Bile Salts: Impact on *In Vitro* Lipid Digestion

Jennifer A. Zornjak

Abstract [Academic]

Elevated levels of lipids and LDL-cholesterol in the blood are significant risk factors associated with developing cardiovascular diseases (CVDs). A potential strategy to combat these risk factors is decreasing lipid absorption by modulating the digestibility of lipids in the human intestinal tract. Since bile salts (BS) play key roles during this process, lipid digestion could be controlled ultimately by limiting the access of BS to the lipid surface. Cellulose ethers (CEs), surface-active dietary fibers and common food additives, might be promising ingredients to control lipid digestion either by creating surface layers around lipid droplets that hinder adsorption of BS, or by sequestering BS in the aqueous phase. However, the precise mechanisms behind these interactions remain unclear. Surface analysis techniques were used to better understand the mechanisms by which CEs with diverse molecular structure and charge (commercial and novel hydroxypropyl-cellulose (HPC)) interact with BSs at the solid surface and in the aqueous phase. The potential of CE-stabilized emulsions to influence lipid digestion was also investigated *in vitro.* Both CEs show potential in modulating lipid digestion; the potential of the commercial HPC to interfere with lipid digestion may be more related to its ability to sequester BS in solution and form mixed HPC-BS complexes that are not easily removed from the surface, whereas the novel HPC seems more effective at creating strong surface layers that resist displacement by BS. These findings can be exploited in developing strategies to design novel food matrices with improved functional properties to optimize lipid digestion and absorption.

Characterizing Interfacial and Bulk Interactions Between Cellulose Ethers and Bile Salts: Impact on *In Vitro* Lipid Digestion

Jennifer A. Zornjak

Abstract [Public]

Diseases of the heart and circulation are the number one cause of death in the United States (US) and it is predicted that at least 45% of the US population (131.2 million) will have some form of these diseases by 2035. Consumption of reduced-fat foods is one strategy to combat CVDs, but fats contribute to various sensory and nutritional properties of foods. Another strategy is to develop foods that incorporate dietary fibers which could interfere with the digestion of fat. However, the mechanism behind the ability of dietary fiber to interfere with fat digestion remains unclear and depends on the fiber type. One of our objectives was to look at the main interactions between a type of dietary fiber, cellulose derivatives (which are ingredients used in the food industry), and two types of bile salts, (BSs) which are important intestinal components present during fat digestion, at a surface representing a fat droplet and in the aqueous phase. Another objective was to look at the digestibility of cellulose derivative systems, compared to another food ingredient (Tween 20). We found that the different BSs played different roles at the surface and interacted differently with the cellulose derivatives. We also found that both cellulose derivatives showed potential in interfering with lipid digestion. This allows a better understanding of how cellulose derivative systems are affected by digestion and could allow us to design new foods with natural products from plants to improve wellness in the US.

Acknowledgements

I would first like to thank my family for constantly providing me with support, guidance, and love throughout my time here at Virginia Tech; I would not have made it through without you all. I would also like to thank my advisor, Dr. Cristina Fernández-Fraguas, for providing me with this wonderful opportunity. I truly appreciate all the support you have provided me throughout my time in grad school. I believe that I have not only grown as a food scientist, but my writing and communication skills have improved as well, which I can take with me in my next adventure. I would also like to thank our lab group (Deepak Poudel, Tiantian Lin, Oumoule Ndiaye, and Jennie Doizer) for providing support in my experiments as well providing feedback on my writing and presentations. I could not have asked for a more fun and supportive group! I would also like to thank Dr. Alan Esker and Jianzhao Liu for their constant guidance throughout my QCM-D and SPR experiments. I truly appreciate the time and effort they put in to help me with these techniques. I would also like to thank Dr. Keven Edgar and Dr. Andrew Neilson for choosing to work with me and providing me with great feedback and support throughout this research. I would also like to thank the students in Dr. Edgar's group, Diana Novo and Yifan Dong, for synthesizing the polymers for my project and providing guidance when I had any questions. I would also like to give a big shout out to my friends back at home (Laura Nibbelink, Connor Adams, Mel Skirkanich, and Allison Bills) as well as the wonderful friends I have made here in grad school at Virginia Tech (Nicole Arnold, Jordan Garry, Anthony Millican, Lily Yang, Chris Winslow, Razieh Farzad, and Mike Hughes). Thank you all for always believing in me and for going on fun adventures when we were not in lab, whether it be hiking, going to an exercise class, or getting a milkshake at midnight. I will truly miss Virginia Tech, the Food Science Department, and all the opportunities that I have been able to do during my 6 years in Blacksburg.

Table of Contents

Attributions

The following individuals made invaluable contributions to this research. Dr. Cristina Fernández-Fraguas provided facilities and project materials, as well as continuous guidance throughout this research. Dr. Alan Esker provided guidance and facilities in research. Dr. Kevin Edgar provided novel cellulose derivatives and support in research. Dr. Andrew Neilson provided guidance and support in research. Diana Novo made the novel amphiphilic cellulose derivatives and provided characterization data. Jianzhao Liu provided guidance and information for the surface analysis techniques.

Abbreviations

Hydroxypropyl cellulose (HPC), cardiovascular disease (CVD), bile salt (BS), quartz crystal microbalance with dissipation monitoring (QCM-D), surface plasmon resonance (SPR), free fatty acids (FFAs), triglycerides (TGs), 5-carboxypentyl hydroxypropyl cellulose (HPC-P)

Chapter 1: Introduction

Introduction

Cardiovascular diseases (CVDs) are a major public health burden worldwide. In the United States, CVDs are the leading cause of death and among the most common causes of disability.[1-3] Hyperlipidemia and hypercholesterolemia, or elevated levels of blood lipid and LDL-cholesterol respectively, are significant risk factors associated with CVDs.[4-5] A potential strategy to combat these risk factors is preventing lipid absorption by modulating the digestibility of lipids within the human gastrointestinal tract.[6-8] In the last decade, a special interest has been focused on the rational design of emulsion-based systems and on studying the role of the interfacial networks in controlling lipid digestion and absorption.[9-17] Lipolysis is a complex, colloidal, and interfacial process that involves different crucial actions by bile salts (BSs)[18-20], biosurfactants produced in the liver from cholesterol. On one hand, BSs have the ability to stabilize lipid droplets in the duodenum by rapidly adsorbing to the oil/water (o/w) interface and displacing previously adsorbed emulsifiers from the interface. As a result, this allows for the adsorption of the co-lipase/lipase complex, which initiates lipolysis. On the other hand, BSs remove and solubilize lipolysis products from the o/w interface in the form of mixed BS micelles and transport these products into the intestinal mucosa for absorption.[18-20] Thus, the interfacial composition of emulsions determines the rate of lipolysis and thus lipid bioavailability. Therefore, ingredients that can interfere with any of these actions of BSs may impact the rate and extent of lipid digestion, hence absorption.

Cellulose ethers (CEs), considered dietary fiber polymers, have received significant attention because of their beneficial metabolic and physiological effects, including lowering cholesterol. [11-12, 21-23] They are commercially relevant ingredients used commonly in processed foods. While they are often used as stabilizers in foods to enhance the viscosity of the aqueous phase of emulsions, they also possess surface active properties which allows them to adsorb to interfaces and act as emulsifiers forming stable emulsions.[24] Therefore, CEs are potential candidates to limit the access of BSs to the lipid surface, either by creating interfacial layers that resist displacement by BSs, which will prevent co-lipase/lipase adsorption, or by sequestering BSs in the duodenum, which will reduce the amount of free BSs available to get the surface. The latter is also a mechanism to prevent BS re-absorption into the enterohepatic circulation and reduce blood cholesterol levels.

Previous studies have shown that CEs can bind to BSs in solution[21, 23] and form interfacial networks not easily disrupted by low concentrations of BSs.[11-12, 14] Those studies have focused on either methyl cellulose (MC), in which methyl groups are the sole substituent, or hydroxypropylmethyl cellulose (HPMC), that contains a predominant proportion of methyl groups and a smaller proportion of hydroxypropyl substituent groups, on lipid digestion. [9, 12, 14, 21-22, 25] Limited attention has been paid to hydroxypropyl cellulose (HPC)[11, 23], despite the fact that CEs with a majority of hydrophilic hydroxypropyl substituent groups seemed to be more effective at binding to BSs in the bulk at high BS concentrations compared to those that contained a majority of hydrophobic substituent groups (MC).[23] However, it is still not known whether interactions between BSs and CEs in the aqueous phase affect the ability of BSs to disrupt the lipid surface. To the best of our knowledge there are no fundamental studies on the competitive adsorption of HPC and BSs and its potential to control lipid digestion. Thus, a systematic approach is needed to identify the mechanisms by which HPC can interact with BSs in the bulk and at the interface to further understand their potential role to control lipid digestion in real, complex food emulsions. Additionally, the diverse behavior shown by BSs, i.e. interfacial activation of lipase and the simultaneous removal of lipolysis products from the interface, is intriguing. Further work is needed to understand how subtle differences in the BS structure impact its interactions with CEs.

Research Objectives and Specific Aims

The long-term goal of this research is to design polysaccharide-based food matrices with improved functionalities to optimize lipid digestion in order to address chronic diseases such as CVDs. The overall objective of this research is to investigate i) the mechanisms by which CEs can control lipid digestion through either bulk or interfacial effects and ii) the impact that BSs structure have on their interfacial behavior and interactions with cellulose ethers. Our hypothesis is that the molecular properties of CEs (i.e. substitution types, charge, and molecular weight) and the degree of hydrophobicity of BSs influence their adsorption/desorption dynamics onto the interface and their interactions in the aqueous phase, which will further impact the rate and extent of lipid digestion. In order to achieve our objectives and test our hypothesis, the following **specific objectives** are proposed:

1. Characterize the (interfacial) interactions between HPC derivatives and diverse BSs at the interface.
2. Determine how interactions between HPC derivatives and BSs in the bulk impact their interfacial properties.
3. Evaluate the impact of HPC derivatives and BS type on lipid digestion *in vitro.*

To address the objectives of this research we will use a combination of surface techniques - quartz crystal microbalance with dissipation monitoring (QCM-D) and surface plasmon resonance (SPR)-coupled with an *in vitro* digestion model. The formation of CE-BS adsorption layers onto a hydrophobic solid-liquid interface have been explored by means of sequential and simultaneous adsorption. Two CEs varying in charge, substitution groups and molecular weight (commercial and novel HPC derivatives) and two BSs have been selected. Sequential adsorption experiments provide insight on the interactions between CE layers and BSs at the interface, while simultaneous adsorption experiments provide insight into how the interactions between CEs and BSs in the aqueous phase impact their adsorption to the interface. Lipolysis experiments under intestinal conditions have been performed to determine whether the CEs adsorbed at the oil–water interface of emulsions can affect the lipolysis under intestinal conditions, in addition to the other bulk mechanisms.

These research studies will provide an improved understanding of the dynamics of interactions between CEs and BSs in the bulk and the impact that has on the interfacial properties, related to access for digestion. This knowledge can be exploited in tailoring dietary fibers/food polysaccharides, and specifically CEs, to high performance in modulating lipid digestion and preventing hyperlipidemia and hypercholesterolemia.

Chapter 2: Literature Review

Cardiovascular Disease (CVD)

Cardiovascular diseases (CVDs) can include atrial fibrillation, congestive heart failure, coronary heart disease, stroke, rheumatic heart disease, and other conditions.[1-2] According to the World Health Organization (WHO), CVDs account for around 31% of all global deaths.[3] In 2015, approximately 17.7 million people worldwide died from some type of CVD and it is predicted that by 2030, this number will rise to 23.6 million deaths worldwide.[3] Not only is this a global issue, but CVDs have been the most prevalent diseases and the No. 1 killer of Americans since 1920.[2] In 2015, 41.5% of the American population (102.7 million) had at least one CVD condition, which included high blood pressure, coronary heart disease, stroke, congestive heart disease, or atrial fibrillation.[2] In addition, CVDs are an economic burden in the United States (US) being the costliest diseases. The American Heart Association predicts these costs will rise in the coming decades. Currently, the total cost for CVDs (including direct and indirect cost) in the US is $555 billion, but it is predicted this will rise to $1.1 trillion by 2035. Direct cost includes money spent on medical services, like trips to the physician, hospital, or health care system, and corresponding costs, like prescription drugs, home health care, or nursing home. Indirect cost is related to the lost productivity in the workplace and at home.[2]

Hyperlipidemia (or elevated blood lipids) and hypercholesterolemia (or elevated low-density lipoprotein cholesterol (LDL-C)) are considered to be major risk factors associated with developing CVDs, especially coronary heart disease.[4-5] The risk associated with elevated cholesterol or lipid levels in the bloodstream is that some cholesterol may become trapped on the artery walls and cause plaque build-up over time; therefore, if the arteries are partially blocked, then it is harder to bring enough oxygen and nutrients to the heart, which can cause chest pain. Additionally, some plaque may dislodge and release cholesterol and lipids in the bloodstream, which can cause the formation of blood clots, consequently causing a heart attack.[2, 5] There are several genetic and environmental factors that may contribute to the development of elevated cholesterol and lipid levels which include, overconsumption of lipids, smoking, stress, physical inactivity, age, income, gender, and ethnicity.[1, 4]

Current Treatment Protocols

Fortunately, hyperlipidemia and hypercholesterolemia may be modifiable through different treatments like drug therapy and lifestyle modifications.[26] Statins are considered one of the most commonly prescribed medications worldwide to reduce LDL-C levels[26]. They work by inhibiting 3-hydroxy-3-methylglutaryl coenzyme A (HMG-CoA) reductase, a rate-controlling enzyme involved in cholesterol biosynthesis. Therefore, LDL-C levels are lowered by reducing its production in the liver and increasing removal from circulation.[27] Currently in the US, the Food Drug Administration has approved six drugs of this class.[4] Atorvastatin (Lipitor) and rosuvastatin (Crestor) are considered to be "strong" reducers, compared to the other types of statins, and on average, they can reduce ~40-60% of LDL-C levels.[4] Even though statins are considered a popular treatment option, there are also side effects that can be associated with taking these drugs.[28-29] One of the most frequent side effects associated with statins is mild muscular symptoms[28-30] and in rare cases, potentially severe side effects of statins, like myopathy which can evolve to muscle fiber destruction, have been reported.[31] Other possible side effects associated with statins may include an increased risk of diabetes mellitus, when taken at high statin doses[32], multiple potential drug interactions resulting in toxicity[29], and derangement of liver function tests during the first three months of statin therapy.[29] Bile acid (BA) sequestrants, like cholestyramine and colestipol, are also commonly used drugs to reduce LDL-C levels. These drugs possess positively charged groups that bind bile acids through electrostatic and hydrophobic interactions, which increases bile acid secretion and consequently increase BA synthesis from blood cholesterol.[33] However, adverse side effects can also be associated with taking these sequestrants. For instance, constipation is one of the major side effects associated with BA sequestrants; other gastrointestinal side effects include bloating and cramping.[34]

Therefore, lifestyle modifications, like change in diet, increase in physical activity, and weight loss, are more appealing options to treat hypercholesterolemia and hyperlipidemia.[26] First of all, lifestyle modifications have the benefits of not requiring a prescription and can be considered a more "natural" approach.[26] Additionally, there has been a strong opinion about the benefits of a diet that consists of consuming dietary fiber, limiting sugar intake, and replacing saturated and trans fats with unsaturated fat.[35] For instance, randomized controlled trials have shown that soluble fibers in oat products decrease LDL-C levels among hypercholesterolemic patients[36] and it was also shown that foods containing pectin, psyllium, oat bran, and guar gum, were equally effective at reducing LDL-C levels, with no significant changes in high-density lipoprotein cholesterol (HDL-C) levels.[37] Consuming reduced fat foods is another lifestyle modification that could lower incidences of hypercholesterolemia and hyperlipidemia.[6] However, lipids play a major role in foods (i.e. enhance texture, taste, flavor, and deliver fat-soluble nutrients[8]); therefore, there is growing interest in understanding and developing novel emulsion-based systems that can potentially modulate the digestibility and bioavailability of lipids in the gastrointestinal tract (GIT).[6-8] To emphasize, there are a number of diseases that impact lipid bioavailability due to reduced lipid digestion or malabsorption, like cystic fibrosis. These diseases can cause trouble for individuals in obtaining essential lipid-soluble nutrients from their diet, thus leading to serious health problems.[6] However, since the overconsumption of lipids is a major contributor to the development of hyperlipidemia and hypercholesterolemia, then it may be desirable to formulate these systems for the individuals with these health conditions.[6] It is also important to note there may be some potential limitations when trying to control lipid digestion. For instance, fat replacers have been formulated into foods with the intent of reducing fat intake; these may be macromolecules that physically and chemically resemble triglycerides (fat substitutes) or substances that imitate the physical properties of triglycerides (fat mimetics).[38] However, there has been reported gastrointestinal side effects when consuming foods that contain fat replacers.[38] Olestra is a sucrose polyester that cannot be absorbed or metabolized in the human body and has been used as a fat substitute in potato chips, cheese puffs, and crackers.[39-40] There have been numerous reports of side effects, like abdominal cramping, diarrhea, stool softening, and inhibition of some vitamin absorption, like A, D, E, and K, so a label statement notifying consumers about these effects above a consumption of 10 g was required to put on all products containing this ingredient.[39-40] Additionally, polydextrose has been used as a bulking agent and texturizer in foods and is only partially metabolizable in the human body.[41] Therefore, there have been previous reports about nausea and diarrhea, so foods that contain more than 15g polydextrose/single serving must provide a label statement that warn consumers about these laxative effects.[41] Another potential consequence of controlling lipid digestion may be an elevated concentration of BAs in the colon, due to inhibition of BA re-absorption through the hepatic portal vein, as well as elevated triglyceride levels in the colon which can induce the secretion of electrolytes and water in the form of diarrhea.[42-43]

Ultimately, these novel emulsion-based systems could lead to the creation of functional foods, which consumed in moderation could improve human health.[6] However, in order to design these novel systems there needs to be an increased understanding of how the interfacial composition and structure of emulsified lipids are impacted by the physiochemical and physiological processes of lipid digestion. In the next section, an overview of the major events that occur during the lipid digestion process is provided.

Overview of Lipid Digestion

Introduction

Dietary lipids may be consumed in a variety of different forms, like bulk fats, water-oil emulsions (margarine and butter), or oil-water emulsions (milk, cream, dressings, soups, and beverages), that differ in composition, physical state, and structural properties.[44] Processed food emulsions are a major source of fat in Western society diets and approximately 50% of all processed foods contain emulsified lipids.[8] Emulsion production involves the creation and stabilization of an interface, between the lipid and water, covered with emulsifiers in order to stabilize them against coalescence and separation. Triglycerides (TGs) are the predominant component of dietary fat and oils[45] and their molecular structure consists of a glycerol backbone esterified with three fatty acid (FA) molecules. The FA positions may be designated as *sn*-1, *sn*-2, and *sn*-3 **(Figure 2.1)**.[46]

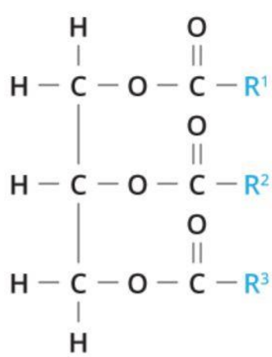

Figure 2.1. Molecular structure of a triglyceride that consists of one glycerol and three fatty acid molecules.

TGs must be hydrolyzed into smaller molecular forms, such as FAs and monoglycerides (MGs), that are less insoluble in water so they can easily be absorbed by the enterocytes in the intestinal epithelium through the mucus barrier and get distributed throughout the body for metabolism.[45] This is achieved during lipid digestion, which involves the enzymatic hydrolysis of emulsified lipids by soluble lipases (lipolysis).[46-48]

Gastric phase

When dietary lipids are ingested, they are chewed and mixed with saliva to form a food bolus.[6, 48] The structural organization within this bolus depends on the initial characteristics of the lipid (composition, rheology, and physical state); in many cases, the lipids in this bolus are present as droplets that vary in size from less than a micrometer (for some food emulsions) to more than a millimeter (for some bulk fats).[6] After the food bolus is swallowed, it gets transported through the esophagus and into the stomach where it mixes with acidic digestive juices, gastric enzymes, and minerals.[49-50] The acidic gastric environment (pH ~1-3) can vary with age, diet, and health status.[48] The shear forces during mixing emulsify the lipid droplets even further by reducing their particle size down to ~10-30 μm and increasing the surface area for the adsorption of gastric lipase to the lipid-water interface.[51] The composition of lipid droplets in the stomach depends on the lipids consumed but typically, lipid droplets consist of a hydrophobic core, containing mostly TGs, esterified cholesterol, and fat soluble vitamins, and an amphiphilic surface layer that contains phospholipids, free cholesterol, and some TGs.[6, 52] The small fraction of TGs (2-5 mol%) present at the droplet surface enables gastric lipase action at the interface.[53] Gastric lipase contains an amphiphilic peptide loop that covers the active site of the enzyme, and when it contacts the lipid-water interface it undergoes conformational rearrangement. The hydrophobic portion of the loop binds to the interface and is activated by the surface energy of the lipid droplet, which allows the active site to hydrolyze the exposed TGs, releasing a single FA at the *sn*-3 position. The products that are formed during gastric lipolysis are *sn*-1,2 diglycerides (DGs) and free fatty acids (FFAs) **(Figure 2.2)**.[51, 54] Over time, the composition changes for both the droplet core and interfacial layer; i.e there is an increase in FFAs, DGs, and free cholesterol and a decrease of TGs at the surface.[55] Gastric lipolysis usually stops when approximately 10-30% of FFAs have been released from the dietary lipids. It is proposed that when ~120-170 $umol{\cdot}m^{-2}$ of FFAs have accumulated at the interface[6], these products force lipase away from the interface, thus inhibiting lipase activity through product inhibition.[45] FFAs and phospholipids are believed to help facilitate lipolysis in the duodenum. Since these molecules are surface active, they may help to stabilize the droplets and change the interfacial composition, which increases the solubilization of the lipid droplets as they pass through the pylorus and into the duodenum of the small intestine.[7, 51, 54, 56]

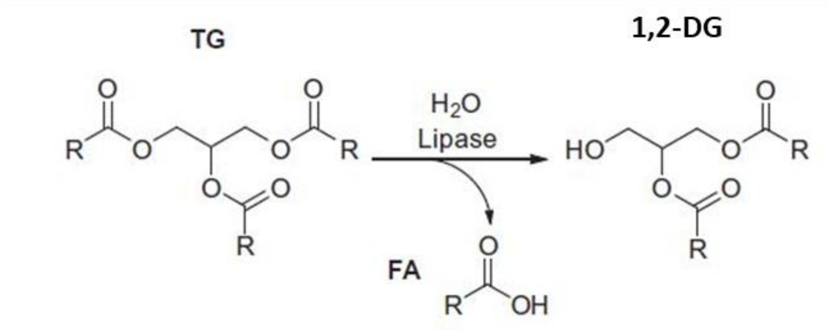

Figure 2.2. Lipolysis of a triglyceride (TG) by gastric lipase to form 1,2-diglyceride (DG) and a fatty acid (FA).

Duodenal phase

The majority of lipolysis (70-90%) occurs in the duodenum, the first section of the small intestine.[7, 51, 54, 56] When the partially digested food bolus enters the duodenum, this initiates secretion of pancreatic lipase and sodium bicarbonate, which drastically increases the pH to ~6-6.6, and induces gall bladder emptying. The gall bladder empties bile, which is then secreted in the duodenum via the bile duct. Bile is a complex fluid that contains water, electrolytes, and organic molecules.[57-58] The major components of bile are bile salts (BSs), key amphiphilic, negatively charged, bio-surfactants (surface active agent) that perform a number of crucial roles in lipid digestion.[20, 59-60]

Table 2.1. Composition of bile. Data collected from O'Connor et al., 1985[57].

Component	**Composition (%w/w)**
Bile Salts	67
Phospholipids	22
Protein	4.5
Cholesterol	4
Bilirubin	0.3

The adsorption of BS promotes the displacement of existing surfactants from the interface and creates a negative charge on the interface that generates electrostatic repulsion at the interface. This helps to stabilize the emulsions and attract the adsorption of the positively charged coenzyme (co-lipase) to the ester bond of the TG through hydrogen bonding.[20, 61] The presence of BSs may promote or inhibit the adsorption of pancreatic lipase depending on their concentration. At low BS concentrations, they promote lipase adsorption but at high physiological BS concentrations, lipase adsorption may be inhibited.[20-21, 62] However, in the presence of co-lipase, lipase adsorption to the interface is enhanced. It is suggested that lipase then couples tightly with the adsorbed co-lipase through electrostatic interactions which forms a stoichiometric complex. This brings lipase into close contact with the lipid substrate, thereby allowing it to bind to the interface and initiating lipolysis thus releasing FFAs (at the *sn*-1 and *sn*-3 positions) and 2-monoglycerides (MGs).[46, 61, 63] The extent of lipase binding to the interface is a key rate-limiting step which is dependent on the interfacial composition and any surface active molecules present in the bulk aqueous phase.[64] Specifically, competitive adsorption for the interface may occur between surface active molecules (like BSs, phospholipids, and digestion products), which could interfere with lipase adsorption.[47] Additionally, the presence of an interfacial barrier (like polysaccharides or proteins emulsifiers) may also impact lipase adsorption.[47] Therefore, this key rate-limiting step controls the concentration of lipase at the interface and, hence, the rate of lipolysis.

As lipolysis continues, products like FFAs and MGs tend to accumulate at the interface, which can decrease the surface area for lipase adsorption, thus inhibiting lipolysis.[6] These accumulated products are removed from the interface and solubilized in the form of mixed micelle vesicles consisting of BSs and phospholipids.[48, 63] The mixed micelles also can carry cholesterol and other fat soluble nutrients.[45] By removing products of lipolysis from the interface, the reaction equilibrium is driven towards continuing lipolysis.[63] Once the mixed micelles move non-polar lipids across the unstirred water layer and the mucosal layer, these products are absorbed by intestinal enterocytes.[47, 50] **Figure 2.3** shows a schematic representation of lipolysis in the small intestine.

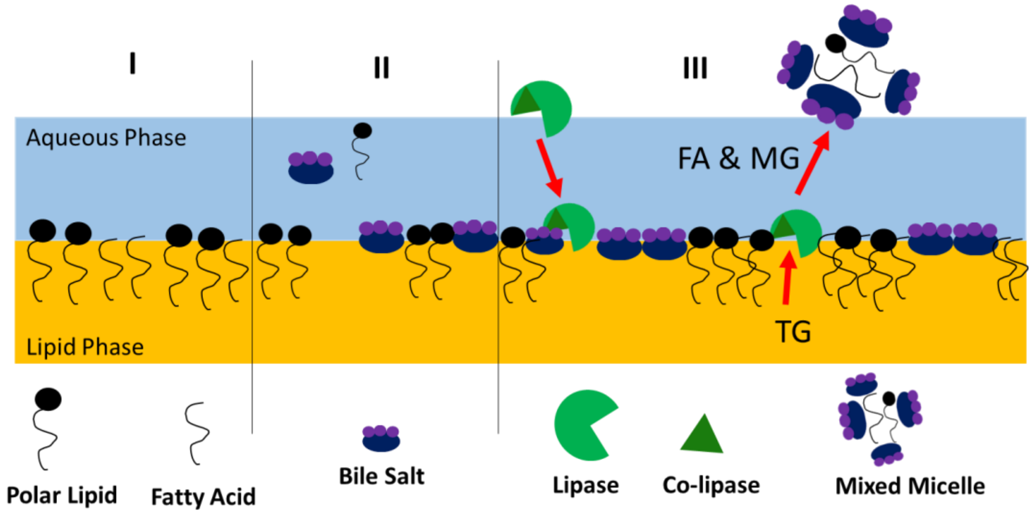

Figure 2.3. Schematic representation of lipolysis in the duodenum. Surface active materials are adsorbed to the lipid-water interface, including polar lipids (I). Then, BSs and phospholipids adsorb to the lipid droplet surface and already adsorbed materials are displaced from the interface (II). This facilitates lipase/co-lipase adsorption, which initiates the enzymatic breakdown of lipid droplets into FAs and 2-monoglycerides. Lipolysis products get removed from the droplet surface and solubilized via BS mixed micelles (III) (Adapted from Wilde and Chu[18]).

Once the lipolysis products get absorbed, their subsequent transport to the systemic circulation depends on the molecular weight of the hydrocarbon chain.[45] Long-chain fatty acids tend to be reconstructed back into TGs within the enterocyte, packaged into lipoproteins (most commonly formed are chylomicrons and very low-density lipoproteins (VLDL)), and then transported to other tissues via the lymphatic system for subsequent metabolism. On the other hand, short-chain fatty acids and medium chain fatty acids tend to be absorbed directly into the portal vein and undergoooo systemic circulation.[45-46]

Bile Salts

Physiology

Bile salts (BSs) are the fully ionized forms of bile acids (BAs), which are synthesized from hepatocyte cholesterol in the liver.[59] Cholesterol is a C_{27} sterol vital for eukaryotic cell growth required as a building block for the formation of cell membranes, mitochondria , and microsomes.[65] Humans obtain cholesterol via two routes; *de novo*, where approximately 700-900 mg are synthesized in the liver every day, and directly from dietary sources, which account for approximately 300-500 mg/day.[58, 65] Cholesterol is eliminated from the body through different pathways; secretion from the gastrointestinal tract (GIT), synthesis of BAs, and synthesis of steroid hormones.[65-66] Its homeostasis is maintained in the liver.[65]

BA synthesis accounts for the largest percentage of hepatocyte cholesterol catabolism, which occurs by the actions of more than 10 enzymes.[65] First, primary BAs are synthesized *de novo* in the liver from hepatocyte cholesterol through two main pathways (neutral or acidic). The major primary BAs consist of cholic acid (3α,7α,12α-trihydroxy-5β-cholanic acid) and chenodeoxycholic acid (3α,7α-dihydroxy-5β-cholanic acid). Then, secondary acids are obtained from the conversion of primary acids through dehydroxylation by intestinal bacteria in the ileum of the small intestine and consist of deoxycholic acid (3α, 12α-dihydroxy-5β-cholanic acid) and lithocholic acid (3α-hydroxy-5β-cholanic acid) **(Table 2.2)**.[59, 67-68]

***Table 2.2**. Molecular structures of primary (cholic and chenodeoxycholic) and secondary (deoxycholic and lithocholic) BAs.*

	Bile Acids	
Primary	**Cholic Acid** 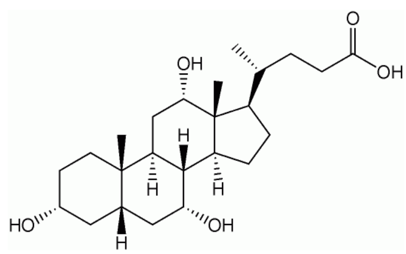	**Chenodeoxycholic Acid** 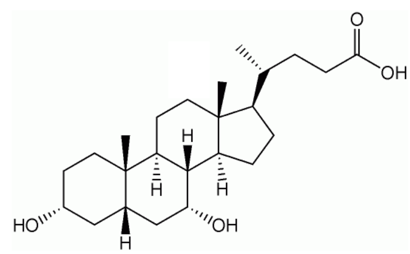
Secondary	**Deoxycholic Acid** 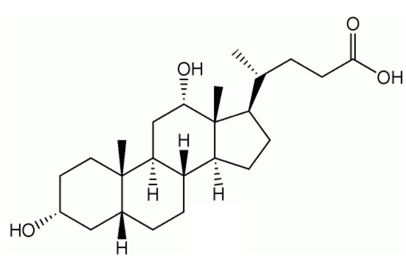	**Lithocholic Acid** 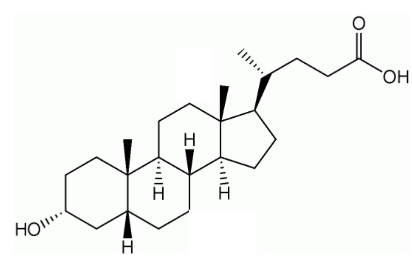

Before being secreted into the gallbladder for storage, BAs are conjugated by *N*-acyl linkage with either glycine or taurine. Conjugation with taurine results in molecules that are fully ionized and highly soluble at the pH in the small intestine during digestion (pH 6-7). Conjugation with glycine results in a slightly stronger acid (pK_a ~4) that also allows them to have higher solubility at the pH of the small intestine. The consequence of conjugation makes them impermeable to cell membranes, which helps to maintain high intraluminal concentration of conjugated BA to facilitate lipid digestion and absorption down the small intestine. Conjugated BAs form sodium salts, which are termed BSs.[57, 59, 67-69] Approximately 95% of BSs are actively absorbed from the small intestine and returned back to the liver via the portal vein in a process called enterohepatic circulation. This is an extremely efficient process that recirculates 5-10 times per day with less than 5% of BSs escaping reabsorption per day and eliminated in the feces.[70] The BSs that are eliminated are replaced by newly synthesized BAs from cholesterol.[69] BAs are also important signaling molecules that are involved in the regulation of lipid, glucose, energy, and drug metabolism. This regulatory function of BAs has been shown to be a result of BA activation of ligand-activated nuclear receptors, like farnesoid X receptor (FXR), cell surface G protein-coupled receptors (GPCRs), vitamin D receptor (VDR), and pregnane X receptor.[71-72] Additionally, BAs and gut microbiota are closely linked. On one hand, BAs control microbiota overgrowth and composition through the activation of FXR signaling. On the other hand, gut microbiota regulate BA biotransformation in the intestine, which alter BA composition and modulate FXR signaling.[72] The activation of FXR has been suggested to play a role in reducing hepatic fat accumulation and plasma TG by inhibiting VLDL overproduction and hepatic de novo lipogenesis[72], lowering fasting plasma glucose and improving insulin sensitivity in obese and diabetic mice[73], and decreasing inflammation of the vasculature, which is involved in the progression of atherosclerosis.[74]

BSs are amphiphilic, bio-surfactant (surface active agents) molecules that have an unusual structure compared to classic surfactants. Typically, classic surfactants have a distinct hydrophilic head that consists of small polar or charged groups and a hydrophobic tail that contains a long hydrocarbon chain.[75] Instead, BSs exhibit planar polarity by having a concave and convex side (**Figure 2.4**).

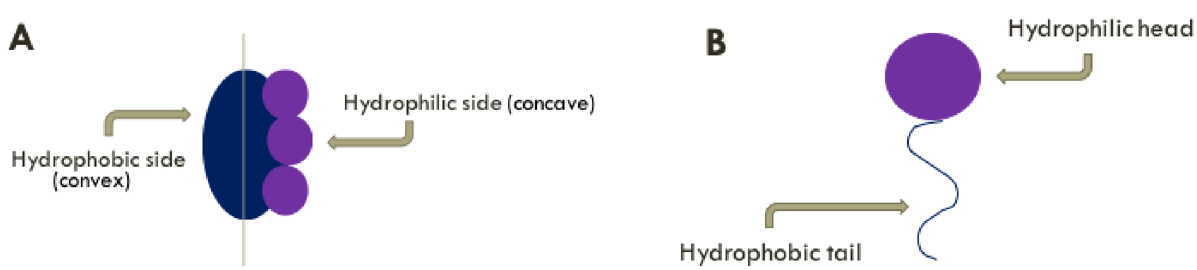

Figure 2.4. Structural comparison between BSs (A) and classic surfactants (B).

BSs comprise two connecting units; a rigid steroid backbone (comprised of a hydrophobic and hydrophilic side) attached to an aliphatic tail. The steroid backbone contains three six-member rings and a five-member ring. The concave side of the rigid steroid ring system bears one, two, or three OH groups and an amino group, making it hydrophilic, and the convex side bears methyl groups, making it hydrophobic. The number, position, and orientation of the hydroxyl groups and the presence or absence of a conjugated amino acid differ between BS species **(Table 2.3)**, making the hydrophobic and hydrophilic sides not as clearly defined as classic surfactants.[19-20, 59, 67, 75] Because of this structure, BSs are important in a variety of different biological functions like antibacterial defense, denaturation of proteins prior to proteolysis, preparation of the lipid-water interface prior to lipolysis, and transportation of lipolysis products in mixed micelles.[20, 76]

Table 2.3. Six major types of BSs that differ in the conjugate amino acid group (glycine or taurine) and the number and position of the hydroxyl groups.

	Bile Salt		
Conjugating Group	**Cholate**	**Chenodeoxycholate**	**Deoxycholate**
Glyco-	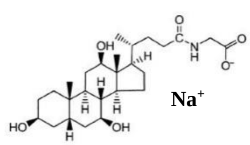	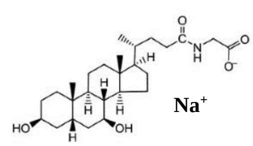	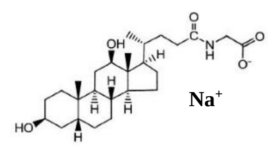
Tauro-	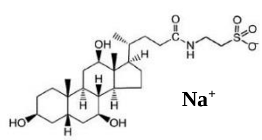	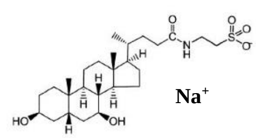	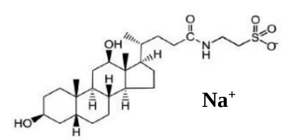

Formation of Bile Salt Micelle

BSs are amphiphilic molecules and consequently, they have the tendency to self-assemble in aqueous solution to form aggregates called micelles. This occurs at a certain BS concentration range known as the critical micelle concentration (CMC)[20, 69, 77], the concentration range at which BS self-assemble in aqueous solutions to form micelles.[20, 69] For typical surfactants, the micelle structure is well established and is characterized by having an exact

CMC value. It is known that the hydrophobic tails assemble together in the interior, while the hydrophilic head groups are on the outer portion in the aqueous phase **(Figure 2.5)**.[20, 76]

Figure 2.5. Surfactant micelle in an aqueous environment with the hydrophilic heads facing outside towards the aqueous phase and the hydrophobic tails tightly packed in the interior.

However, due BS unusual structures, it is believed that BS micelles are more complex in nature. The rigidity of the BS steroid ring may lead to an incomplete separation of hydrophobic / hydrophilic sides with some hydrophobic parts remaining in the aqueous phase while some hydrophilic parts might remain inside the micelle.[75]

The two driving mechanisms involved in BS micelle formation include hydrogen bonding and the hydrophobic effect.[77] Three models of BS micelle formation have been proposed.[78-80] The two-step model proposed by Small *et al.* states that primary aggregates form as a result of hydrophobic interactions at low BS concentrations. Secondary aggregates form as a result of hydrogen bonding between hydroxyl groups from smaller, primary aggregates at high BS concentration. This model proposes that the primary aggregates have a globular shape and secondary aggregates have a oblate ellipsoidal shape.[80] Kawamura *et al.* proposed a second model that states the secondary aggregates have a disc-like structure. In this structure, the hydrophobic sides face each other, making the interior of the aggregate hydrophobic, while the hydrophilic sides face toward the aqueous phase.[78] The third model proposed by Giglio *et al.* states that the anions are arranged as a helix structure, with the hydrophobic sides facing the outside and the center of the aggregate is filled with cations. The helix is stabilized by ion-ion, ion-dipole, and hydrogen bond interactions.[79] However, a recent study performed with molecular dynamics simulations discounts the helical structure, making the two-step model and disc-like structure more widely recognized.[76, 81]

Micelles can be characterized by their CMC and aggregation number. The CMC is characterized by the concentration at which free surfactants in solution begin to self-assemble to form aggregates and the interfacial tension remains constant. It has been suggested that BS have a broader range of CMC values compared to typical surfactants, which can be a consequence from its planar polarity.[20, 57, 75-76] The CMC value depends on several factors like solution parameters (temperature, pH, ionic strength) and BS species. An increased ionic strength lowers the electrostatic repulsion between the charged groups favoring aggregation between BS molecules, and consequently decreasing the CMC value.[75, 82] The pH value affects BS ionization; at a pH higher than the pK_a of the BS species (glycine species = ~4.3-5.3; taurine species= ~2[83]), they will be ionized. However, at a pH close to the pK_a, the dissociated and undissociated molecules will aggregate together to form micelles, thus lowering the CMC value.[75] Finally, the higher BS hydrophobicity, the lower CMC value. The general trend indicates that there is a decrease in CMC value in this order: Ursodeoxycholate (UDC) ≥ cholate (C) ≥ chenodexoycholate (CDC) ≥ deoxycholate (DC).[84] In regards to the conjugated amino acid groups, the general trend is CMC unconjugated BSs > glycine conjugates ≥ taurine conjugates. **Table 2.4** presents CMC values for various BSs. These values have been determined using several techniques such as surface tension, conductivity, calorimetry, chromatography and fluorescence spectroscopy.[20, 75, 84-85]

Table 2.4. Critical micelle concentration (CMC) and aggregation number (*N_{agg}*) values for various sodium salts of conjugated and unconjugated bile acids collected from various sources (*[1]*Maldonado-Valderrama et al., 2011, and *[2]*Madenci et al., 2010).

Bile Salt (all sodium)	CMC (mM)	Aggregation Number (N_{agg})
Cholate (NaC)	4-20[1]	3-8[1]
Deoxycholate (NaDC)	2-5[1]	6-11[1]
Taurocholate (NaTC)	3-18[2]	3-7[2]
Glycocholate (NaGC)	4[2]	9[2]
Taurodeoxycholate (NaTDC)	2-3[2]	12-19[2]
Glycodeoxycholate (NaGDC)	1-2[2]	13-16[2]
Taurochenodeoxycholate (NaTCDC)	0.9-7[2]	5-26[2]
Glycochenodeoxycholate (NaGCDC)	1-2[2]	15[2]

The aggregation number (N_{agg}) is characterized by the micelle size and average number of surfactant molecules that make up the micelle. For typical surfactants and BSs, N_{agg} is related to their CMC value. However, BSs have shown to have N_{agg} values (typically having a range of $2 \leq N_{agg} \leq 15$) about an order of magnitude smaller compared to classic surfactants, which is due to their planar polarity. The N_{agg} value also depends on the type of BS species. The trend N_{agg} typically is DC ≥ CDC > C ≥ UDC, which is similar to the trend for CMC values. This shows how important hydrophobicity, number and position of hydroxyl groups, and the conjugated amino acid are to determine N_{agg} and CMC values.[20, 75, 82]

Adsorption and Desorption of Bile Salts to Interfaces

In order to better understand the adsorption/desorption behaviors of BSs to interfaces, studies have been performed at both the air-water and oil-water interfaces. BSs have been shown to have a strong adsorption affinity and reach a lower final surface pressure at the air-water and oil-water interface (~30 mN/m), compared to classic surfactants (~50 mN/m).[20, 86-88] It has been suggested that a low surface pressure at an interface may correlate BSs adopting a flat conformation at interfaces. This is because a flat conformation may exert different physical forces on the surface, thus resulting in a different surface pressure than classic surfactants. This conclusion would also correlate to BS facial amphiphilic structure and their rapid adsorption time because one molecule would cover a larger surface area of the interface.[86] Differences in adsorption/desorption behaviors between BS types have also been observed.[20, 23, 89] Maldonado-Valderrama *et al.* studied the adsorption process of two BS, NaTC and NaGDC, and found that both BS species rapidly adsorbed to the air-water interface, even at low concentrations, with NaGDC adsorbing faster than NaTC.[20] These results correlate well with another study by Parker *et al.*, who found that cholates had slower adsorption rates than deoxycholates and chenodeoxycholates to a solid hydrophobic surface.[89] By using pendant drop tensiometry, Maldonado-Valderrama *et al.* observed that NaGDC desorbed faster than NaTC from the air-water interface, indicating that NaTC had a stronger affinity to the interface.[20] It is important to note that, while the conjugation type (i.e. with taurine or glycine) has little effect on BS adsorption/desorption behavior, subtle differences in structure (i.e. difference by a single hydroxyl group) influence CMC values and aggregation numbers which could greatly impact BS behavior at the interface.[89]

As previously mentioned, BSs perform a number of different roles in lipid digestion; i.e BS emulsify lipids, displace materials from the droplet interface, bind to the co-lipase/lipase complex to facilitate its adsorption to the interface and then initiate lipolysis, and solubilize lipolysis products via mixed micelles.[20] The fact that studies have shown different adsorption-desorption behaviors to interfaces between BS species[20, 89], suggests that it is unlikely that one single BS species can perform all of these roles in digestion. Therefore, it is thought that there might be a cooperative adsorption process between certain BS species during lipid digestion.[89]

More specifically, it is postulated that the BSs that have a slower adsorption and longer residence time at the interface may help promote lipase/co-lipase adsorption to the interface, thus facilitating lipolysis. On the other hand, BS showing a largely reversible adsorption may favor the displacement of lipolysis products from the interface and solubilization into mixed micelles.[89] However, further work is needed to improve the understanding of how minor subtle differences in BS molecular structure could impact their behavior and functions during the lipid digestion process and their interactions with food emulsifiers.

Cellulose

Cellulose is one of the most abundant renewable resources that is available worldwide and it is estimated that raw cellulose shares around 10^{12} tons of the annual biomass production.[90] It is a major building block of the cell wall structure of higher plants, and constitutes approximately 40-50% of wood, 80% of flax, and 90% of cotton fiber.[24] Cellulose consists of β-1,4 di-equatorial glucose repeating units (**Figure 2.6)** that are linked firmly together through glyosidic bonds, making a very rigid, linear structure.[91] This configuration contributes to the strength shown in plant structures, as well as its insolubility in common solvents, like water.[90] Cellulose is considered a source of dietary fiber because humans lack the digestive enzymes necessary to hydrolyze the β-1,4 glycosidic linkages.[90] Additionally, cellulose can be modified into cellulose derivatives and be used in industrial applications, like cosmetics, drug delivery systems, films, coatings, and foods. Two main groups of cellulose derivatives include cellulose ethers and cellulose esters. The general structure of esters is $RCOOR^-$ and ethers is ROR^-.[92-93]

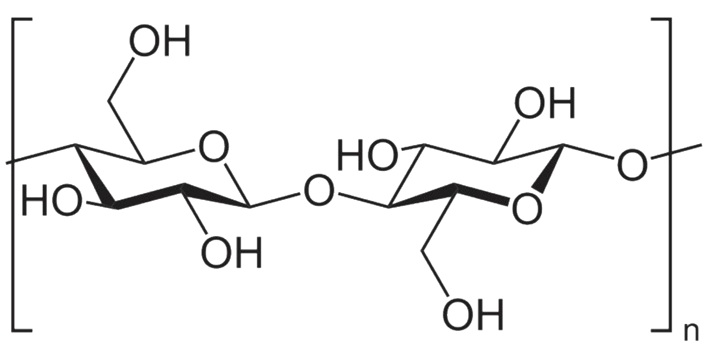

Figure 2.6. Repeating unit of cellulose.

Cellulose Derivatives

Cellulose is modified into cellulose ethers (CEs) by these steps, 1) generation of alkali cellulose 2) alkylation or hydroxyalkylation and 3) product purification.[94] First, cellulose is treated with a caustic alkaline solution that breaks up the hydrogen bonding between polymeric strands, opening hydroxyl groups available for modification.[24] Alkylation or hydroxylalkylation is carried out next resulting in CEs and purification is performed through water washing and filtration procedures.[24] After production, the substituent groups of these derivatives can be identified by ^{1}H NMR and cellulose derivatives can be characterized by degree of substitution (DS) and molar substitution (MS). The term DS refers to the average number of substituted hydroxyl group positions per anhydroglucose unit, whereas MS refers to the average number of moles of substituents per mole of anhydroglucose.[24] Even though there are a wide variety of cellulose derivatives, only a few are approved for use in food manufacturing. **Figure 2.7** shows examples of some CEs used in food applications.[95-96]

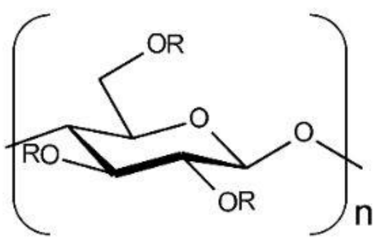

Cellulose Ether	R group
Methylcellulose (MC)	H, CH_3
Ethylcellulose (EC)	H, CH_2CH_3
Hydroxypropylcellulose (HPC)	H, $CH_2CH(OH)CH_3$
Hydroxypropylmethylcellulose (HPMC)	H, $CH_3CH_2CH(OH)CH_3$
Carboxymethylcellulose (CMC)	H, CH_2COOH

Figure 2.7. Anhydroglucose unit of cellulose ethers used in food manufacturing. (Adapted from Stephen and Phillips, 2016[24])

Properties & Applications in Food

CEs play important roles in food applications, including the modification of rheological properties, emulsification, stabilization of foams, modification of ice crystal formation and growth, and water-binding capacity.[97] They can form gels when heated (thermal gelation), contrary to other polysaccharides that form gels during cooling, which can especially be important in bread making because it can impart added dough strength and uniformity throughout baking, giving a consistent crumb structure to the final product.[94] This property is also important to prevent oil absorption during deep frying. However, thermal gelation is dependent on the type of CE and temperature. It has been observed that an increase in methyl substitution gives a firmer gel, whereas an increase in hydroxypropyl substitution gives a softer gel, which can be attributed to hydrophobic interactions between substituent ether groups.[94, 98] Some studies also suggest that not only do hydrophobic interactions play a role in gelation, but hydrogen bonding as well.[99] An increase in temperature also increases the number of hydrophobic interactions and cross-linking, thus creating an even firmer gel.[98] Some CEs are used as fat-replacers in foods because they can provide desirable fat-like mouthfeel and viscosity to these systems. CEs are amphiphilic molecules, i.e. they have hydrophobic and hydrophilic domains, and, consequently, they have surface active properties and can be used as emulsifiers to stabilize emulsions. Emulsions are thermodynamically unstable systems consisting of a dispersion of one immiscible liquid in another liquid in the form of droplets that can separate into individual phases over a period of time.[7] When they are prepared through high pressure homogenization, the droplets are disrupted by intense shear flow and CEs can adsorb to the emulsion oil-water (o/w) interface with their hydrophobic domains interacting with the oil droplet surface while the hydrophilic domains dissolve the aqueous phase.[7, 44] By adsorbing to the oil-water interface, this imposes a protective barrier around the oil droplets and reduces the interfacial tension, which can help reduce flocculation or coalescence.[21, 100-101] Another manner that CEs can stabilize emulsion systems is by imparting increased viscosity in the continuous phase, which slows down the rate of creaming.[102] The molecular weight of the polymer influences solution viscosity; therefore, if the molecular weight increases, the solution viscosity increases.[24] An example of how CEs can exist both in the continuous phase and at the o/w interface of emulsions is provided in **Figure 2.8.** Due to the above functional properties, CEs have received great interest recently in their potential to control lipid digestion.[11-12, 21-23]

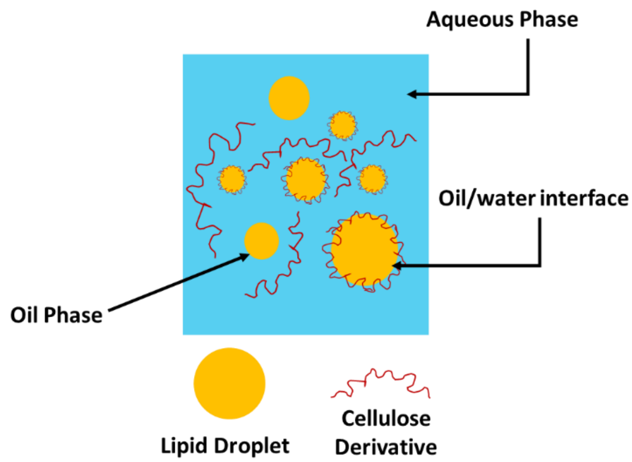

Figure 2.8. Surface active and thickening properties of cellulose ethers to help create/maintain stable emulsions.

Strategies to Modulate Lipid Digestion

Formulating novel strategies to control lipid digestion depends on the key physiochemical processes that may impact the digestion of lipids in the small intestine.[6] First of all, interfacial properties of lipids change as they pass through the gastrointestinal tract (GIT). For food emulsions, the lipid droplets contain emulsifiers that are adsorbed to the interface. These original emulsifiers may be digested by enzymes and/or displaced by surface active molecules in the system, which may impact the ability of the emulsifier to stabilize the lipid droplets.[6, 63, 103] Also, if the interfacial layers are not strong enough, then coalescence may occur as they collide with each other within the GIT, thus increasing the particle size and inhibiting lipase adsorption. Additionally, particle sizes decrease as the droplets are digested by lipase which may be due to the removal of digestion products into the surrounding aqueous phase.[6, 104] The matrix surrounding the lipids may also be disrupted during digestion, which determines how easily biosurfactants and enzymes can access the interface. For example, if lipid droplets are trapped in a solid matrix, that may inhibit lipase adsorption. On the other hand, if the droplets are dispersed in a low viscosity fluid, then the surface would be more accessible to any surface active molecules and enzymes in the surrounding medium.[6] Since food systems are highly complex and can contain many components, binding interactions also may occur with each other and form electrostatic and hydrophobic complexes that control the rate and extent of lipid digestion.[6]

It was previously hypothesized that strengthening the interfacial barrier against lipase action may help control the rate and extent of lipolysis.[105] However, these barriers have shown to not significantly inhibit lipase action.[105] Nonetheless, many studies have investigated the effect of the interactions between components of interfacial films (adsorbed and/or unadsorbed) and biosurfactants, like BSs, which could potentially control the rate and extent of lipolysis.[9, 11-14, 21-23, 25, 106-110]

Since many proteins play major roles in the formation and stabilization of food emulsions[111], various studies have looked at the behavior of protein-stabilized emulsions to influence lipid digestion.[9, 106-109] Milk proteins, like caseins and whey proteins, exhibit excellent surface active properties, due to the amphiphilicity and molecular flexibility of the polypeptide chains, which allows them to form interfacial layers that have desirable rheological properties.[111-112] For example, whey proteins, like β-lactoglobulin, can form a compact rigid layer that is ~2 nm thick and caseins can form extended layers up to ~10 nm thick.[111] Some commercial milk products (like calcium caseinate) are present as aggregates, due to cross-linking by calcium-induced interactions, that allow them to form thick interfacial layers. All of these interfacial layers are desirable when creating emulsions because they contribute to long term stability against coalescence by both electrostatic and steric mechanisms.[111] For this reason, it was thought that these interfacial films may serve as good candidates to resist the displacement by BSs, which could control BS and lipase adsorption, and ultimately lipolysis. In general, results have shown that the susceptibility of proteins to be displaced by BSs seems to depend on the type of protein adsorbed at the interface. If a protein poorly covers the interface, then it may be more susceptible to BS displacement[107], whereas if a protein saturates the interface, then it seems be more resistant to BS displacement.[109] For example, it was found that β-lactoglobulin (β-lg) networks were weakened, broken up, and pushed off by BS at both air-water[107] and oil-water interfaces[107-108] but soy proteins seemed more resistant to displacement by BS.[9, 109] It was also found that if a protein can interact and compete with BSs for the interface, then that may impact its displacement by BSs, thus impact the further action of co-lipase/lipase.[109] However, it seems that only soy proteins have shown to interact and compete with BSs for the interface, compared to β-lactoglobulin and egg white proteins.[109]

Polysaccharides have also received great interest in their potential to interact with BSs and control lipid digestion. Soluble dietary fibers (SDFs) have demonstrated positive metabolic effects in the GIT[113-115] and one of the proposed mechanisms behind this effect is the prevention of BS re-absorption.[58] Studies that have investigated soluble dietary fibers (SDFs) have found that they may interact with BSs in a number of different ways, including, 1) SDFs and BSs are bound / complexed at a molecular level[110, 116-117], 2) SDFs entrap BS micelles by forming a viscous or gelatinous network[118-119], or 3) SDF increases the barrier properties of the unstirred water layer between micelles and absorptive cells.[120-121] For example, it has been shown that chitosan and a BS (NaTC) bound together through electrostatic interactions.[110] It was also found that BS micelles were entrapped by an arabinoxylan[58] and β-glucan matrix.[122] Cellulose ethers are also promising candidates to control lipid digestion[11-12, 14, 23, 32] because, unlike proteins, they can exist at both the interface and in aqueous phase of food emulsions.[24] Overall, studies have demonstrated that cellulose ethers can delay lipolysis.[12, 21-22, 25] It is suggested that these results can be attributed to their ability to bound or "sequester" BSs in the bulk[21], through hydrophobic interactions[11, 21, 23] , which may affect BS adsorption to the interface, thus contributing to their resistance to displacement by BSs at the interface.[21] Based on these studies, polysaccharides, like cellulose ethers, seem to be more efficient at controlling lipid digestion, compared to proteins, which may be more attributed to their ability to interact with BSs rather than to their role as a strong interfacial barrier.[105]

Surface Analysis Techniques

Understanding the surface behavior of materials in biological systems has become an increasingly popular field and there has been great progress in techniques that help to characterize the interactions between molecules at biological surfaces.[123,124] In particular, quartz crystal microbalance with dissipation monitoring (QCM-D) and surface plasmon resonance (SPR) are two surface analysis techniques that provide qualitative and quantitative information about the real-time and label-free monitoring of molecular adsorption / interactions at solid surfaces.[124] They are increasingly used to investigate structural aspects and mechanisms of biological systems and have been used in a broad range of applications. Information behind the theory of these two techniques is provided below.

Quartz Crystal Microbalance with Dissipation Monitoring (QCM-D)

QCM-D is an acoustic technique that is based upon the use of a QCM sensor that contains a thin quartz crystal, which is piezoelectric in nature, and is sandwiched between two gold electrodes (**Figure 2.9A)**. The QCM crystal is mounted on a flow cell in a temperature controlled setting. The application of an electrical current in the flow cell causes mechanical stress to the crystal. Because the crystal is piezoelectric, when an alternating electrical current is applied across the electrodes, the crystal oscillates and a vibrational wave is generated that propagates through the crystal in a direction that is perpendicular to the surface. A standing, acoustic wave is generated when the oscillating crystal creates an acoustic wave that is two times the thickness of the crystal (**Figure 2.9B)**. At this point, the crystal is said to be oscillating at its resonant frequency. When an applied stress is introduced in the system, like a change in mass on the crystal or an adsorbate contacting the crystal surface, the resonant frequency of the oscillating crystal is changed. This change in frequency can be detected at sub-nanogram limits, making this technique very sensitive.[125-131]

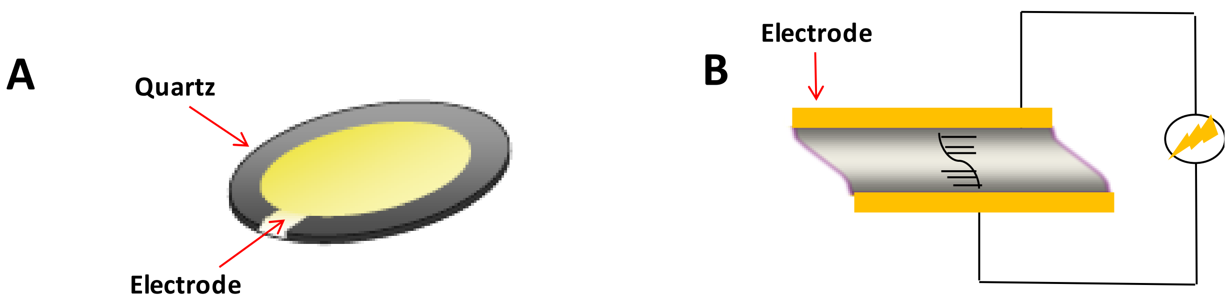

Figure 2.9. Schematic representation of (A) a QCM crystal with gold electrodes and (B) a QCM crystal oscillating under an alternating electrical current with a standing, acoustic wave propagating through the thickness of the crystal.

The basic theory behind the QCM technique is that there is a linear relationship between the change in frequency of the quartz crystal and the mass of the adsorbed rigid film. Sauerbrey developed this theory after looking at the adsorption of rigid films onto quartz crystals a vacuum.[132] Based off this study, it was reported that the decrease in resonant frequency translated to the increase in distance that the resonant wave travelled, which translated into the increase in thickness of the crystal. Therefore, the Sauerbrey equation was derived:[132]

$$\Gamma = \Delta\mathrm{m} = -\frac{C\Delta\mathrm{f}}{n}$$

where Δm is the mass per unit area, C is the crystal specific constant (0.177 $\mathrm{mg \cdot m^{-2} \cdot Hz^{-1}}$ or 17.7 $\mathrm{ng \cdot cm^{-2} \cdot Hz^{-1}}$ for a 5 MHz crystal), n is the overtone number (n = 1,3,5,7,9,11, and 13), and Δf is the change in frequency.

It is also possible to calculate the layer's effective thickness (d_{eff}) by estimating the adhering layer's effective density (ρ_{eff}):[125]

$$d_{eff} = \frac{\Delta m}{\rho_{eff}}$$

The Sauerbrey equation applies to thin films that are rigid and evenly distributed on the crystal surface. This relationship has been applied to studies involving adsorption of gas-phase species, like volatile organic compounds[133], environmental pollutants[134], and gas-phase chromatography detectors[135], metal surface oxidation, and gas desorption.[130] However, the Sauerbrey equation underestimates the adsorbed masses when the attached film is not rigid because a viscoelastic (soft) film cannot fully couple to the oscillatory motion of the QCM crystal.[125, 127-128, 130-131]

Therefore, a QCM equipped with dissipation monitoring (QCM-D) has been used more frequently when looking at viscoelastic films in a liquid environment because it measures both change in frequency and dissipation of the quartz crystal. Information about the rigidness/softness of the adsorbed film can be determined because a QCM-D measures the oscillation decay of the crystal after the electric current is switched off. The change in dissipation is defined as:[125, 131, 136]

$$\Delta D = \frac{E_{dissipated}}{2\pi E_{stored}}$$

where $E_{dissipated}$ is the energy dissipated by the viscous nature of the surrounding medium and E_{stored} is the energy stored in the crystal. When a ΔD is small, then the energy dissipates slowly indicating a rigid film. However, a soft film has a large ΔD compared to a rigid film because soft films interact with the liquid environment more, which generates more resistant force. Therefore, this creates a faster energy dissipation (**Figure 2.10).**[125, 131]

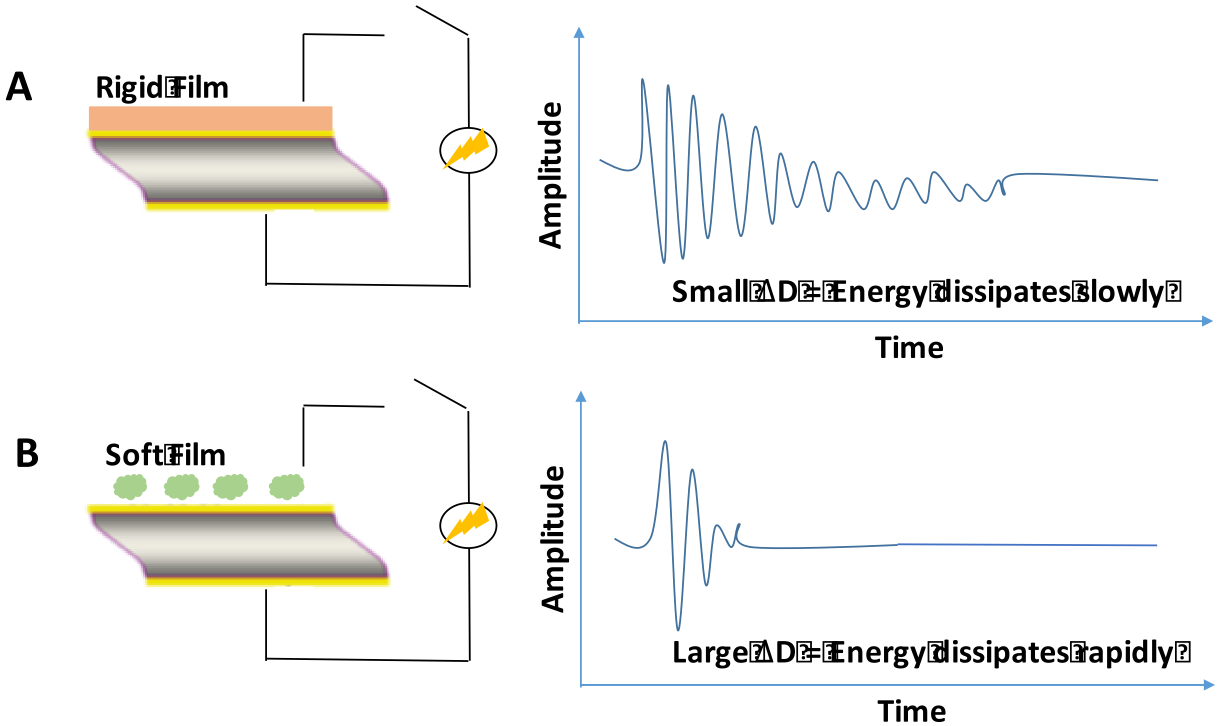

Figure 2.10. Schematic representation of a QCM crystal with gold electrodes (A) coated with a thin, rigid film where energy dissipates slowly and (B) coated with a viscoelastic (soft) film where energy dissipates rapidly after the electrical current is turned off.

When looking at viscoelastic films at the liquid / solid interface, a QCM-D can provide both qualitative and quantitative information. For qualitative information, the validity of the Sauerbrey relationship and structural changes to the surface can be checked. If the ΔD is less than 10^{-6}, then the adsorbed film may be considered rigid. However, if the ΔD is greater than 10^{-6} then the Sauerbrey equation may be invalid, so modeling may be required by using both Δf and ΔD to determine its mass and structural properties. For structural changes, a large ΔD and spreading of the overtones may indicate a soft, hydrated film because there are more interactions between the adsorbing film and the liquid environment.[125, 128, 131]

If the Sauerbrey equation is not applicable, modeling is necessary to determine the loss due to the shear motion of the film. The Voigt model is the most commonly used method for polymers that conserve their shape, but do not flow. In this model, the adsorbed viscoelastic film is treated as a no-slip layer between the elastic QCM crystal and semi-infinite viscous (Newtonian) liquid. Four parameters are used in the Voigt model to describe the viscoelastic film, as shown in **Figure 2.11**, which include density (ρ_f), viscosity (n_f), thickness (h_f), and elastic shear modulus (μ_f).[137] With these four parameters, the QCM-D data can be fit to obtain the thickness, elastic shear modulus, and viscosity values of the viscoelastic film.[125, 137]

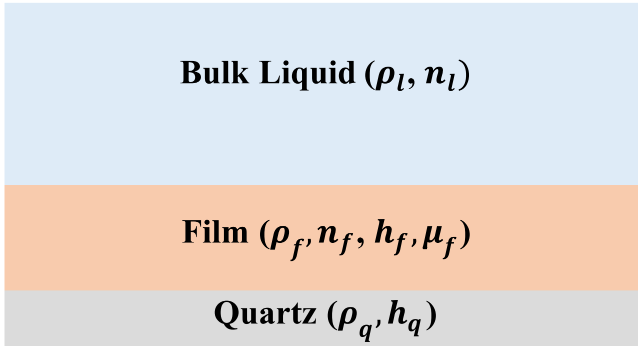

Figure 2.11. Schematic representation of the Voigt model parameters used in a QCM-D study. The viscoelastic film is in contact between a quartz crystal (represented by a density, ρ_q, and a thickness, h_q) and a semi-infinite Newtonian liquid (represented by a density, ρ_l, and a viscosity, n_l). Adapted from Liu et al.[138].

Because of its flexibility and precision, the QCM-D technique is now widely used to study interactions among proteins, DNA, lipids, cells, and other biomolecules. Some studies include looking at adsorption / desorption kinetics of cellulose derivatives onto gold and citrate-covered surfaces[139], adsorption behaviors of polyelectrolyte multilayers on SiO_2 surfaces[140], interactions between pectin and BSA surfaces[141], monitoring hydration changes in adhered mussel-adhesive proteins[142], and detecting *Salmonella typhimurium* for food safety interests.[110]

Surface Plasmon Resonance (SPR)

Surface plasmon resonance (SPR) is an optical technique that is widely used to obtain both quantitative information about adsorbed mass, kinetics, concentrations, or thermodynamics in biological systems and qualitative information about molecular interactions. This is achieved by measuring the change in resonant angle caused by refractive index changes associated with analyte composition changes near the interface.[143-145] SPR has become a versatile technique used in a variety of applications like drug screening[146], epitope mapping[147], reaction kinetics, stoichiometry[148], food safety analysis, and environmental monitoring.[149]

The Kretschmann configuration[150] is the most commonly used design in modern SPR instruments, consisting of a *p*-polarized light source, metal film, glass prism, and a photodetector (**Figure 2.12**). The metal film is placed at the interface of two dielectric media; medium 1 is the glass prism and medium 2 is air or the aqueous solution that is studied. The *p*-polarized light travels from the higher refractive index (medium 1) to the lower refractive index (medium 2), resulting in total internal reflection (TIR) which allows the light to travel back into the glass prism. Under TIR conditions, evanescent waves are formed in the lower refractive index medium (medium 2). These evanescent waves have the ability to penetrate through the metal film and excite the surface plasmon, an electromagnetic wave that propagates through metal / dielectric interfaces[151], which creates surface plasmon resonance. Once this occurs, the intensity of the reflected light decreases sharply, and the incident angle at which the minimum reflectivity is observed is called the SPR angle.

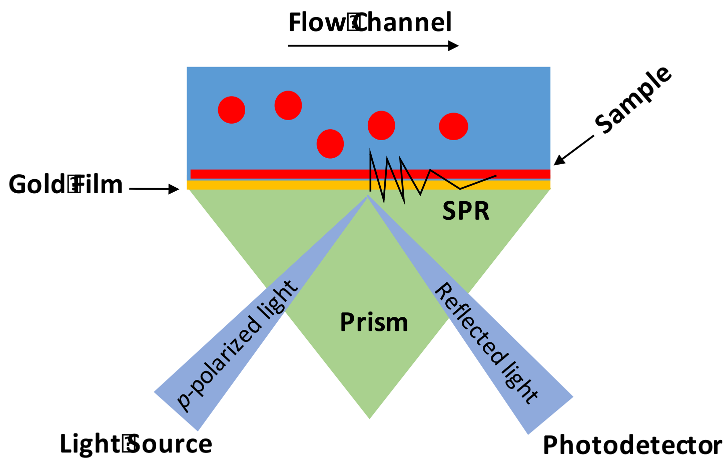

Figure 2.12. Schematic diagram of the Kretschmann configuration.

The SPR angle changes with changes in refractive indexes. Because the refractive index of the glass prism and metal film are fixed and do not change, the SPR angle changes when the refractive index of the aqueous solution at the interface changes. This is primarily caused by sample adsorption to the surface.[143-145, 152] Therefore, SPR instruments monitor the change in SPR angle as a function of time, which is further used to calculate the adsorbed mass (Γ_{SPR}). The total change in SPR angle ($\Delta\theta_{tot}$) relates to the changes in resonant angle that is caused by reversible adsorption ($\Delta\theta_{rev}$), irreversible adsorption ($\Delta\theta_{irr}$), and the bulk effect ($\Delta\theta_{bulk}$) (**Figure 2.13**). Using the change in resonant angle, adsorbed mass (Γ_{SPR}) can be determined with the equation of de Feijter *et al.*:[153]

$$\Gamma_{SPR} = \frac{L\,(n_f - n_s)}{\left({dn}/{dc}\right)} = \frac{\Delta\theta_a\,(n_f - n_s)}{\left({d\theta}/{dL}\right)\left({dn}/{dc}\right)}$$

where L is the thickness of the adsorbed layer, n_f is the refractive index of the film, n_s is the refractive index of the solvent, $\Delta\theta_a$ is the change in resonant angle caused by a change in refractive index of the aqueous solution, $d\theta/_{dL}$ is the change in the resonant angle with respect to layer thickness which can be calculated by Fresnel simulations[154-155], and $dn/_{dc}$ is the refractive index increment measured by differential refractometer. For a case in which the original solvent is returned into the system after adsorption, irreversible adsorption is measured and $\Delta\theta_a$ is the same as $\Delta\theta_{irr}$.

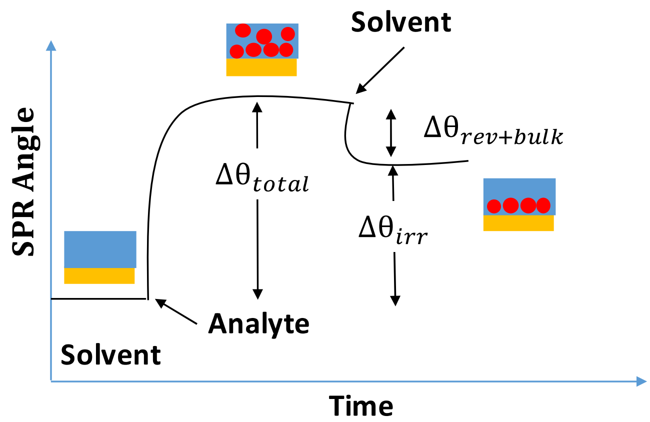

Figure 2.13. Schematic representation of adsorption profiles in SPR depicting both reversible and irreversible adsorption.

Coupling QCM-D and SPR Techniques

It is common to couple information from surface analysis techniques, like QCM-D and SPR, because there are limitations to using single technique measurements. Optical techniques have the advantage of directly measuring the amount of adsorbed mass on the sensor surface through changes in optics, but it is difficult to give the adsorbed mass kinetics if there are large conformational changes. On the other hand, acoustic techniques (QCM-D) provide information regarding conformational changes, but also takes into account the coupled liquid in the system, which can give misleading information about the true amount of adsorbed mass to the surface.[156] Therefore, studies have coupled these techniques in order to gain more information about the adsorbed material.[138, 157] Combining these two techniques have been shown successful in studies looking at the adsorption behavior of dianionic amino acid-based surfactants to various solid surfaces[158] and the adsorption and cross-linking of ethyl(hydroxyethyl) cellulose to hydrophilic and hydrophobic surfaces.[159] Previous studies that have looked at the interactions between cellulose ethers and BS at the oil-water interface and in the aqueous phase have used drop profile analysis tensiometer[11-12, 14] and micro-differential scanning calorimetry techniques.[11, 23]

However, to the best of our knowledge there are no studies that have utilized the coupling of QCM-D and SPR techniques with the purpose of studying the interactions between cellulose ethers and BS to control lipid digestion.

In vitro Digestion Models

In vitro digestion models are commonly used experimental models to study the behavior of foods in the GIT. Although, *in vivo* studies have the advantage of providing the most accurate results, they are more expensive, time consuming, difficult to undertake and often not justifiable due to ethical restrictions.[160-162] On the other hand, *in vitro* digestion models have the advantage of allowing for rapid screening of larger amounts of samples and/or conditions for *in vivo* trials and for studying the separate or combined effects of each stage of digestion (oral, gastric, and intestinal).[160] They can also be used as a pre-treatment for bioavailability assays and simulated colonic fermentation. Depending on the type of research that is performed, whether it being a screening application or confirmative study, static or dynamic *in vitro* digestion models can be employed to simulate different stages of digestion.

Static vs Dynamic Models

Static models are simple simulations of digestion which is mimicked in consecutive steps.[162] They are useful for screening and ranking of large amounts of samples within limited range of variation. At each step, fixed concentrations of enzymes, salts, digestive fluids are usually employed and incubated for a specific time and the pH is generally maintained at a fixed value using a pH-stat or buffer.[162-163] Static models have been used to study the digestibility of macronutrients (e.g. starch[164-165], lipids[12], and proteins[166]) and bioaccessibility of a great variety of micronutrients (e.g. polyphenols[167], carotenoids[168], and vitamins[169]). The advantage that dynamic models have over static models is that they simulate the continuous changes of physiochemical conditions throughout digestion, including pH variation, enzyme/salt concentration secretion, and peristaltic forces in the GIT and removal of digested products.[170] Different dynamic systems have been designed to confirm results obtained from static models and gain more insight in the changes occurring during digestion.[171-174] For example, a gastrointestinal model (TIM-1) has been developed that consists of compartments representing the stomach, duodenal, jejunal, and ileal parts of the GIT which simulates the gastric emptying rate, peristaltic movements, and gradual pH changes through the different compartments.[173] This model has been useful for gaining information about the bioaccessibility of folate from foods[175] and digestive stability of lipid-soluble nutrients from different food matrices.[176] A similar dynamic model to TIM-1 has also been developed (Tiny-TIM) that contains 2 compartments representing the stomach and small intestine, which has allowed for rapid screening to assess the bioaccessibility of phenolic acids in breads.[174] However, the majority of studies reported in the literature investigating food digestion are static models because dynamic models are more expensive, labor intensive, and time consuming.[170] Nonetheless, there has been much effort in developing a standardized digestion procedure for both static and dynamic models because there is diversity among the existing models, like the number and type of steps included in the digestion experiments (mouth, stomach, small intestine) and composition of digestive fluids (varying pH, enzyme/salt concentrations), which makes it difficult to compare results and infer findings.[161-162] As a result, an improved and amended version of a previously reported standardized protocol based on an international consensus developed by the European COST INFOGEST network has been recently developed. This can be used to assess the gastro-intestinal breakdown of complex foods or pure food components, by analyzing the digestion products of macronutrients (e.g. peptides/amino acids, fatty acids, and mono-/disaccharides), and evaluating the release of micronutrients from the food matrix.

A large number of research studies using static models include the pH-stat titration method to examine lipid digestion **(Table 2.2).** In these systems, digestion is simulated in different steps (either mouth, stomach, and/or intestinal phase) and samples are exposed to digestive fluids that can contain enzymes, like pancreatin, various salts, like NaCl and $CaCl_2$, and biosurfactants, like BS and phospholipids, to best mimic *in vivo* conditions. During lipolysis in the intestinal phase, a pH-stat titration is employed to determine the relative rate and extent of FFAs released from TGs after enzyme addition around a neutral pH.[161, 177] An alkali solution (typically NaOH) is added to neutralize the FFAs released in order to maintain the pH at the initial set value (pH 6.5-7.0).[177] Although this method does not provide information on the absolute value of FFA released[15] and the formation of monoglycerides or diglycerides[178], it is a simple, rapid and convenient tool to rapidly screen the impact of certain variables on lipid digestion and has been widely used in pharmaceutical and food research to study lipolysis occurring in the duodenal compartment and to monitor the reaction kinetics.

Nonetheless, a limited number of static *in vitro* digestion models using the pH-stat method have been employed to evaluate the effect of both cellulose ethers, especially the effect of HPC, and BS type on the rate and extent of lipid digestion.[10, 12, 21-22] Therefore, the *in vitro* digestion study explored in this thesis will provide us a better fundamental understanding of the mechanisms by which HPC adsorbed at the oil–water interface of emulsions and/or present in the bulk influence lipolysis under intestinal conditions. It will also provide further insight on the role that different BS structures may play at different stages in the lipid digestion process. These findings may be incorporated into a dynamic *in vitro* model or *in vivo* study in the future.

Table 2.5. Overview of some in vitro digestion studies that have employed the pH-stat method to analysis FFA release from o/w emulsion based systems. Adapted from McClements & Li, 2010.

Test Samples	Variable tested	Characterization	Digestion step	Reference
O = olive oil E = galactolipids	Emulsifier type	ζ-potential, Particle size, FFA, Interfacial tension	**Intestinal**: pH 7, pancreatic lipase, BS	Hu *et al.*, 2010b[179]
O = SCT, LCT E = Lecithin	Tea extract	Particle size, FFA	**Stomach:** pH 5.4, gastric juice **Intestinal:** pH 7.5, pancreatin, bile	Juhuel, 2010[180]
O = SCT, MCT, LCT E = monoglyceride,	Oil [Lipase]	FFA, Microstructure	**Intestinal:** pH 6.5, pancreatin	Brogard, 2007[181]
O = olive oil E = Pluronic®	Emulsifier Particle size	Microscopy, ζ-potential, Particle size, FFA, Interfacial tension, Appearance	**Intestinal:** pH 7, BS, pancreatic lipase	Torcello-Gomez *et al.*, 2011[13]
O = olive oil E = β-lactoglobulin, lactoferrin	Interfacial composition	Microscopy, ζ-potential, Particle size, FFA	**Intestinal:** pH 7, BS, pancreatic lipase	Schmelz *et al.*, 2011[182]
O = corn oil E = caseinate, lactoferrin	Emulsifier Multilayer	ζ-potential, Particle size, FFA	**Intestinal:** pH 7, pancreatic lipase, BS	Lesmes *et al.*, 2010[103]
O = sunflower oil E = HPMC	Molecular weight of emulsifier	ζ-potential, Particle size, FFA	**Stomach:** pH 2.5, gastric juice, **Intestinal:** pH 7, bile extract, pancreatic lipase, protease	Pizones Ruiz-Henestrosa *et al.*, 2017[21]
O = olive oil E = HPMC, Tween 20	Molecular weight and methoxyl content of emulsifier	ζ-potential, Particle size, FFA, Microscopy	**Intestinal:** pH 7, bile extract, pancreatic lipase	Torcello-Gomez *et al.*, 2016[12]
O = sunflower oil E = HHPMC, HPMC, MC, and HMC	Emulsifier	FFA, Texture, Microscopy	**Stomach:** pH 2.0, gastric juice, pepsin **Intestinal:** pH 7.0, bile extract, pancreatin, pancreatic lipase	Borreani *et al.*, 2017[22]
O = corn oil E = Pectin, chitosan, MC	Emulsifier	Appearance, Microscopy, FFA, Particle size, ζ-potential, Viscosity	**Mouth:** pH 6.8, saliva fluid **Stomach:** pH 2.5, gastric fluid, pepsin **Intestinal:** pH 7.0, pancreatic lipase, bile extract	Espinal-Ruiz *et al.*, 2014[25]

Abbreviations: O = oil ; E = emulsifier ; SCT = short chain triglyceride; LCT = long chain triglyceride; MCT = medium chain triglyceride; HPMC = hydroxypropylmethylcellulose; HHPMC = high hydroxypropylmethylcellulose; MC = methylcellulose; HMC = high methylcellulos

Chapter 3: Materials and Methods

3.1 Materials

The cellulose ethers (CEs) used in these experiments were powdered hydroxypropyl cellulose (HPC, M_w ~100 kg/mol , 20 mesh particle size (99% through, viscosity of 5% (w/w) in H_2O, η = 75-150 cP, DS(HP) = 2.2, MS(HP) = 4.4), which was purchased from Sigma Aldrich (St. Louis, MO), and 5-carboxypentyl hydroxypropyl cellulose (HPC-P), which was synthesized as previously reported in Dong *et al.* 2016 **(Figure 3.1).**[183] See **Appendix A** for full details. **Table 3.1** provides a summary of the polymer properties.

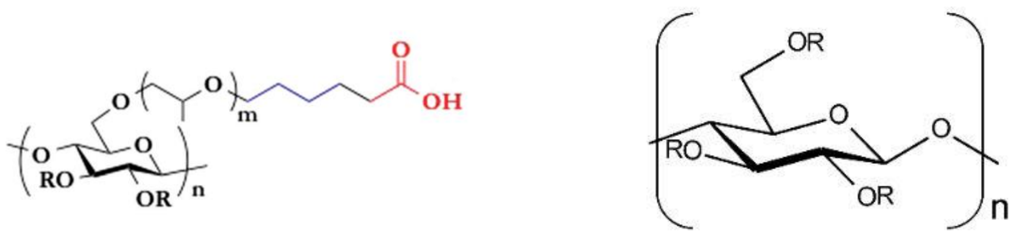

R = -H, -(CH_2CHCH_3O)$_m$ **R = -H, -($CH_2CH(OH)CH_3$)**

HPC-P **HPC**

Figure 3.1. Structures of 5-carboxypentyl hydroxypropyl cellulose (HPC-P) and hydroxypropyl cellulose (HPC). The HPC-P structure is not meant to convey regioselective substitution; depictions of substituent location are merely for convenience and clarity of depiction.

Table 3.1. Summary of polymer properties. Abbreviations: hydroxypropyl (HP), DS (degree of substitution), MS (molar substitution), M_w (molecular weight), M_n (average molecular weight), DP (degree of polymerization)

Parameter	Polymer	
	Commercial HPC	HPC-Pen106-AA-H
DS (COOH)	-	1.06
DS (HP)	2.2	2.2
MS (HP)	4.4	4.4
M_w (g/mol)	206,100	70,400
M_n (g/mol)	112,000	69,000
DP	268	129

The bile salts (BSs) used in these experiments were sodium taurocholate (NaTC, ≥97.0% purity) and sodium taurodeoxycholate (NaTDC, ≥95.0% purity) from Sigma-Aldrich (St. Louis, MO). They are negatively charged at a pH 7 and their molecular weights are 537.68 and 521.69 g/mol, respectively **(Figure 3.2)**.

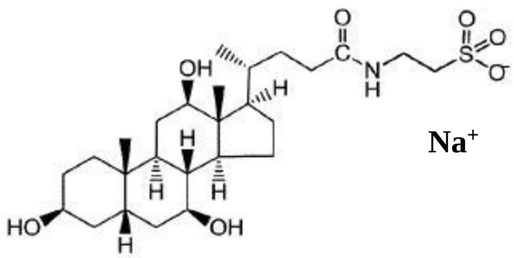

NaTC

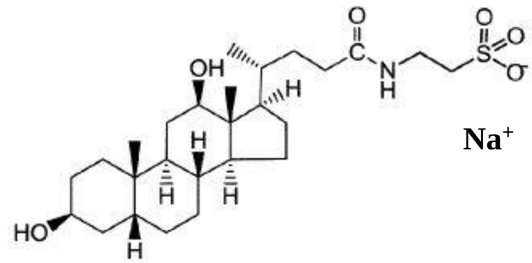

NaTDC

Figure 3.2. Structures of sodium taurocholate (NaTC) and sodium taurodeoxycholate (NaTDC)

The buffer used in all solutions was 2 mM Bis-Tris (Sigma-Aldrich, ≥98.0% purity) prepared with ultrapure water and adjusted to pH 7 with 1 M HCl (Thermo Fisher Scientific).

Pancreatin from porcine pancreas (8 x USP specifications, P7545) was purchased from Sigma-Aldrich (St. Louis, MO). Calcium chloride dihydrate ($CaCl_2$), sodium chloride (NaCl), and Tween® 20 were purchased from Thermo Fisher Scientific (Waltham, MA).

Olive oil (oleic acid**)** was chosen for the *in vitro* digestion experiments because it is mainly constituted by triglycerides (>98%).[184] It has been shown that emulsions containing different types of oil, including olive, sunflower, and canola, were rapidly and fully digested under simulated gastrointestinal (GIT) conditions, regardless of their initial free fatty acid composition.[185] However, the rate and extent of lipid digestion of emulsions containing krill oil was lower than the other emulsions, which may have been due to appreciable amounts of phospholipids and pre-digested triglycerides.[185] The olive oil (Flippo Berio) was purchased from a local grocery store (Kroger) and was purified with activated magnesium silicate (Florisil®, Sigma-Aldrich, <200 mesh), in order to eliminate impurities. A proportion of 2:1 w/w (oil:Florisil) was mixed using a disperser homogenizer (VirTishear, VirTis) at speed 50, while being simultaneously shaken on a shaker (Innova® 2000, New Brunswick Scientific™) at 80 rpm for 3h. The mixture was centrifuged (Eppendorf™ 5804R) at 1340 x g (rcf) for 30 min and the supernatant was filtered under vacuum filtration to remove any remaining resin. The purified olive oil was transferred to round narrow-mouth amber bottles (Thermo Fisher Scientific) and stored under nitrogen in the dark to prevent lipid oxidation.

3.2 Preparation of Polymer and Bile Salts solutions

Commercial HPC stock solution (1.5% (w/v)) was prepared as follows. Approximately two-thirds of the final volume of Bis-Tris buffer was heated to ~80°C and the HPC powder was added carefully under stirring. After 5 minutes, the temperature was lowered to 22°C and continued to stir at room temperature for at least 2 hours. The remaining volume of Bis-Tris buffer was added to the solution to complete the solubilization. These stock solutions were then stored at 4°C overnight, in order to achieve maximum hydration before use and without stirring to eliminate air bubbles. HPC-P stock solution (3.75% (w/v)) was prepared as follows. Approximately half of the final volume of DMSO was heated to ~60°C and the HPC-P sample was added carefully under stirring and was continuously stirred for at least 4 hours. Then, the sample was sonicated (FS20 Ultrasonic Bath, Thermo Fisher Scientific) for at least 30 minutes or until fully dissolved. The sample was stored under room temperature until use.

NaTC and NaTDC stock solutions (30 mM) were prepared by dissolving the powder in the required amount of Bis-Tris buffer at room temperature under stirring for at least 1 hour. These solutions were stored in 4°C until use.

For the sequential experiments, CE stock solutions were diluted with Bis-Tris buffer to achieve a final concentration of 0.1% (w/v); this concentration was chosen to allow for the formation a continuous, saturated CE layer on the QCM-D and SPR sensor surfaces.[11, 139] For the HPC-P sample, the final concentration of DMSO in the solution was 5% (v/v). In order to control for presence of DMSO, the buffer and BS solutions used for the experiments with HPC-P were also prepared with 5% DMSO. BS stock solutions were diluted to obtain concentrations of 2, 5, and 10 mM. These are BS concentrations above and below the critical micelle concentration (CMC) of NaTC (3-18 mM[89, 186]) and NaTDC (2-3 mM[89, 186]) in order to test the effect of BS micelles and monomers. After preparation, these solutions were ready for the Quartz Crystal Microbalance with Dissipation Monitoring (QCM-D) and Surface Plasmon Resonance (SPR) experiments. For the simultaneous experiments, mixed CE-BS solutions were prepared at room temperature from stock solutions. The final concentration of CE was fixed at 0.1% (w/v), whereas the BS concentration was either 2, 5, or 10 mM. After preparation, these mixtures were allowed to sit at room temperature for 30 minutes before the QCM-D experiments. For the lipolysis experiments, HPC stock solutions were diluted with Bis-Tris buffer to achieve a final concentration of 1.0% (w/v).

3.3 Quartz Crystal Microbalance with Dissipation Monitoring (QCM-D)

Measurements were performed using a QCM-D Multi-Channel E4 system (Q-sense AB, Sweden). The QCM-D sensors used were gold, consisting of quartz crystal covered with 5 nm of chromium and 100 nm of gold (QSX 301, Q-Sense), and hydrophobic polystyrene (PS) sensors, consisting of 40 nm of PS (QSX 305, Q-Sense). They were placed into flow cells and mounted on the E4 system prior to the experiments. Sensors were then excited to oscillate by applying an alternating electrical voltage across the surface at their fundamental resonant frequency (4.95 MHz) and at the 3^{rd}-11^{th} odd overtone (15-55 MHz). Changes in frequency (Δf) and dissipation (ΔD) due to CE and BS adsorption and desorption from the sensors were monitored simultaneously. A typical representative profile for changes in frequency (Δf) and dissipation (ΔD) to obtain the total and irreversible adsorption values measured at the fifth overtone for this study is shown in **Figure 3.3.** For example, the system was initially equilibrated with buffer for at least 10-min. Then a solution containing adsorbate was introduced into the flow cell and material, coupled with water, adsorbed onto the sensor surface, causing a decrease in the measured resonant frequency (total adsorption). Then, buffer was introduced into the flow cell to wash away reversibly bound mass and coupled water, which gave rise to an increase in frequency and irreversible adsorption values. Dissipation increased upon adsorption, based on its elastic or viscoelastic properties, and decreased during the buffer rinse.

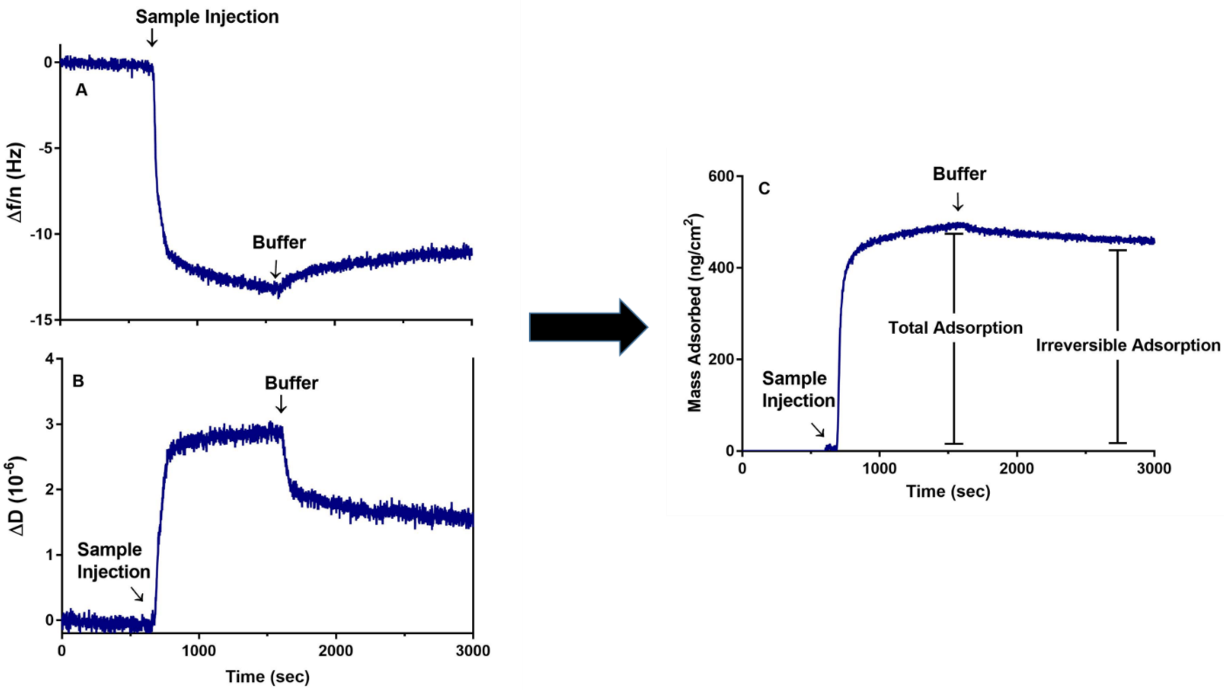

Figure 3.3. Representative QCM-D data for the changes in (A) frequency (Δf/n) and (B) dissipation (ΔD) measured at the 5th overtone where the system is initially buffer, followed by adsorption of a solution, and a subsequent buffer rinse. (C) Output data from the QCM-D measurement depicting reversible and irreversible adsorbed mass values obtained from the Sauerbrey model.

<u>*Sensor Preparation*</u>

Gold sensors were cleaned by boiling them in a 5:1:1 solution of ultrapure water:ammonium hydroxide:hydrogen peroxide, respectively, for 45 minutes. Sensors were rinsed exhaustively with ultrapure water and dried with nitrogen gas prior to being used. PS sensors were cleaned by immersing them in a 2% (w/v) Hellmanex III^{TM} solution, that was prepared in ultrapure water, for 1 hour. The sensors were then exhaustively rinsed and kept in ultrapure water for at least 2 hours. Then, they were rinsed with 99% ethanol and dried with nitrogen gas prior to being used.

All CE and BS solutions were degassed for 10 minutes prior to QCM-D experiments in order to minimize bubbles in the solutions. First, Bis-Tris buffer was introduced into the flow cells at a flow rate of 0.25 mL/min with a cartridge pump (ISMATEC-ISM935) until the system stabilized. Next, sequential and simultaneous adsorption experiments were performed.

<u>*Sequential Adsorption of Cellulose Ethers and Bile Salts*</u>

Once the system was stabilized, 0.1% (w/v) CE solutions were flowed over the gold or PS sensors at a flow rate of 0.25 mL/min for 15 minutes until the system reached a new constant value. Once the initial formation of a saturated surface layer of CE was ensured, Bis-Tris buffer was flowed through the system for 25 minutes to examine the stability of the adsorbed CE layers. Subsequent injections of one concentration (2, 5, or 10 mM) of BS (NaTC or NaTDC) were made and adsorption over the CE film was recorded for 10 minutes. BS injections were followed by a buffer rinse step for 10 minutes. Total and irreversible adsorption values for 2, 5, and 10 mM BS were obtained after 10 min adsorption and post buffer rinse. For commercial HPC, experiments were performed in triplicate for both BS (NaTC and NaTDC) at 2,5, and 10 mM on gold and PS sensors. For HPC-P, experiments were performed in duplicate for both 10 mM BS (NaTC and NaTDC) on PS sensors.

Simultaneous Adsorption of Cellulose Ethers and Bile Salts

Simultaneous adsorption experiments were performed only on PS sensors. Once the system was stabilized, mixed CE-BS solutions containing a fixed concentration of CE (0.1% (w/v)) and BS concentrations ranging from 2-10 mM were flowed onto the PS sensors at a flow rate of 0.25 mL/min for 15 minutes. Then, Bis-Tris buffer was flowed into the system for 25 minutes to examine the stability of the adsorbed film on the PS sensors. Total and irreversible adsorption values for 0.1% CE + 2, 5, and 10 mM BS were obtained after 10 min adsorption and post buffer rinse. For commercial HPC, experiments were performed in triplicate for both BSs (NaTC and NaTDC) at 2, 5, and 10 mM. For HPC-P, experiments were performed in duplicate for both 10 mM BS (NaTC and NaTDC).

Analysis of QCM-D Data

Changes in frequency ($\Delta f_n/n$) correspond to changes in the oscillation frequency of the sensor divided by the overtone. These changes were related to the changes in the hydrated mass adsorbing on the sensor via the Sauerbrey and Voigt model. If the adsorbed layer was evenly distributed, fully elastic, and rigidly attached, the Sauerbrey equation was used to calculate the adsorbed mass in the software package QSense Dfind (version 1.1):[132]

$$\Gamma_{QCM-D} = -\frac{C\Delta f}{n}$$

where Γ_{QCM-D} is the adsorbed mass per unit area ($ng\cdot cm^{-2}$), C is the crystal specific constant ($17.7\ ng\cdot cm^{-2}\cdot Hz^{-1}$), n is the overtone number (n = 5 for this work) and Δf is the change in frequency (Hz).

Changes in dissipation (or dampening) are related to the structural properties of the adsorbed layer. The QCM-D E4 system stops the electrical voltage and allows the sensor to freely oscillate until a standstill, while measuring the decay of the resonating sensor. The change in dissipation is:[136]

$$\Delta D = \frac{E_{dissipated}}{2\pi E_{stored}}$$

where $E_{dissipated}$ is the energy dissipated by the viscous nature of the surrounding medium and E_{stored} is the energy stored in the sensor after a single oscillation. If the ΔD is greater than 10^{-6} and if the scaled frequencies (Δf/n) do not overlap, use of the Sauerbrey equation underestimates adsorbed mass/thickness, so adsorption curves for these viscoelastic layers were fit with a Voigt-based viscoelastic model.[137] The adsorbed layer was treated as a viscoelastic layer between the quartz crystal and a semi-infinite Newtonian liquid layer. The quartz crystal was assumed to be purely elastic (thickness (h_f) = 3 x 10^{-4} m and density (ρ_f) = 2650 g·L^{-1}) and the surrounding buffer solution was assumed to be purely viscous (density (ρ_f) = 1000 g·L^{-1} and viscosity (n_f) = 1.00 mPa·s^{-1}). The adsorption curves for multiple overtones (n = 5, 7, 9 for this work) were used for estimates of thickness, elastic shear modulus, and viscosity of the adsorbed layer in the software package QSense Dfind (version 1.1). All results were reported as average values with standard errors. Data were graphed and statistically analyzed using Prism v. 7.04 (GraphPad, la Jolla, CA). Significant differences in total adsorbed mass (ng/cm^2) and mass desorbed (%) in relation to BS concentration for each CE were determined by one-way ANOVA and Tukey post hoc analysis for the sequential and simultaneous adsorption experiments. Significant differences in adsorbed mass and thickness in relation to HPC and HPC-P layers were determined by two sample t-test at the two different time points. Level of significance was set at $p<0.05$.

3.4 Surface Plasmon Resonance (SPR)

Measurements were performed on a SPR SR7000 system (Reichert Inc). Gold-coated SPR sensor slides, consisting of a glass slide covered with 2 nm of chromium and 48 nm of gold (Reichert Inc), were used for the experiments. The glass sides were soda-lime float glass (refractive index = 1.523). A drop of immersion oil was first placed on the prism. This oil matched the refractive index of the prism (n_D= 1.5150). The sensors were placed on the prism and a Viton gasket (DuPont Dow Elastomers, LLC) was mounted on top of the sensor slide. Changes in resonant angle ($\Delta\theta_{sp}$) due to CE and BS adsorption and desorption from the sensor were directly detected by the SPR sensor. A typical representative profile of SPR data is depicted in **Figure 3.4** which shows the total change in SPR angle ($\Delta\theta_{tot}$) corresponed to the change in resonance angle caused by reversible adsorption ($\Delta\theta_{rev}$), irreversible adsorption ($\Delta\theta_{irr}$), and the bulk effect ($\Delta\theta_{bulk}$).

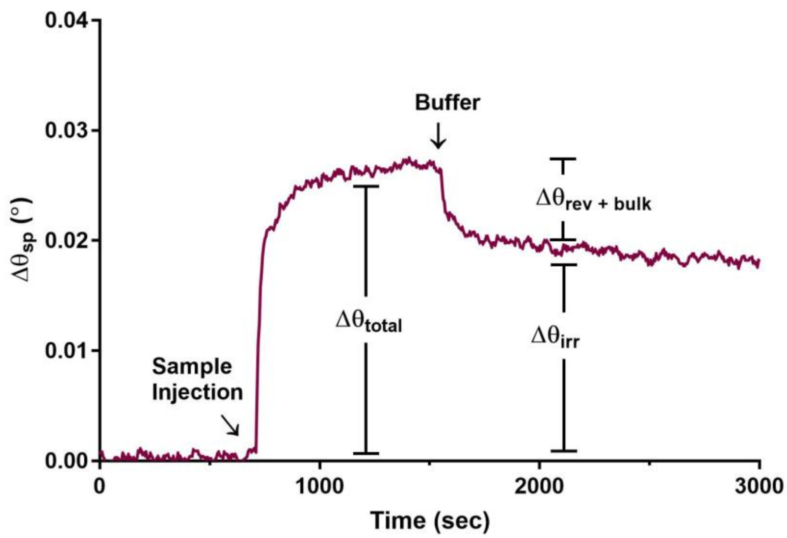

Figure 3.4. Representative SPR data depicting the changes in resonant angle during total, reversible and irreversible adsorption.

Sensor Preparation

Sensors were cleaned by boiling them in a 5:1:1 solution of ultrapure water:ammonium hydroxide:hydrogen peroxide, respectively, for 45 minutes. They were rinsed exhaustively with ultrapure water and dried with nitrogen gas prior to being used.

Sequential Adsorption of Cellulose Ethers and Bile Salts

All solutions were degassed for at least 10 minutes prior to flowing in order to reduce the introduction of air bubbles into the system. Then, Bis-Tris buffer was introduced into the system at flow rate of 0.25 mL/min via Teflon tubing connected to a cartridge pump (Masterflex). This cartridge pump contained a switch valve that allowed switching between samples. After the system stabilized, sequential adsorption experiments were performed as described in the **Chapter 3.3.** For commercial HPC, experiments were performed in triplicate for both BS (NaTC and NaTDC) at 2,5, and 10 mM on gold sensors. For HPC-P, experiments were performed in duplicate for both 10 mM BS (NaTC and NaTDC) on gold sensors.

Analysis of SPR data

The total change in SPR angle ($\Delta\theta_{tot}$) corresponded to the change in resonance angle caused by reversible adsorption ($\Delta\theta_{rev}$), irreversible adsorption ($\Delta\theta_{irr}$), and the bulk effect ($\Delta\theta_{bulk}$). The different changes in resonant angles ($\Delta\theta_{sp}$) were monitored as a function of time and were used to calculate the adsorbed amount with the equation of de Feijter *et al:*[153]

$$\Gamma_{SPR} = \frac{\Delta\theta_a\,(n_f - n_s)}{\left(\frac{d\theta}{dL}\right)\left(\frac{dn}{dc}\right)}$$

$$\Delta\theta_a = \Delta\theta_{sp} - c\left(\frac{d\theta_{sp}}{dc}\right) = \Delta\theta_{sp} - c\left(\frac{d\theta_{sp}}{dn}\frac{dn}{dc}\right)$$

where $\Delta\theta_a$ is the corrected resonance angle change by subtracting the contribution of bulk refractive index changes in the dielectric medium from the observed $\Delta\theta_{sp}$. c is the bulk concentration of the CE or BS solution. $d\theta_{sp}/dn$ is an instrument specific constant obtained via the calibration of the instrument with ethylene glycol standards. Γ_{SPR} was the adsorbed mass per unit area ($ng{\cdot}cm^{-2}$), n_f was the refractive index of the film, n_s was the refractive index of buffer, $d\theta/dL$ was the change in resonant angle with respect to adsorbed layer thickness changes as model by Fresnel equations, and dn/dc was the refractive index increment of the sample solution. Values for each parameter used in the de Feijter equation are summarized in **Table 3.2.** For the data used in this thesis, reversible CE and BS adsorbed mass values were obtained from $\Delta\theta_{tot}$, where the corrected resonance angle change ($\Delta\theta_a$) was calculated to subtract the contribution of the bulk refractive index changes. Irreversible adsorption values for CEs and BSs were obtained from $\Delta\theta_{irr}$, which corresponds to the difference between the initial θ_{sp} when the solution was injected (after baseline was achieved) and the final θ_{sp} post buffer rinse. All results were reported as average values with standard error. Statistical analysis of the sequential adsorption experiments was performed as described in **Chapter 3.3.**

Table 3.2: Parameters used in the de Feijter et al. equation to convert SPR data into adsorbed masses.

Parameter	Value
$d\theta_{sp}/dn$	61.5 (deg)
c	1 mg/mL (HPC & HPC-P); 2, 5, and 10 mM BS
n_f	1.56
n_s	1.33 (buffer)
$d\theta/dL$	4.3 x 10^{-3} deg·$Å^{-1}$ (Au)[187] and 4.3 x 10^{-3} deg·$Å^{-1}$ (cellulose)[187]
dn/dc	Determined by differential refractometer

Refractive Index Increment Measurements

The refractive index increment (dn/dc) of the CE and BS solutions were determined with a Wyatt Optilab rEX differential refractometer. The experiments were carried out at 22°C with a λ = 658 nm. Samples were flowed in at a flow rate = 0.25 mL/min using a syringe pump. For commercial HPC and HPC-P, dn/dc values were evaluated over a concentration range of 0 to 2.0 mg/mL and for BS solutions, dn/dc values were evaluated over a concentration range of 0 to 10 mM. The dn/dc values are summarized in **Table 3.3** and were determined using the Wyatt Astra V software package. All results were performed twice and were reported as average values with standard deviations.

Table 3.3: Values of dn/dc for solutions used in the SPR experiments

Sample	dn/dc value (mL·g^{-1})
HPC	0.131 ± 0.002
HPC-P	1.723 ± 0.362
NaTC	0.160 ± 0.001
NaTDC	0.170 ± 0.002

3.5 *In vitro* Lipid Digestion

Emulsion Preparation

Emulsion premixes containing 1.0% (w/v) commercial HPC, Tween 20, or BS (NaTC or NaTDC) and 20% (w/w) olive oil were vortexed for 30 seconds before being treated with an ultrasonic processer (Model 505, 500 W, 20 kHz, Fisher Scientific Inc., Waltham, MA) equipped with a 3.0 mm diameter ultrasound probe at 30% amplitude. While submerged in an ice bath, a series of ultrasonic pulses of 10 seconds with 10 second rest periods were performed to limit the temperature increase. The ultrasonic treatment was performed for a total of 10 minutes (5 minutes of pulsing and 5 minutes of rest periods). The emulsions were then left out for one hour to reach room temperature before carrying out any further treatment and/or analysis.

In vitro Digestion Model

Static *in vitro* digestions simulating a gastric-conditioning and intestinal step were carried out using a pH-stat automatic titration double unit equipped with two pH meters and two Dosino 800 dosing units (Metrohm Instruments)**.** Before beginning each experiment, pH meters were calibrated with 3 buffer solutions (pH 4, 7, and 9 (Metrohm)) to ensure a correlation of coefficient at least 98%. *In vitro* digestions began with a gastric conditioning step containing a 1.5 mL of freshly prepared emulsion, 2 mM Bis-Tris buffer, and 2.25 mL of 3M NaCl solution in a clean vessel. Gastric enzymes were not used since the emulsions did not contain any proteins. Once the mixture maintained a constant temperature of 37°C, the pH was adjusted manually to 2.5 with 1M HCl. The pH was stabilized for 10 minutes and adjusted back to 2.5 if necessary. Then, the mixture was stirred for 1 h at 37°C and the pH was recorded during this time. After 1h, the mixture was adjusted automatically to pH 7.0 with 0.1M NaOH. Next, 1.35 mL of 1M $CaCl_2$ followed by 15 mL of 30 mM BS solution was added and the mixture was adjusted back to pH 7 if necessary. Freshly prepared pancreatin solution (5.25 mL of 150 mg/mL; 8 x USP) was added and the mixture was stirred at 37°C for 2h. During this time, appropriate amounts of 0.1M NaOH were dispensed to neutralize the free fatty acids (FFAs) produced by lipid digestion and maintain the pH at a constant value of 7.0. The final concentration of NaCl, $CaCl_2$, BS, and pancreatin were 150 mM, 3 mM, 10 mM, and 17.5 mg/mL, respectively, which mimics the conditions found in the gastrointestinal tract under fed state conditions.[177, 188-189]

In order to obtain the most accurate amount of % FFAs released, a back titration was performed by increasing the pH to 9.0 with 0.1M NaOH after the intestinal phase. This step was performed because there was a risk of incomplete ionization of FFAs at a neutral pH environment due to the higher pK_a value of oleic acid (apparent pK_a ~7.45-7.78 at 37°C[190]). Therefore, there was a possibility of underestimating the % FFAs released during the intestinal phase.[191]

Control experiments were performed without the addition of 1) emulsion or 2) pancreatin/BS to correct for the amount of NaOH solution that was needed to neutralize the FFAs released as a consequence of the emulsion or any impurities in the pancreatin extract. Bis-Tris buffer was added instead in order to keep the same volume of final digestion mixture. Control experiments were performed for every emulsion that was prepared and the amount of NaOH that was dispensed during these experiments was subtracted out from the tested experiments.

The concentration of FFAs released during lipolysis and the back titration were calculated from the volume of NaOH consumed during lipolysis. The percentage of FFAs released was calculated from the number of moles required to neutralize the FFAs divided by the number of moles of FFAs that could be produced from the triglyceride (TG) assuming all were digested. It is assumed that one TG initially releases two FAs and one 2-monoglyceride (2-MG).[188] However, it has been reported that the 2-MG isomerizes to 1/3-monoglyceride and subsequently gets lipolysed to release a third FA and glycerol.[188, 192-193] Therefore, 3 FFA molecules are assumed to be produced by 1 TG. The following equation was used to calculate the percentage of FFAs released during lipolysis:

$$\%\ \text{FFA} = 100\ \text{x} \left(\frac{V_{NaOH} \times m_{NaOH} \times M_{Lipid}}{w_{Lipid} \times 3}\right)$$

where V_{NaOH} is the volume of NaOH required to neutralize the FFAs produced (mL), m_{NaOH} is the molarity of the NaOH used (0.1M), M_{Lipid} is the molecular weight of the oil (assumed to be 800 g/mol[13]) and w_{Lipid} is the total weight of oil initially present in the vessel.

The following mathematical model was used to determine the percentage of total FFAs released (Φ) as a function of time (*t*):[194]

$$\Phi = \phi_{max}\left(1 - \left(1 + \frac{3kMt}{3d_0\rho_0}\right)^{-2}\right)$$

where k is the μmoles of FFA released per unit droplet surface per unit time (rate of digestion), ϕ_{max} is the maximum percentage of the total FFA present that is released at the end of the reaction (extent of digestion), d_0 is the initial droplet diameter, ρ_0 is the oil droplet density (910 kg/m^3 for olive oil[13]), and M is the molar mass of the oil (0.8 kg/mol for olive oil[13]).

Particle Size Distribution Measurements

The particle sizes of the emulsions were determined using a dynamic light scattering instrument (Zetasizer Nano ZS, Malvern Panalytical) at room temperature. The emulsions were diluted at a 1:1000 proportion with 2 mM Bis-Tris buffer solution before each measurement to avoid multiple scattering effects. In order to determine the particle size distributions, the refractive indices of the oil (olive oil) and aqueous phase used in the calculations were 1.47 and 1.33, respectively. Particle size measurements were taken after emulsion preparation and after the stimulated intestinal step. Each measurement was calculated from the average of 10 readings made for the sample and these experiments were performed in triplicates.

Analysis of Lipolysis Data

Results are reported as the average and standard deviation of duplicate measurements made on at least two freshly prepared emulsion samples. Data were graph and statistically analyzed in Prism v. 7.04 (GraphPad, la Jolla, CA). Significant differences in the rate and extent of lipolysis in relation to emulsifier type for each BS was determined by a one-way ANOVA and Tukey post hoc analysis. Level of significance was set at $p<0.05$.

Chapter 4: Results and Discussion

The interactions between cellulose ethers (CEs) and bile salts (BSs) at solid surfaces were investigated by means of sequential and simultaneous adsorption using complementary real-time surface analysis techniques, quartz crystal microbalance with dissipation monitoring (QCM-D) and surface plasmon resonance (SPR). Together QCM-D and SPR yield quantitative information on changes in the surface layer structure in terms of (hydrated and "dry") adsorbed mass, thickness, and viscoelasticity of the cellulose film as the adsorption of BS progresses. Previous studies have shown this combination of surface analysis techniques successfully characterized interactions between biological molecules.[195-199] Two CEs with potential to control lipid digestion were employed in this study. Hydroxypropyl cellulose (HPC) is a commercial non-ionic cellulose ether, in which the hydroxypropyl group is the sole substituent, while the novel HPC-derivative (HPC Pen-AA-H) that contains a moderate balance of hydrophobic (5-carboxypentyl) and hydrophilic (hydroxypropyl) substituent groups, has been developed by the Edgar lab.[183] At a physiological pH, the carboxylic acid groups in the novel HPC derivative are largely deprotonated, since it is above their pK_a (~5), resulting in a net negative charge.[200] Two common BSs found in the human body, sodium taurocholate (NaTC) and sodium taurodeoxycholate NaTDC, (that differ only on the cholate conjugation group) were selected to study the effect of the degree of hydrophobicity in the BS. A range of BS concentrations above and below the critical micelle concentration (CMC) was used to test the effect of BS micelles and monomers.

4.1 Adsorption of Cellulose Ethers onto Sensor Surfaces

The adsorption/desorption behavior of the CEs onto QCM-D & SPR sensor surfaces was first evaluated. There are a few investigations of adsorption of non-ionic CEs onto solid surfaces using QCM-D.[139, 201-202] However, this is the first study characterizing the adsorption/desorption behavior of commercial HPC and novel HPC-P at solid surfaces using a combination of QCM-D and SPR techniques. Preliminary experiments were conducted to determine the ideal conditions for CE adsorption onto the solid surfaces. The adsorption of macromolecules onto interfaces is a dynamic process that involves 1) the diffusion of the polymer from the bulk solution to the interface as a consequence of a concentration gradient and 2) adsorption onto the interface.[101, 203] The first is a mass transfer process controlled by diffusion whereas the second is a pure adsorption/desorption process. As the interface becomes saturated with polymer molecules, the net transfer of mass decreases approaching equilibrium. The rate and extent of these processes can depend upon certain factors, like type, viscosity, and concentration of polymer[11, 204-205] as well as the type of interface onto which polymer is adsorbing.[139, 201] For example, it has shown that several hours (12-24 h) are needed for equilibrium for low concentrations of CE (10^{-4} to $2x10^{-4}$ g/L)[203-204] but for high concentrations (>0.01 g/L), equilibrium was achieved in a very short timeframe (less than a couple of seconds).[204] The adsorption kinetics for HPC was also shown to be slower than methyl cellulose (MC) at low bulk concentrations (10^{-5} to 10^{-2} %wt).[11] The hydrophilic hydroxypropyl groups may have attributed to the slower adsorption for HPC[11] since it has suggested that hydrophobic groups (like methyl groups) act as a driving force for a faster diffusion to the interface due to their higher incompatibility with the aqueous phase.[206] Therefore, a 50-minute adsorption time for HPC was first conducted, but ultimately a 15-minute adsorption period was selected due to several reasons. It was found that after 15 minutes of adsorption to the sensor surface, the rate of adsorption decreased to 4 $ng{\cdot}cm^{-2}$/min and after a buffer rinse step there were no significant differences between 50 and 15 min adsorption times for the amount of irreversible adsorption. Also, a shorter adsorption period was necessary in order to minimize the masses of polymers needed (due to the limited quantity of novel HPC-P that was able to be synthesized) because a 0.25 mL/min flow rate requires 12.5 mL of CE solution for a 50-minute adsorption time, whereas a 15-minute adsorption time requires 3.75 mL of CE solution. Adsorption times need to be consistent in order to compare results between commercial HPC and HPC-P; therefore, a 15 minute-adsorption was selected to provide a CE continuous interface, while at the same time limiting the amount of HPC-P polymer needed to complete the study. It should be noted that this is an experimental limitation; use of a longer adsorption period could potentially provide a more saturated cellulose ether interface.

Preliminary experiments were also conducted to determine the best sensor surface for CE adsorption. Gold, hydrophobic polystyrene (PS), and various self-assembled monolayers (SAMs) with different degrees of hydrophobicity (SAM-CH_3 and SAM-OH) were tested. It was found that HPC had the same affinity for the gold and SAM-CH_3 surface with no significant difference in the frequency change (Δf) during HPC adsorption and desorption. Ultimately, the pre-coated PS surface was chosen for performing the sequential and simultaneous adsorption experiments because HPC had the greatest affinity for this surface (discussed later in this section) and this hydrophobic surface best mimics a lipid droplet surface.

4.1.1 Effect of the Surface Hydrophobicity on the Adsorption of Commercial HPC

In order to study the effect of type and hydrophobicity of the surface on the adsorption/desorption behavior of HPC, two different sensors, gold and PS, were used. **Figure 4.1** shows the representative profile of the changes in frequency ($\Delta f/n$) and dissipation (ΔD) during the adsorption of HPC onto gold and PS sensor surfaces, followed by a buffer rinse using QCM-D. Frequency ($\Delta f/n$) and dissipation (ΔD) changes of the oscillating crystal provide information about hydrated mass changes on the sensor and viscoelastic properties of the adsorbed layer, respectively. For example, a decrease in frequency relates to an increase in adsorbed mass onto the sensor and an increase in dissipation relates to the formation of a softer, viscoelastic film, whereas an increase in frequency relates to a decrease in adsorbed mass and decrease in dissipation relates the formation of a more rigid, elastic film.[207-208] It is important to note that the changes in adsorbed mass measured by QCM-D involve the adsorbed molecule (in this case the HPC adsorbed layer) as well as the water associated within the adsorbed HPC layer.[124] **Table 4.1** provides the rate of HPC layer formation (($ng \cdot cm^{-2}$)/min), after the 1st min of HPC adsorption, 15 min of adsorption, and during the buffer rinse step. **Table 4.2** summarizes values of hydrated adsorbed mass ($ng \cdot cm^{-2}$) and thickness (nm) of HPC layers formed onto gold and PS surfaces. Total adsorption values correspond to the adsorbed mass/thickness after the adsorption of HPC for 15-min and irreversible adsorption values correspond to the mass/thickness remaining on the sensor after the buffer rinse. These values were obtained from the frequency data **(Figure 4.1A)** based upon a rigid elastic film (using the Sauerbrey model) and from both frequency and dissipation data **(Figure 4.1A and Figure 4.1B)** for a softer more viscoelastic film (Voigt modeling) as described in the Experimental Section**.**

In general, a sharp decrease in frequency ($\Delta f/n$) was observed on both surfaces ~1 min after HPC was introduced into the system **(Figure 4.1A)**. This result indicates the sudden deposition of mass onto the sensors with a significantly faster rate of formation on the PS sensor ($p<0.05$), compared to gold **(Table 4.1).** This was followed by a slower decrease in frequency until buffer was introduced into the system, suggesting that HPC was most likely interacting with the already adsorbed layer, rather than the sensor itself.[209] A larger frequency change ($\Delta f/n$) and rate of formation was observed on the PS sensor, compared to gold, during the 15-min adsorption period, meaning a larger amount of mass adsorbed onto PS **(Table 4.2)** at a faster rate. Increases in dissipation (ΔD) were associated with frequency changes during HPC adsorption, indicating a viscoelastic film **(Figure 3.3B).**

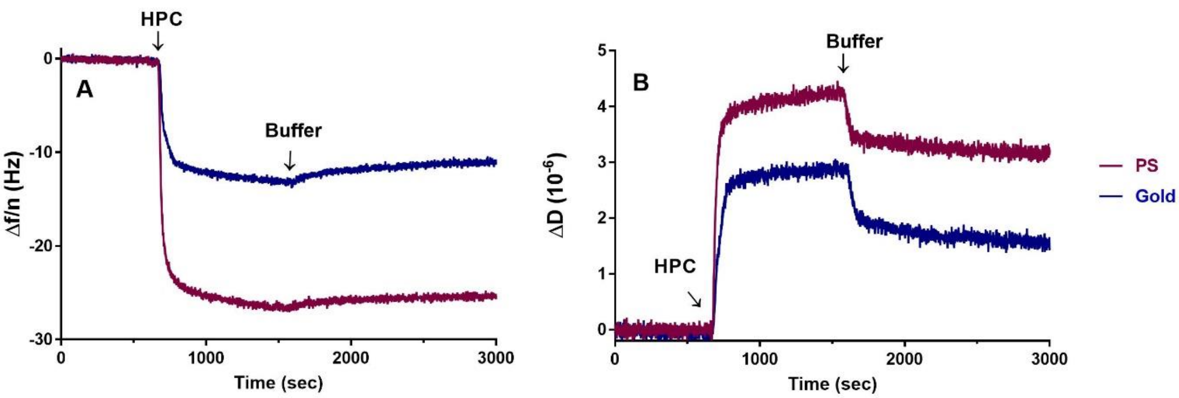

Figure 4.1. Representative profile of changes in frequency ($\Delta f/n$) (A) and dissipation (ΔD) (B) versus time for the adsorption of commercial HPC onto gold and PS and buffer rinse step measured at the 5th overtone (25 MHz). Arrows and labels indicate when solutions were introduced in the flow cell after the initial baselines were set.

Overall, the mean total adsorbed mass and thickness values calculated from the Voigt model were ~2.0 times higher than the Sauerbrey values for both surfaces **(Table 4.2)**, indicating that viscoelastic films, containing coupled water, were formed on both surfaces after the 15-min adsorption period.[210] During the buffer rinse, the increases in frequency **(Figure 4.1A)** and the negative rate of formation values **(Table 4.1)** observed on both surfaces, indicated the removal of weakly bound HPC molecules and associated water in the film.[209] The irreversible HPC adsorbed on both surfaces still had a dissipation value ΔD>0, suggesting that the polymer assumes different configurations (i.e. trains, loops, and tails) at the surface. [11, 101] Only a small portion of HPC (trains) may adsorb to the surfaces while the rest of the segments (loops and tails) extend into the bulk solution[211], thus having coupled water attached to the film. Since the irreversible adsorbed mass and thickness values obtained from Voigt modeling are only about 0.25 times larger than the values obtained from the Sauerbrey equation, the Sauerbrey equation may be more appropriate in this situation **(Table 4.2).**[159] Regardless of modeling type, there was a significantly ($p<0.05$) higher amount of adsorbed mass/thicker layer remaining on PS, compared to gold, after the buffer rinse step **(Table 4.2)**. It is also important to note that the amount of mass that was removed during the buffer rinse was about the same on both sensors and that the adsorption of HPC is almost irreversible regardless of sensor type (i.e. a high proportion of HPC remained on both sensors after the buffer rinse step).

Table 4.1. Rate of mass formation values [(ng·cm^{-2})/min] during the 1st min of HPC adsorption, after 15 min adsorption, and during the buffer rinse step on gold and PS. Values represent mean ± SEM. Values at each stage of HPC adsorption not sharing a common superscript are statistically significantly different (two sample t-test, p<0.05).

Sensor Surface		Rate of Formation [(ng·cm^{-2})/min]
1 min adsorption	PS	522 ± 46^a
	Gold	304 ± 28^b
15 min adsorption	PS	51.9 ± 2^a
	Gold	29.9 ± 2^b
During buffer rinse	PS	-7 ± 1^a
	Gold	-7 ± 0^a

Table 4.2. QCM-D values of the Sauerbrey and Voigt adsorbed mass (ng·cm^{-2}) and thickness (nm) for HPC adsorption determined on gold and PS after 15 min of adsorption (total adsorption) and after the buffer rinse (irreversible adsorption). Values represent mean ± SEM. Values for total adsorption not sharing a common superscript are statistically significantly different (two sample t-test, p<0.05) and values for irreversible adsorption not sharing a common superscript are statistically significantly different (two sample t-test, p<0.05).

Sensor Surface		Sauerbrey Model		Voigt Model	
		Mass (ng·cm^{-2})	Thickness (nm)	Mass (ng·cm^{-2})	Thickness (nm)
Total Adsorption	PS	457 ± 19^a	4.6 ± 0.2	727 ± 30^a	7.2 ± 0.3
	Gold	226 ± 20^b	2.2 ± 0.2	416 ± 32^b	4.2 ± 0.3
Irreversible Adsorption	PS	416 ± 17^a	4.2 ± 0.2	560 ± 21^a	5.6 ± 0.2
	Gold	187 ± 18^b	1.8 ± 0.2	247 ± 24^b	2.5 ± 0.2

The observed differences in $\Delta f/n$ and ΔD **(Figure 4.1)** and adsorbed mass/thickness **(Table 4.2)** can be explained by different physical or chemical interactions taking place at the sensor surfaces: On gold, segments of the HPC polymer chain may interact with the metal through weak Van der Waals forces[212], leading to physisorption (physical interactions) of HPC, and thus a lower adsorption of HPC to the surface. On the other hand, the main driving force for adsorption onto the hydrophobic PS surface may be attributed to chemisorption due to hydrophobic interactions between the polymer and the surface[213]. Additionally, it was found that the adsorption of non-ionic cellulose ethers, hydroxyethylcellulose (HEC) and EHEC, was higher on the surface that contained more adsorption sites (citrate-covered gold surface) compared to a bare gold surface.[139] Therefore, in our study, it is also possible that the PS surface contained more adsorption sites than gold, which may have allowed for a more efficient adsorption of the hydrophobic unsubstituted parts of the HPC backbone to the hydrophobic PS surface.

Figure 4.2 shows the $(\Delta f/n)/\ \Delta D$ ratios during the 1st min of HPC adsorption, 15 min of adsorption, and after the buffer rinse step. The $(\Delta f/n)/\ \Delta D$ ratio provides information about the viscoelastic properties of the adsorbed HPC molecules with respect to the induced energy dissipation of the sensor per coupled unit mass. For example, a more negative $(\Delta f/n)/\ \Delta D$ value corresponds to a more rigid, elastic film because the addition of mass does not elicit a significant increase in dissipation, whereas a less negative $(\Delta f/n)/\ \Delta D$ value corresponds to a softer, more dissipative viscoelastic film.[214] Additional information about HPC conformational changes occurring at the surface can be seen in **Figure 4.3,** which shows the evolution of the elastic modulus during the adsorption and desorption of HPC on both sensors.

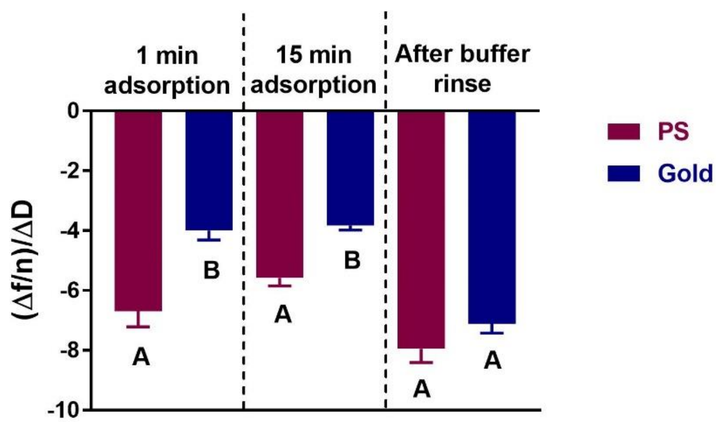

Figure 4.2. Bar chart displaying the ratio of $(\Delta f/n)/\Delta D$ on gold and PS during three stages of HPC adsorption. Values represent mean ± SEM. Values at each stage of HPC adsorption not sharing a common superscript are statistically significantly different (two sample t-test, p<0.05).

During the early stages of HPC adsorption (1st min), a significantly more rigid film ($p<0.05$) was formed on the PS surface than on the gold surface (-6.7 ± 0.5 and -4.0 ± 0.3 $(\Delta f/n)/\Delta D$ respectively) **(Figure 4.2)**. A slight decrease in elastic modulus was observed on both sensors after ~90 sec of HPC adsorption **(Figure 4.3)**. Nonetheless, a significantly more rigid film ($p<0.05$) was formed on the PS surface than on the gold surface after 15 min of adsorption (-5.6 ± 0.3 and -3.8 ± 0.2 $(\Delta f/n)/\Delta D$ respectively).

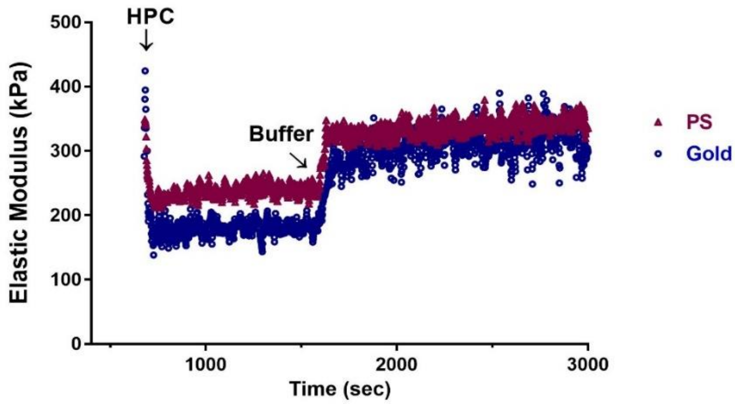

Figure 4.3. Change in elastic modulus (kPa) versus time during the adsorption of HPC onto gold and PS and buffer rinse step. Values calculated from Voigt modeling as previously described in the Experiment Section. Arrows and labels indicate when solutions were introduced in the flow cell after the initial baselines were set.

It is likely that the first HPC molecules adsorbed to the interface through trains because there was little competition for adsorption, leading to a denser, compact conformation with a larger elastic modulus.[215] However, as more HPC chains adsorbed and competed for adsorption onto the sensor, some type of reorganization likely occurred, and the film may have contained more diffuse HPC chains in the aqueous solution, as indicated by the slight decrease in elastic modulus.[204, 215] Similar findings were found by Mezdour *et al.* when studying the adsorption of HPC onto an oil-water interface.[102] They interpreted a decrease in modulus/surface pressure during adsorption as a brush organization of HPC macromolecules at the interface[102], which may be proposed to explain our results. For example, in our study, it is possible that as adsorption continued, HPC chains that arrived near the interface had to stretch, in order to penetrate the already adsorbed layer of HPC, which helped the formation of a brush. As a result, only a few hydrophobic segments per chain may have interacted with the hydrophobic surface while the chains in the brush configuration were in the bulk solution, thus decreasing the elastic modulus. Hydrophobic interactions may have stabilized this brush.[102, 216-217] Increases in elasticity during the buffer rinse step suggests that the diffuse HPC chains on both sensors were likely removed **(Figure 4.3),** while an elastic HPC layer, that contained less coupled water, remained on the sensor surfaces (as indicated by the higher negative $(\Delta f/n)/\,\Delta D$ values in **Figure 4.2**).

The adsorption of commercial HPC on a gold surface using SPR was also investigated. **Figure 4.4** compares the changes in adsorbed mass ($ng{\cdot}cm^{-2}$) versus time (sec) during the adsorption of HPC onto gold, followed by a buffer rinse, using QCM-D and SPR. These adsorbed mass values were obtained with the Sauerbrey model (QCM-D) and the equation of de Feijter *et al*. (SPR).[153] A significantly higher amount of total adsorbed mass (226±20 ng·cm^{-2} vs. 76±8 ng·cm^{-2}, respectively) and irreversible adsorbed mass (187±18 ng·cm^{-2} vs. 69±7 ng·cm^{-2}) was observed using QCM-D, compared to SPR, after the 15-min adsorption period. This result is due to the hydrodynamically coupled water that is associated with the HPC film, which is considered in the QCM-D technique, whereas SPR only considers the adsorbed film.[218] The water content (%) of the irreversible adsorbed mass was calculated to be 63.1%±7. Similar qualitative adsorption/desorption trends were observed for both QCM-D and SPR. Specifically, there was a quick increase in adsorbed mass, followed by a gradual increase to equilibrium. When buffer was introduced into the system, a small amount of mass was removed which was most likely due to the removal of a diffuse HPC layer.

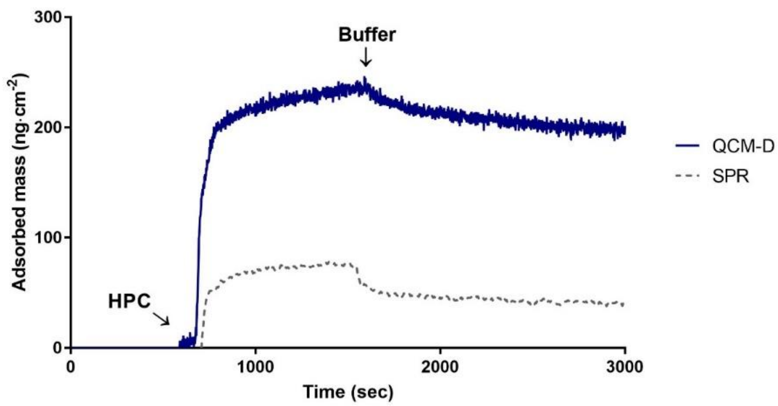

Figure 4.4. Changes in adsorbed mass (ng·cm^{-2}) versus time during the adsorption of HPC onto gold sensors using QCM-D and SPR. Adsorbed mass values were obtained using the Sauerbrey model (QCM-D) and the equation of de Feijter et al. (SPR). Arrows and labels indicate when solutions were introduced in the flow cell after the initial baselines were set.

In conclusion, this study shows that the type and hydrophobicity of the solid surface has an impact on the adsorption of commercial HPC. More specifically, a higher amount of HPC adsorbs onto the PS surface than on gold which may be due to more adsorption sites for HPC and stronger hydrophobic interactions taking place between HPC and PS, whereas weak van der Waals interactions may occur with the gold surface. Nonetheless, HPC shows high irreversible adsorption (i.e. a very high proportion of HPC initially adsorbed remains on both surfaces after the buffer rinse step), regardless of sensor type. By combining QCM-D and SPR, we have shown similar adsorption/desorption trends of HPC on gold surfaces. Also, we have shown that water is associated within the HPC film, which contributes to higher adsorbed mass values for QCM-D, compared to SPR.

4.1.2 Effect of the Molecular Properties of Cellulose Ethers on their Adsorption onto Hydrophobic Surfaces

In order to explain the impact of HPC structure and hydrophobicity on their adsorption features and layer structures formed on hydrophobic surfaces, we compared the adsorption / desorption behavior of commercial HPC and novel HPC-P using QCM-D. Because of the greater HPC adsorption observed on hydrophobic PS sensors, in this and following studies, we will only consider adsorption of CEs onto PS sensors. We studied the adsorption/desorption of HPC-P using SPR. However, the *dn/dc* value obtained using the differential refractometer seems to not be an accurate value since negative HPC-P adsorbed mass values were obtained with SPR. Since a small amount of DMSO had to be added in order to dissolve HPC-P, we believe that presence of a mixed solvent system (buffer + DMSO) made it difficult to obtain an accurate value since these solvents have different refractive indexes. Due to the limited amount of the novel HPC-P sample that could be synthesized for this project, we could not perform the *dn/dc* experiments more than 4 times to try to obtain a more accurate value. Therefore, SPR experiments investigating the adsorption of HPC-P and the sequential adsorption of BSs on the HPC-P layer will not be discussed in this thesis.

Figure 4.5 shows representative QCM-D data for the changes in frequency ($\Delta f/n$) and dissipation (ΔD) during the adsorption of HPC and HPC-P, followed by a buffer rinse, onto PS sensors. **Table 4.3** summarizes estimated values of adsorbed (hydrated) mass ($ng{\cdot}cm^{-2}$) and thickness (nm) of HPC and HPC-P layers formed onto PS sensors. Total and irreversible adsorption values were obtained from the changes in frequency based upon a rigid elastic film (using the Sauerbrey model) and a softer more viscoelastic film (Voigt modeling) as described in the Experimental Section **(Chapter 3)**.

As a general trend, a sharp decrease in frequency ($\Delta f/n$) was observed ~1 min after HPC and HPC-P were introduced into the system, indicating the sudden deposition of mass onto the PS surface **(Figure 4.5A).** However, the $\Delta f/n$ was substantially larger for HPC-P than HPC during the adsorption period **(Figure 4.5A),** resulting in a significantly higher amount of initial (total) adsorbed mass and thickness of the HPC-P layer ($p<0.05$), regardless of modeling type **(Table 4.3)**. Similar findings were reported during the adsorption of EHEC and hydrophobically modified EHEC (HM-EHEC) onto a hydrophobic SAM surface.[159] It was found that HM-EHEC had a substantial increase in adsorption onto the hydrophobic surface, compared EHEC.[159] In our study, the extra hydrophobic modification of HPC-P with the pendent carboxyl groups most likely enhanced its adsorption onto the PS sensor by having more hydrophobic parts to adsorb onto the hydrophobic surface. However, the changes in frequency for HPC-P continued to decrease during the entire 15-min period, whereas HPC adsorption almost reached equilibrium before the introduction of buffer. This result suggests that HPC-P adsorbed onto the PS surface at a slower rate than HPC **(Figure 4.5A).** The slower rate of adsorption observed for HPC-P could be related to the partial formation of self-aggregates in the bulk solution, probably caused by the presence of pendent carboxyl groups at the ends of the polymer branches, which was recently reported by Dong *et. al* through dynamic light scattering measurements.[183] Therefore, HPC-P self-association may have slowed down HPC-P adsorption since the polymer would first need to disorganize in order to anchor to the PS surface.[206, 219] Increases in dissipation (ΔD) were associated with frequency changes during HPC and HPC-P adsorption, indicating an increase in the viscoelasticity of the films **(Figure 4.5B).**

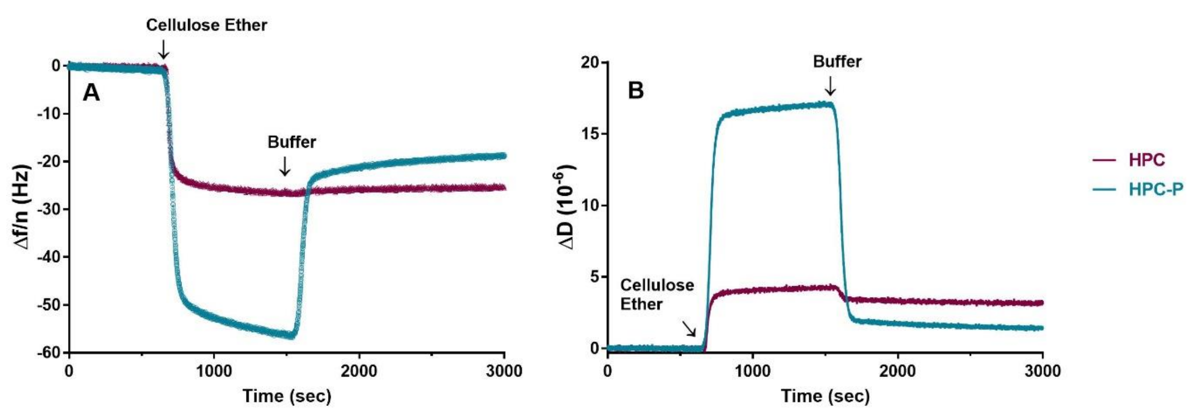

Figure 4.5. Representative QCM-D data of changes in frequency (A) and dissipation (B) versus time for the adsorption of commercial HPC and HPC-P onto the PS surface measured at the 5th overtone (25 MHz). Arrows and labels indicate when solutions were introduced in the flow cell after the initial baselines were set.

Overall, the mean total adsorbed mass and thickness values calculated from the Voigt model were ~2 times higher than the Sauerbrey values for both surfaces **(Table 4.3)**. This shows that the HPC and HPC-P films were viscoelastic after the 15-min adsorption period.[210] During the buffer rinse step, a significant frequency increase and dissipation decrease was observed for the HPC-P layer, indicating a high reversibility of HPC-P (more than 50%) from the PS surface compared to HPC **(Figure 4.5)**. As a result, the final (irreversible) mass and thickness of the HPC layer was significantly higher than HPC-P ($p<0.05$), regardless of modeling type **(Table 4.3).** This result suggests the presence of an electrostatic adsorption barrier during HPC-P adsorption, which was previously postulated for the adsorption of hydrophobically modified polyelectrolytes onto a hydrophobic PS surface at a high physiological pH.[220] HPC-P is negatively charged at a neutral pH, due to the dissociation of the carboxyl groups located at the end of the polymer branches, which may result in electrostatic repulsions of the charged groups.[183] These repulsions may have caused the HPC-P polymer to initially adopt a linear, more extended conformation at the interface, leading to a thin layer structure on the PS surface.[221] However, as more HPC-P accumulated at the surface, the repulsions most likely increased, resulting in a long range repulsive barrier. In order for HPC-P to overcome this barrier and attach/gain anchoring energy on PS, short range attractions (in this case, hydrophobic interactions) must have occurred between the polymer and the substrate.[220] It is possible that a significant amount of HPC-P could not fully overcome this electrostatic barrier during the 15-min adsorption period, resulting in high desorption during the buffer rinse.

Table 4.3. QCM-D values of the Sauerbrey and Voigt adsorbed mass (ng·cm^{-2}) and thickness (nm) for HPC and HPC-P adsorption determined onto the PS surface after 15 min of adsorption (total adsorption) and after the buffer rinse (irreversible adsorption). Values for total adsorption not sharing a common superscript are statistically significantly different (two sample t-test, p<0.05) and values for irreversible adsorption not sharing a common superscript are statistically significantly different (two sample t-test, p<0.05).

Cellulose Ether		Sauerbrey Model		Voigt Model	
		Mass (ng·cm^{-2})	Thickness (nm)	Mass (ng·cm^{-2})	Thickness (nm)
Total Adsorption	HPC-P	1049 ± 104^{a}	10.5 ± 1.0	2926 ± 271^{a}	29.3 ± 3.0
	HPC	457 ± 19^{b}	4.6 ± 0.2	727 ± 30^{b}	7.2 ± 0.3
Irreversible Adsorption	HPC-P	306 ± 13^{b}	3.0 ± 0.2	389 ± 12^{b}	3.9 ± 0.1
	HPC	416 ± 17^{a}	4.2 ± 0.2	560 ± 21^{a}	5.6 ± 0.2

Figure 4.6 shows the $(\Delta f/n)/\,\Delta D$ ratios (a measure of film rigidity) during the 1st min of cellulose ether adsorption, after 15 min of adsorption, and during the buffer rinse step. Additional information about HPC conformational changes occurring at the surface can be seen

in **Figure 4.7,** which shows the evolution of the elastic modulus during the adsorption of HPC and HPC-P onto the PS surface.

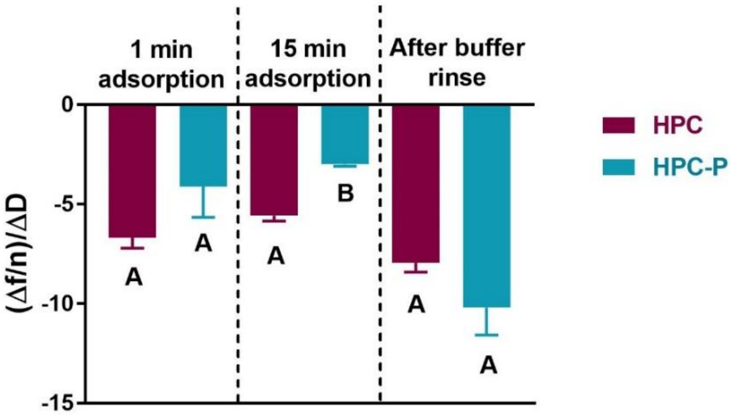

Figure 4.6. Bar chart displaying the ratio of $(\Delta f/n)/\Delta D$ during three stages of adsorption for HPC and HPC-P onto the PS surface. Values represent mean ± SEM. Values at each stage of cellulose ether adsorption not sharing a common superscript are statistically significantly different (two sample t-test, $p<0.05$).

After 15-min of adsorption, HPC-P had a significantly less negative $(\Delta f/n)/\ \Delta D$ value ($p<0.05$) **(Figure 4.6)** and a lower elastic modulus value **(Figure 4.7)** which indicates that it formed a more viscoelastic film, compared to HPC. However, for both cellulose ethers, there were observed increases in elasticity and decreases in the $(\Delta f/n)/\ \Delta D$ values when buffer was introduced into the system, indicating that the resulting irreversible films were rigid. This result indicates that a diffuse layer of HPC and HPC-P, that entrapped more water, was most likely removed when buffer was introduced into the system.

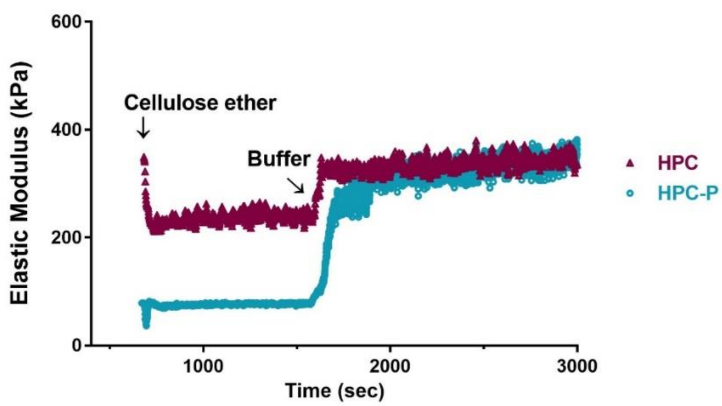

Figure 4.7. Change in elastic modulus (kPa) versus time during the adsorption of HPC and HPC-P onto the PS surface followed by a buffer rinse step. Values calculated from Voigt modeling as previously described in the Experiment Section. Arrows and labels indicate when solutions were introduced in the flow cell after the initial baselines were set.

In conclusion, we have shown that the molecular properties (i.e. charge and substituent groups) of the cellulose ether impact its adsorption onto a hydrophobic substrate (PS) and the properties of the adsorbed film. The more hydrophobic character of HPC-P enhances its adsorption onto the PS surface, compared to HPC. However, the adsorption of HPC-P was highly reversible, with more than 50% of HPC-P being removed during the buffer rinse, leading to a final lower surface concentration compared to HPC. This could be due to electrostatic repulsions between HPC-P adsorbed chains which contain negatively charged carboxyl groups. Additionally, the cellulose ether films irreversibly adsorbed onto the hydrophobic surface are both relatively elastic. The smaller thickness of the HPC-P layer may suggest that this polymer adsorbs with a flat conformation, whereas HPC assumes a train, loop, and tail conformation at the surface that entraps more water.

These studies have helped us gain insight into the conformational changes that occurred at the surface during adsorption/desorption of cellulose ethers as well as the different properties of the irreversible adsorbed cellulose ether films. Knowledge about the interfacial properties of the cellulose ether films is key to understand the interactions that take place at the interface during the subsequent sequential and simultaneous adsorption of bile salts (BSs).

4.2 Sequential Adsorption of Cellulose Ethers and Bile Salts

In order to gain insight into the resistance of CE films against displacement by BSs, sequential adsorption experiments were performed using both QCM-D and SPR. The experiment tries to emulate the closest scenario of what happens to the emulsion interface during lipid digestion and shows the interaction of pre-adsorbed layers of CEs with BSs at the interface. These experiments consisted of flowing 0.1% wt CE for 15 min onto hydrophobic (PS) and/or gold substrates to provide a cellulose ether continuous surface, followed by a 25 min exchange of buffer to remove any reversible adsorbed mass. Then, low and high concentrations of BSs were injected into the flow cell for 10 min to observe the adsorption behavior of BSs onto the pre-adsorbed cellulose layer. After each BS injection, buffer was introduced into the system to remove any loosely adsorbed material from the solid surface. For comparison, the same experiment was performed without HPC (i.e. BSs were adsorbed at the bare solid surface followed by the buffer rinse step). Three individual experiments were performed for each BS concentration. We investigated i) the effect of BS type (NaTC and NaTDC) and concentration (2, 5, and 10 mM) on the displacement of a commercial HPC layer and ii) the impact of the molecular properties (i.e. charge, molecular weight, substituent type) on the resistance of the CE to displacement by a more physiological BS concentration (10 mM). This BS concentration would be equivalent to the individual BS concentration used in the *in vitro* lipid digestion studies (**Chapter 4.4**).

4.2.1 Effect of Bile Salt Type and Concentration on the Displacement of a HPC Layer

QCM-D study: PS sensors

Using QCM-D, the changes in frequency ($\Delta f/n$) and dissipation (ΔD) were monitored as a function of time during the sequential adsorption of commercial HPC and BS onto PS surfaces. **Figure 4.8** shows the representative profile corresponding to the sequential adsorption of 2, 5, and 10 mM BS onto both the HPC layer and PS sensor, followed by a buffer rinse step, measured at the fifth overtone. As a general trend, a sudden decrease in frequency was observed after the injection of BSs into the flow cell, indicating the initial adsorption of BSs onto the HPC layer and consequently the formation of a mixed HPC-BS layer **(Figure 4.8)**. This initial response was followed by a smaller decrease in frequency as the adsorption of BSs proceeded. An initial increase in dissipation was also observed for all BS samples, which indicates an increase in the viscoelasticity of the HPC-BS mixed layer and the pure BS layer. To further elucidate the interfacial mechanism of BS adsorption, the experiment was finished with a rinse step with buffer. During the rinse step, an initial sudden increase in frequency was observed, followed by a steady increase in frequency reaching a steady value by the end of this step, which suggested some desorption of mass from the surface. Additionally, a decrease in dissipation was observed, indicating that the films became more rigid. The changes in the frequency and dissipation profile during the adsorption of BSs and posterior exchange with buffer are different depending on the type and concentration of BS.

Namely, the **adsorption and desorption of the two BSs onto the bare hydrophobic PS surface showed diverse behaviors**. The adsorption of NaTC (2, 5, and 10 mM) continued to increase during the entire 10-min period, suggesting a slow adsorption process **(Figure 4.8A)**. On the other hand, the adsorption of NaTDC (2, 5, and 10 mM) reached a steady state within the 10-min period **(Figure 4.8C)**. During the buffer rinse, a larger desorption was observed for 5 and 10 mM NaTDC, compared to NaTC **(Figure 4.9A)**. The adsorption/desorption behavior of pure BSs may be influenced by their critical micelle concentration (CMC)[89], the concentration range at which BS self-assemble in aqueous solutions to form micelles.[20, 69] The BSs employed in our study have different CMC values: NaTC has a broad CMC (3-18 mM) and tends to aggregate into small micelles, whereas NaTDC has a low CMC value (2-3 mM) and tends to aggregate into larger micelles.[89, 186] A recent study investigating the adsorption-desorption behavior of BSs at C18-functionalized hydrophobic surfaces using dual polarization interferometry, an optical surface technique,[89] showed results with similar qualitative features as seen in **Figure 4.8.** For concentrations below the CMC, an initial rapid increase followed by a slow adsorption process was reported on a hydrophobic surface.[89] In this study, 2 mM NaTC is the only concentration that is below the CMC. However, a slow adsorption was observed for all three concentrations of NaTC **(Figure 4.8A).** Because the reported CMC for NaTC is very broad (3-18 mM[89, 186]), it is possible that the range of concentrations that we tested in this study may be below the actual CMC. On the other hand, for concentrations above the CMC (5 and 10 mM NaTDC), the behavior appears to be rapid adsorption followed by equilibrium (**Figure 4.8C).** This could indicate that the formation of micelles in the bulk may play a role in the adsorption process.[89]

Figure 4.9A presents the % BS desorption from the PS surface during the buffer rinse. During the buffer rinse, there was a significantly higher % of BS desorption from the PS surface for 5 mM NaTDC (75% ± 5) compared to NaTC (34% ± 6%). Although the result was not significantly different, 10 mM NaTDC (87% ± 1) showed a higher % of desorption from the PS surface, compared to NaTC (65% ± 8) **(Figure 4.9A)**. These results indicated a higher reversible behavior for NaTDC whereas a more irreversible behavior for NaTC during the buffer rinse. The lack of complete desorption for NaTDC (5 and 10 mM) from the PS substrate **(Figure 4.9A)** was an unexpected result because micelle forming surfactants usually fully desorb from a surface during a rinse step. This is because during a rinse step, the surfactant concentration decreases below the CMC. Therefore, surfactants will desorb from the surface in order to maintain equilibrium in the bulk solution, until the solute is removed and the surfactant is fully desorbed from the surface.[89, 222-223] These differing adsorption/desorption profiles between NaTC and NaTDC on the PS surface may support the idea that a subtle difference in the BS structure (in this case, one less hydroxyl group for NaTDC at the C7 position) influences different phases of the lipolysis process.[89] It has postulated that a slower adsorption and irreversible behavior, seen with NaTC, may promote the adsorption and residence time of a co-lipase/lipase complex.[89] In contrast, a faster adsorption to the surface and higher reversible behavior, seen with NaTDC, may favor the displacement and solubilization of lipolysis products.

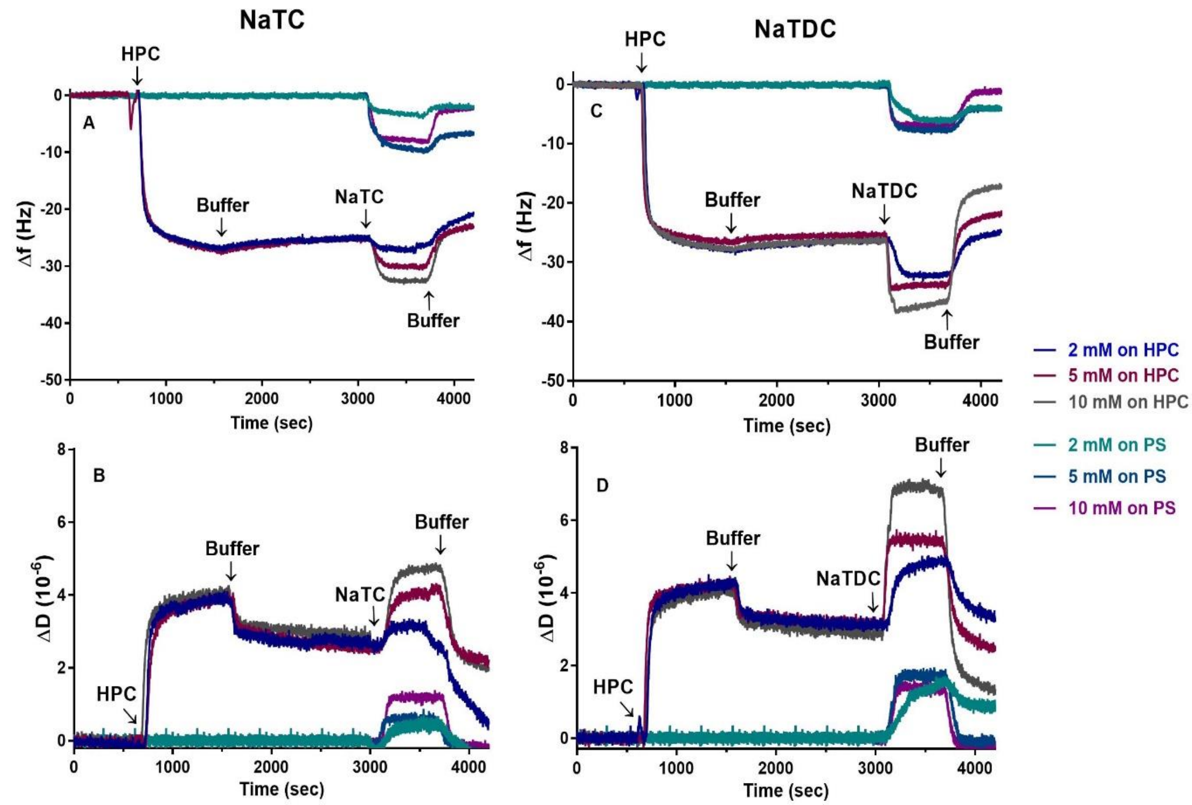

Figure 4.8. Representative QCM-D data of the changes in frequency ($\Delta f/n$) and dissipation (ΔD) versus time measured at the 5th overtone (25 MHz) for the adsorption of 2, 5, and 10 mM NaTC (A and B) and NaTDC (C and D) onto commercial HPC and the PS surface. Arrows and labels indicate when solutions were introduced in the flow cell after the initial baselines were set.

When examining the **adsorption of both BSs onto the HPC layer**, the frequency gradually drops with the increase in BS concentration, which means that more BS molecules adsorbed onto the surface at a higher concentration. The higher the BS concentration, the lower the frequency plateau is for the mixed adsorption layer. The BS molecules may penetrate into the HPC layer, modifying the surface structure and forming a mixed polymer/biosurfactant layer. A more gradual decrease in frequency was observed in the NaTC system, for all three concentrations, which suggests a slower adsorption onto HPC than NaTDC **(Figure 4.8A)**. On the other hand, 5 and 10 mM NaTDC showed a sharp decrease in frequency followed by a quick equilibrium, while 2 mM NaTDC showed a slower decrease in frequency before reaching a steady state **(Figure 4.8C)**. It is interesting to point out that there was a slight increase in frequency during the adsorption of 5 and 10 mM NaTDC **(Figure 4.8C)**. This result suggests that some HPC layer may have been removed from the sensor during this time since an increase in frequency was not observed during the adsorption of 5 and 10 mM NaTDC onto the PS sensor. Also, the dissipation did not seem to decrease during this time of frequency increase, suggesting NaTDC may have displaced some HPC layer and then adsorbed to the sensor without changing viscoelastic properties **(Figure 4.8D)**. Similar results were found by Torcello-Gómez and Foster when examining the sequential adsorption of HPMC and NaTDC onto an oil/water interface.[12] It was reported that a drop in the dilatational modulus of the HPMC layer during the adsorption of NaTDC suggested some of the HPMC layer was displaced by NaTDC before the exchange of buffer.[12]

Figure 4.9B presents the % total mass (BS, HPC, or BS+HPC) that desorbed from the PS surface during the final buffer rinse. Regardless of BS type and concentration, the frequency values obtained after the buffer rinse of the HPC/BS systems (4200 sec) were higher than the values when the BSs were first injected in the system (3000 sec), suggesting that at least some HPC was removed from the PS surface **(Figure 4.8).** Therefore, **Figure 4.9C** presents the minimum % of HPC mass that may have been displaced by BSs from the PS surface (if the assumption is that all the BSs were removed during the final buffer rinse). A slightly higher % of mass desorbed from the PS surface in the HPC/NaTDC system (5 and 10 mM), compared to the same concentrations of NaTC **(Figure 4.9B)**. Additionally, a slightly higher % of HPC was displaced by 5 and 10 mM NaTDC, compared to NaTC **(Figure 4.9C)**. Also, as the concentration of NaTDC increased, more mass was displaced from the PS surface **(Figure 4.9B)**. Fernández-Fraguas *et al.* reported that HPMC adsorbed films on an oil/water interface were not easily disrupted by a mixture of BS (NaTC and sodium glycodeoxycholate (NaGDC)) at low concentrations (BS≤10 mM), however the HPMC layer was eventually displaced with increasing BS concentrations (BS=10 mM).[14] On the other hand, 2 mM NaTC seems slightly more effective at removing HPC, compared to 2 mM NaTDC **(Figure 4.9C).** All of these findings suggest that NaTDC (5 and 10 mM) was more effective at interacting with HPC at the interface and displacing some of the HPC layer during the buffer rinse, compared to NaTC. As a result, the degree of hydrophobicity in the BS plays an important role in its interactions with HPC and displacement during the buffer rinse. Since NaTC has an extra –OH group, more hydrogen bond formation may have occurred with the hydroxypropyl groups in HPC at 2 mM NaTC, which could have allowed more desorption from the interface, compared to NaTDC. However, the higher desorption of mass at 5 and 10 mM NaTDC could be due to its ability to desorb quickly from an interface. Surface complexes/aggregations have been shown to form for high concentrations of NaTC (10 mM) on an interface, which made desorption unlikely at the interface.[60] However, these complexes were not shown to form by deoxycholates, which allowed it desorb faster from an interface.[60] Therefore, the hydrophilic face of the NaTDC micelles may have interacted with HPC, but NaTDC aggregates may not have formed, which allowed more desorption from the interface.

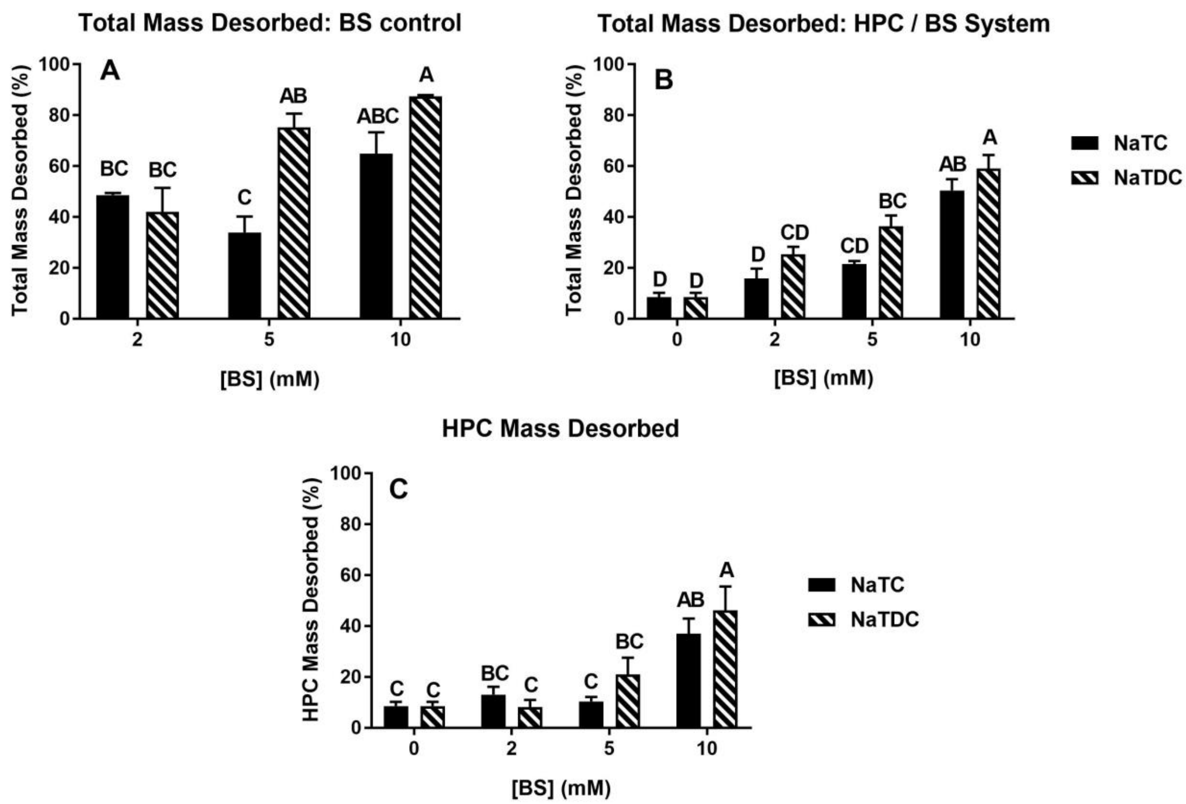

Figure 4.9. % BS desorbed from the PS surface during the buffer rinse (A), % total mass desorbed of the HPC/BS systems during the buffer rinse (B) and the minimum % HPC removed from the PS surface during the buffer rinse assuming that all the BSs were removed during the final buffer rinse (C). Values obtained by the Sauerbrey model and represent mean ± SEM. Values of % BS desorbed not sharing a common superscript are statistically significantly different (1-way ANOVA with Tukey's post hoc test for all possible comparisons, p<0.05). Values of % total mass desorbed of the HPC/BS systems not sharing a common superscript are statistically significantly different (1-way ANOVA with Tukey's post hoc test for all possible comparisons, p<0.05). Values of % HPC mass removed not sharing a common superscript are statistically significantly different (1-way ANOVA with Tukey's post hoc test for all possible comparisons, p<0.05).

On the other hand, 2 mM NaTC seems slightly more effective at removing HPC, compared to 2 mM NaTDC **(Figure 4.9C).** Therefore, the degree of hydrophobicity in the BS may play a key role in its interactions with HPC and displacement during the buffer rinse. It is important to note that since the BS control samples did not completely desorb from the PS sensor **(Figure 4.9A)**, some BS may have remained in the HPC/BS systems. Similar observations were reported by Torcello-Gómez and Foster who postulated that a complex of 5 mM NaTDC and HPMC remained on an oil-water interface after a buffer rinse. After the buffer rinse, they suggested that the NaTDC molecules may have been embedded in the HPMC layer formed by trains and loops at the oil/water interface.[12] As a result, our finding indicates that the % of HPC removed during the buffer rinse may have been higher than the values presented in **Figure 4.9C.** Nonetheless, a certain amount of HPC remained on the PS surface since there was not a complete desorption of the HPC/BS systems after the buffer rinse. This result indicates that HPC was resistant to displacement by both BSs at concentrations ranging from 2 to 10 mM. This result was surprising because BSs are extremely surface active and previous studies investigating other interfacial films, like β-lactoglobulin[224], HPMC[9, 14], and sugar beet pectin[14] have been shown to get diminished by high BS concentrations (e.g. 10 mM). These contrasting results could be due to different conditions employed in the experiments; that is some studies have investigated the displacement of interfacial films by a mixture of different types of BSs.[14, 224] Therefore, it might be possible that the mixture of these BSs influence a greater displacement of the interfacial film.

To gain more information on the adsorption behavior of BSs onto HPC, the change in dissipation (ΔD) vs frequency ($\Delta f/n$) during the adsorption of 2, 5, and 10 mM BSs onto the HPC layer was represented **(Figure 4.10)**. This plot displays the energy dissipation per coupled unit mass independently of time. Hydrated mass increases with decreases in frequency, so in this case, **Figure 4.10** shows mass increasing from right to left. The solid lines represent the best fits of the data. The slope of the correlation, provided next to best fit lines, gives information on the viscoelastic properties of the adsorbed layer, so we can therefore infer conformational changes that occur on the HPC layer.[225-226] A large slope (i.e. high dissipation per frequency change) characterizes a soft viscoelastic layer, while a small slope (i.e. small dissipation increase per frequency change) describes more rigid layers.[227] **Figure 4.11** presents the thickness layers formed by 2, 5, and 10 mM NaTC on PS and HPC (these values do not consider the thickness of the HPC layer). The Sauerbrey model was used to calculate the layer thickness since the changes in dissipation on the PS sensor were too low to obtain values with the Voigt model. Frequency and dissipation changes are proportional to the thickness of thin films; as the layer gets thicker, both the negative change in frequency and positive change in dissipation increases.[137, 210]

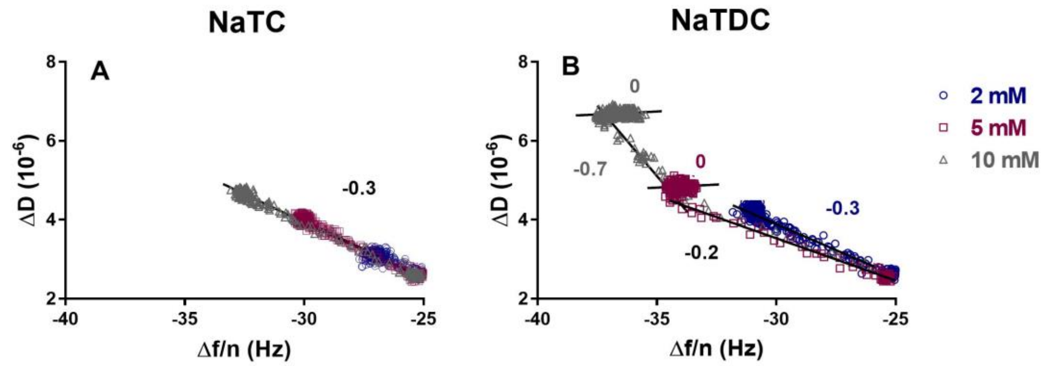

Figure 4.10. Change in dissipation (ΔD) versus frequency (Δf) measured at the 5th overtone (25 MHz) during the adsorption of 2, 5, and 10 mM NaTC (A) and NaTDC (B) onto the HPC layer. Values on the graph indicate the slope of the lines.

As the concentration of NaTC increased from 2 to 10 mM, the frequency and dissipation changes increased during its adsorption onto the HPC layer **(Figure 4.10A).** As a result, the NaTC adsorbed films on the HPC layer got significantly thicker ($p<0.05$) as the concentration of NaTC increased **(Figure 4.11).** The thickness of the layer formed by 2 and 5 mM NaTC was lower on HPC (0.2 ± 0.1 and 0.6 ± 0.1 nm, respectively) than on the PS surface (0.6 ± 0.1 and 1.7 ± 0.1 nm, respectively). However, the thickness of 10 mM NaTC was about the same on PS and HPC (1.3 ± 0.1 and 1.2 ± 0.1 nm, respectively). This result may indicate that 2 and 5 mM NaTC adopted a flatter conformation on HPC, compared to the PS surface, or that HPC could adopt a more compact configuration after interaction with NaTC and form a less diffuse layer at 2 and 5 mM NaTC**.**

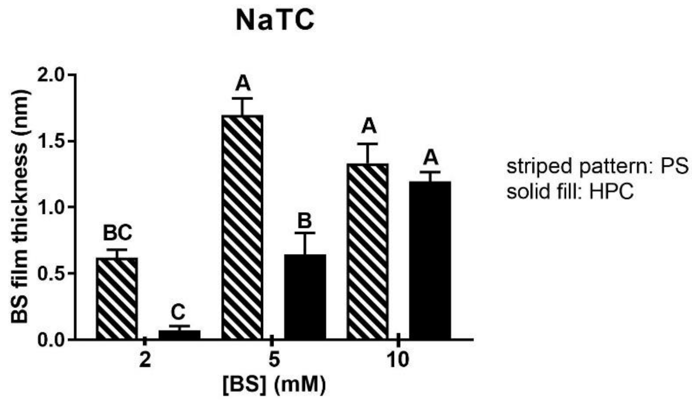

Figure 4.11. Thickness values obtained by the Sauerbrey model after the adsorption of 2, 5, and 10 mM NaTC onto the PS surface and HPC layer. Values represent mean ± SEM and do not consider the HPC layer. Values obtained on the PS surface and HPC layer not sharing a common superscript are statistically significantly different (1-way ANOVA with Tukey's post hoc test for all possible comparisons, p<0.05).

A linear relationship between the changes in dissipation and frequency was also observed during the adsorption of NaTC, regardless of NaTC concentration **(Figure 4.10A).** A linear behavior may suggest that no significant conformational changes occurred on the adsorbed layer as the adsorption of NaTC progressed.[140, 227] Similar findings were found during the adsorption of cellulose derivatives[139] and proteins[227] to solid surfaces and it was suggested that a linear behavior means that the already adsorbed layer does not undergo significant conformational alterations as polymers chains are progressively added to the surface.[139] Similar slopes also indicate that the viscoelasticity of the films was the same, regardless of NaTC concentration, which could suggest that individual NaTC molecules would be adsorbing at all the tested NaTC concentrations (2,5, and 10 mM) and therefore at none of these NaTC concentrations micelles are formed (note that NaTC has a broad CMC (3-18 mM)).

On the other hand, there were observed differences in ΔD vs $\Delta f/n$ in the NaTDC system **(Figure 4.10B)**. The different slope of correlations at different NaTDC concentrations indicates differences in the viscoelasticity of the films. Like NaTC, a linear relationship in the changes of frequency and dissipation was observed for the adsorption of 2 mM NaTDC. However, there were observed shifts in slopes for 5 and 10 mM NaTDC, which may indicate that the nature of the adsorption process for these BSs changed, i.e there were different kinetic regimes **(Figure 4.10B)**. For 5 mM NaTDC, an initial linear behavior was observed, but towards the end of the adsorption process, there was a shift in slopes and an increase in frequency. This result suggests that 5 mM NaTDC may have initially adsorbed onto HPC and produced an elastic film, but towards the end of adsorption, some mass may have been removed from the layer. An initial linear behavior was also observed for 10 mM NaTDC, but there was a shift to a larger dissipation increase with little decrease in frequency (slope=-0.7). This slope change may suggest that there was a viscous second layer of 10 mM NaTDC.[73] A recent study by Euston *et al.* suggested that above the CMC value, BS micelles become the dominant adsorbing species and adsorb over a saturated monolayer of individual BS molecules.[228] Since 10 mM is above the CMC for NaTDC, it is possible that the initial NaTDC molecules adsorbed as individual molecules to create a monolayer. As more micelles formed in the bulk solution, a viscous second layer may have been formed that consisted of NaTDC micelles. It is also possible that the NaTDC micelles were starting to remove some HPC, so some HPC polymer chains were dangling off the sensor, thus increasing the dissipation.

Overall, this QCM-D study has provided qualitative and quantitative information about the adsorption-desorption behaviors of NaTC and NaTDC onto both a hydrophobic surface (PS) and a HPC layer at various BS concentrations below and above their CMC concentrations. Contrasting behaviors were shown between the BS types and concentrations on the PS surface and HPC layer. NaTC adsorbed more slowly and generated more elastic films, regardless of NaTC concentration, compared to NaTDC at higher concentrations (5 and 10 mM). These results suggest that NaTC may adsorb onto PS and the HPC layer as individual monomers at 2, 5, and 10 mM, since these concentrations are at the lower end of its CMC range. However, NaTDC may adsorb in the form of micelles at 10 mM, since this concentration is above the reported CMC, thus creating viscous multilayer films. Additionally, NaTDC seems to be more effective at interacting and displacing HPC, compared to NaTC, which may be due to NaTDC micelles and/or the slightly higher degree of hydrophobicity for NaTDC. Nonetheless, it seems that some HPC remained on the surface, which suggests that HPC is resistant to the displacement by both BSs. The contrasting behaviors obtained on the PS surface support the idea that different BSs may play different roles in lipolysis. Specifically, the slow adsorption of NaTC and irreversible behavior may promote the adsorption of co-lipase/lipase complex, whereas the fast adsorption/desorption of NaTDC may favor the displacement of lipolysis products from the interface.

4.2.2 Effect of Cellulose Ether Molecular Properties

QCM-D study: PS sensors

The sequential adsorption of both cellulose ethers (CEs), HPC and HPC-P, and 10 mM BS onto solid surfaces was investigated using both QCM-D. The aim of this study was to identify whether different molecular properties of CEs impact the strength of interfacial CE layers and their resistance to the adsorption/displacement by different BSs. A concentration of 10 mM BS was used for these experiments because it is within the range of physiological BS concentrations found during lipid digestion in the duodenum in the fed state.[48, 189] **Figure 4.12** shows the representative QCM-D data for the changes in frequency ($\Delta f/n$) and dissipation (ΔD) for the adsorption of HPC and HPC-P followed by the adsorption of 10 mM BS on the CE layers and a final buffer rinse step. When both BSs were first introduced into the flow cell, a decrease in frequency was observed followed by a simultaneous increase in dissipation, which indicates the initial adsorption of the BSs onto the CE layers and the formation of a viscoelastic mixed layer. BS adsorption continued onto the CE layers at a slower rate until a steady state was reached. When buffer was introduced, an increase in frequency and decrease in dissipation was observed, which indicates the removal of mass from a loosely bound viscoelastic layer.[73]

There were observed differences in regards to the adsorption profile of BSs onto the CE layers as well as the desorption of the mixed layer formed. The adsorption of NaTC onto the HPC and HPC-P layers was initially slow (-3.2±1.5 and -1.9±0.3 Hz/min, respectively) until it reached a steady state ~3400 seconds **(Figure 4.12A).** On the other hand, a faster initial adsorption of NaTDC onto the HPC and HPC-P layers was observed during the 1st min of adsorption (-6.7±1.4 and -5.8±1.1 Hz/min, respectively) **(Figure 4.12C).** An increase in frequency during adsorption of NaTDC onto HPC, suggests that some mass (BS, HPC, or HPC+BS) started to be removed during this time. On the contrary, the adsorption of NaTDC onto HPC-P reached a plateau **(Figure 4.12C),** which suggests that HPC-P may have been more resistant to displacement by NaTDC during the adsorption period. Larger changes in dissipation were observed during the adsorption of both BSs onto HPC-P, compared to HPC, which indicates HPC-P-BS mixed layers are more viscous **(Figure 4.12B and D)**.

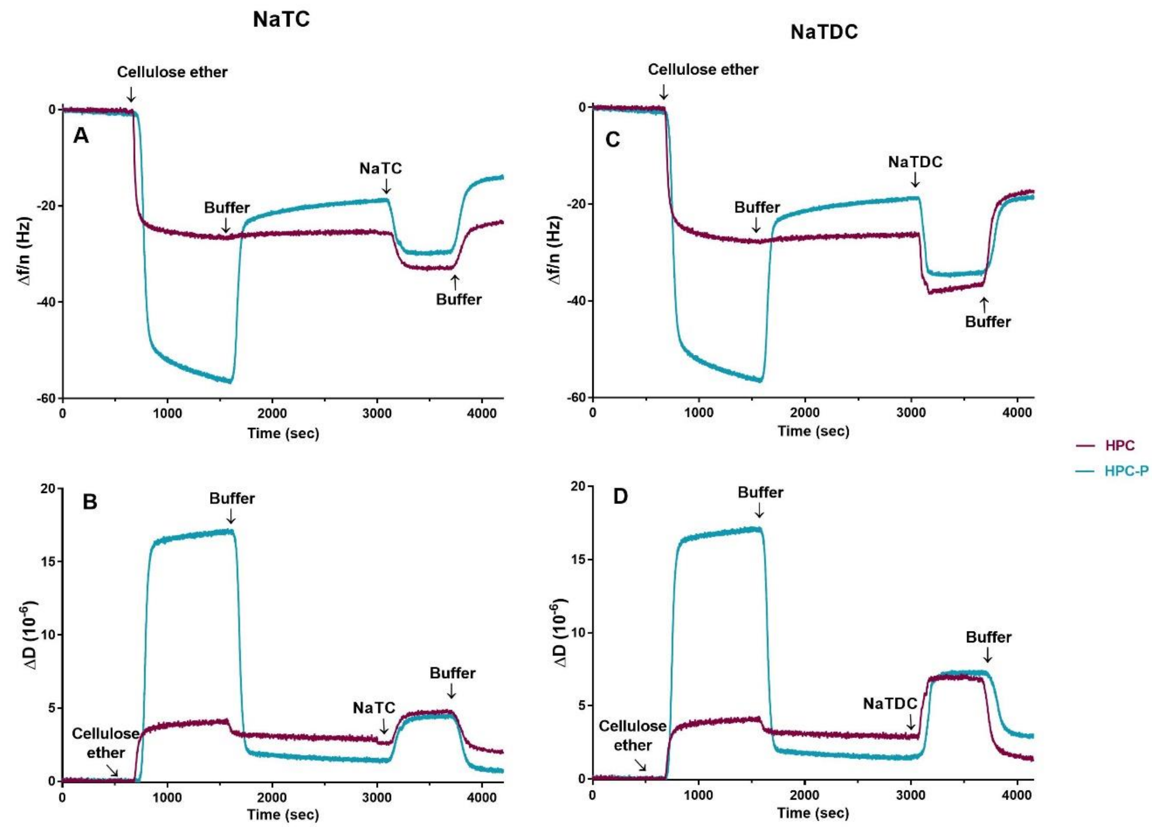

Figure 4.12. Representative QCM-D data of the changes in frequency ($\Delta f/n$) and dissipation (ΔD) versus time measured at the 5th overtone (25 MHz) for the adsorption 10 mM NaTC (A and B) and NaTDC (C and D) onto commercial HPC and HPC-P). Arrows and labels indicate when solutions were introduced in the flow cell after the initial baselines were set.

Figure 4.13B presents the % total mass (BS, CE, or BS+CE) that desorbed from the PS surface during the final buffer rinse. **Figure 4.13C** shows the minimum % of CE mass that may have been displaced by BSs from the PS surface (if it is assumed that all BSs were removed during the buffer rinse). Regarding NaTC, the % total masses desorbed in the HPC systems were not significantly different from the HPC-P systems (p>0.05). Although the mass values for the CE/NaTDC systems are not significantly different from one another (p>0.05), the % of total mass desorbed was slightly larger in the HPC system compared to the HPC-P system **(Figure 4.13B).** In addition, NaTDC displaced a higher amount of HPC than HPC-P **(Figure 4.13C)** indicating that NaTDC was slightly more effective at interacting with HPC than HPC-P at the interface. When comparing the impact of the BS type on the displacement of HPC-P, more mass was removed in the HPC-P/NaTC system than in the HPC-P/NaTDC system during the buffer rinse **(Figure 4.13B**). Additionally, a higher amount of HPC-P was displaced by NaTC than by

NaTDC **(Figure 4.13C),** suggesting that NaTC was slightly more effective at interacting and displacing HPC-P, compared to NaTDC.

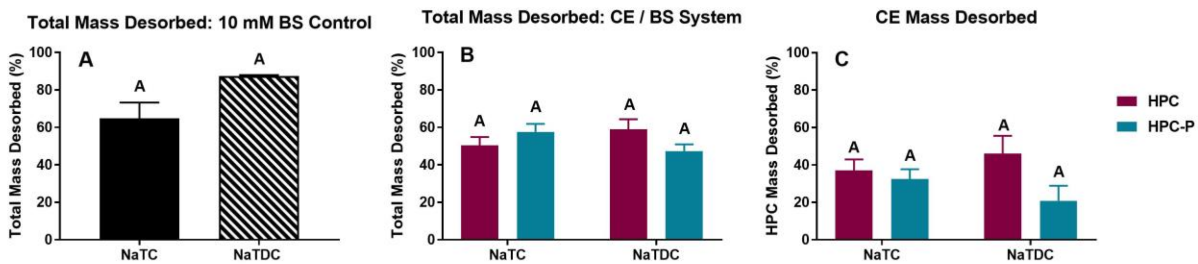

Figure 4.13. % BS (10 mM) desorbed from the PS surface during the buffer rinse (A), % total mass of the CE/BS systems desorbed during the buffer rinse (B) and the minimum % CE removed from the PS surface during the buffer rinse (C). Values were obtained using the Sauerbrey model and represent mean ± SEM. Values of % BS desorbed not sharing a common superscript are statistically significantly different (*two sample t-test, p<0.05*). Values of % total mass of the CE/BS systems not sharing a common superscript are statistically significantly different (1-way ANOVA with Tukey's post hoc test for all possible comparisons, p<0.05).Values of % CE mass removed not sharing a common superscript are statistically significantly different (1-way ANOVA with Tukey's post hoc test for all possible comparisons, p<0.05).

Since both HPC-P and BSs are negatively charged at pH 7, it is expected for there to be unfavorable electrostatic repulsions resulting in weak or even absent interactions between the molecules.[229] Repulsive electrostatic interactions most likely occurred between HPC-P and NaTDC at the interface. NaTDC form micelles at the concentration studied (10mM >CMC NaTDC) which means that the hydrophobic faces of NaTDC molecules were hidden on the micelle core[186] and consequently there was less opportunity for hydrophobic attractions with the hydrophobic groups of the HPC-P layer. However, NaTC molecules may not form micelles at 10 mM due to their broad CMC range (3-18 mM), and most likely adsorbed at the interface as monomers. Consequently, interactions between HPC-P and NaTC will be given by a net balance of hydrophobic attractions and electrostatic repulsions. Since the hydrophobic faces of NaTC are exposed, there was more opportunity of hydrophobic interactions[228], thus allowing for a greater interaction and displacement of HPC-P. Previous studies have suggested that interactions between an anionic polysaccharide (pectin) and (NaTC)[230-233] take place probably through binding between the non-polar faces of the BS and the non-polar methyl groups of the pectin chain.[230-233] In addition, NaTC has one more -OH group than NaTDC, therefore a higher probability of hydrogen bond formation between hydroxyl groups -OH from NaTC and cellulose exists. These results confirm that the BS hydrophobicity and/or formation of micelles play a role in the interactions between BS and the CE adsorbed layer.

It is also possible that the HPC-P interfacial layer was more strongly adhered to the PS surface than the HPC layer. HPC-P is modified with 5-carboxy pentyl groups which creates a more moderate balance of hydrophobicity and hydrophilicity[183] compared to HPC. Hence, it is possible that the extra hydrophobic groups allowed HPC-P for more hydrophobic interactions with the PS surface and to be more resistant to disruption by NaTDC.[159] These findings suggest that the molecular structure of CE affect interactions with BS at the interface.

Figure 4.14 represents the ΔD vs $(\Delta f/n)$ plots for the adsorption of 10 mM BS onto HPC, HPC-P, and the bare PS surface and shows mass increasing from right to left (these values do not consider the CE layer). The solid lines represent the best fits of the data. A large slope (i.e. high dissipation per frequency change) characterizes a soft viscoelastic layer, while a small slope (i.e. small dissipation increase per frequency change) describes more rigid layers.[227] **Figure 4.15** shows the thickness of the BS layers formed after the adsorption of 10 mM BS onto the PS surface, HPC, and HPC-P preformed layers (these values do not consider the thickness of the CE layer). The Sauerbrey model was used to calculate the layer thickness since the changes in dissipation on the PS surface were too low to obtain values with the Voigt model. Frequency and dissipation changes are proportional to the thickness of thin films; as the layer gets thicker, both the negative change in frequency and positive change in dissipation increases.[137, 210]

There were clear differences in the ΔD vs $(\Delta f/n)$ plot during the adsorption of NaTC and NaTDC. Regarding NaTC, a linear trend was observed in the ΔD vs $(\Delta f/n)$ plot for the entire adsorption period of NaTC onto all three surfaces (HPC, HPC-P, and bare PS surface) **(Figure 4.14A)**. This indicates that as the adsorption of NaTC proceeded on all of the surfaces, the adsorbed layers did not undergo significant conformational changes.[139, 227] Larger dissipation and frequency changes were observed during adsorption of NaTC onto the HPC-P layer, compared to the other surfaces **(Figure 4.14A).** Since frequency and dissipation changes are proportional to the thickness of thin film[137, 210], this result corresponded to significantly thicker film of NaTC onto the HPC-P layer ($p<0.05$) **(Figure 4.15A).**

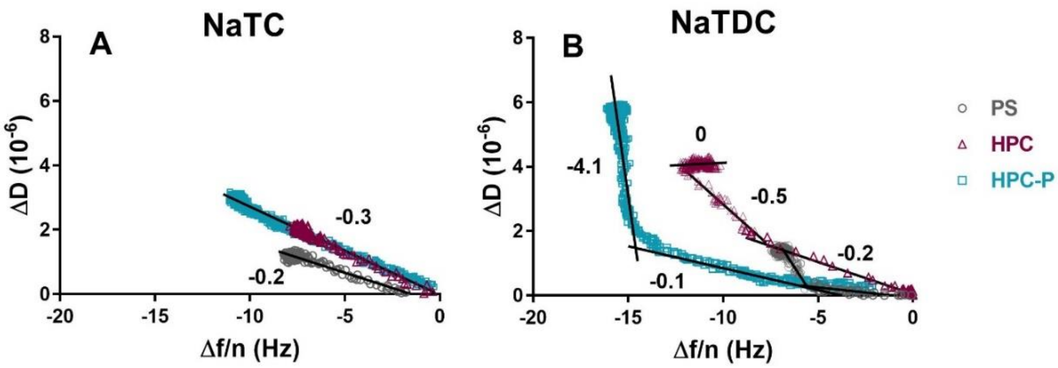

Figure 4.14. Changes in dissipation (ΔD) versus frequency (Δf) measured at the 5th overtone (25 MHz) during the adsorption of 10 mM NaTC (A) and NaTDC (B) onto PS, HPC, and HPC-P.

On the other hand, multiple adsorption processes (i.e. kinetic regimes) were observed during the adsorption of NaTDC onto all three surfaces **(Figure 4.14B)**. A linear behavior with moderately small slopes (i.e. smaller change in dissipation per frequency change) was observed during the initial adsorption of NaTDC. This suggests the formation of a rigid initial NaTDC layer on the PS sensor as well as a rigid mixed layer of CE/NaTDC, with the NaTDC layer formed on HPC-P being similar to the one formed on the bare PS surface and more rigid than the layer formed on HPC. As adsorption of NaTDC proceeded, there was a shift to larger slopes, which indicates that the dissipation changes per added mass increased, thus the adsorbed layer became more viscoelastic.[227] However, these slopes were drastically different between surfaces; specifically, the HPC-P system had a much larger slope than the other surfaces. This result indicates the HPC-P layer became much more viscoelastic and diffuse than the HPC layer and the PS surface, as NaTDC adsorption proceeded. The highest viscoelasticity of the HPC-P system corresponded to a thickest layer **(Figure 4.14B).** The shift in slopes could indicate that NaTDC micelles were beginning to adsorb onto the mixed layer and/or the CE polymer chains were beginning to dangle off of the PS surface.

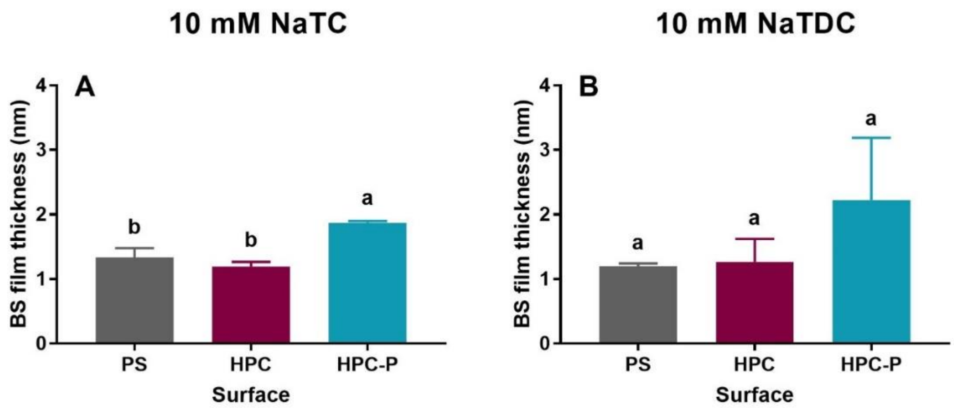

Figure 4.15. Thickness values obtained by the Sauerbrey model after the adsorption of 10 mM NaTC (A) and NaTDC (B) onto PS, HPC, and HPC-P. Values represent mean ± SEM and do not consider the cellulose ether layer. Values obtained for NaTC and NaTDC not sharing a common superscript are statistically significantly different (1-way ANOVA with Tukey's post hoc test for all possible comparisons, $p<0.05$).

Overall, this study has shown that NaTDC is more effective at interacting and displacing HPC, compared to HPC-P. This may be attributed to more electrostatic repulsive interactions between NaTDC and HPC-P due the formation of NaTDC micelles, which hides the hydrophobic domains, that provides a lower opportunity for hydrophobic interactions and prevents some adsorption of NaTDC onto the HPC-P layer. Moreover, NaTC is more effective at displacing HPC-P, compared to NaTDC, which may be attributed to its adsorption onto the HPC-P layer as individual molecules. As a result, a net balance of electrostatic repulsive and hydrophobic interactions may have occurred, which allowed for greater interactions and displacement of HPC-P. Additionally, more hydrophobic interactions between HPC-P and the PS surface may occur, which may allow HPC-P to be more resistant than HPC to displacement by NaTDC. Finally, as the adsorption of NaTDC proceeds onto the CE layers, it produces more diffuse layers, compared to NaTC. This may be attributed to NaTDC micelles adsorbing onto the layers or the CE polymer chain hanging off of the surface.

4.3 Simultaneous Adsorption of Cellulose Ether + BS Mixtures

The simultaneous adsorption of CEs and BSs was carried out in order to gain insight on the impact that dynamic interactions between both components in the bulk has on the adsorption of both surface-active materials to a hydrophobic (PS) solid surface. These experiments were performed using QCM-D and consisted of flowing mixed (CE + BS) solutions for 15 min onto a PS surface, followed by a 25-min exchange of buffer to remove any loosely bound components.

We investigated the effect of type of BS (NaTC and NaTDC) and BS concentration (2,5, or 10 mM) as well as the effect of the molecular properties (i.e. charge, molecular weight, substituent type) of the CE. Three individual experiments were performed for each BS concentration.

4.3.1. Effect of Bile Salt Type and Concentration

The changes in frequency ($\Delta f/n$) and dissipation (ΔD) were monitored as a function of time during the simultaneous adsorption of mixed HPC+BS solutions onto the PS surface. The representative profile corresponding to the adsorption of mixed HPC+BS solutions (containing a fixed amount of HPC (0.1 (w/v)) and 2, 5, or 10 mM BS, respectively) onto the PS surface, followed by a buffer rinse step, is shown in **Figure 4.16**. This figure also shows the adsorption profile of control samples (BS and HPC alone). As a general trend, a rapid decrease in frequency was observed after the injection of the mixed HPC+BS and control samples into the flow cell, indicating the initial adsorption of mass onto the PS surface. This initial response was followed by a smaller decrease in frequency (except for 5 and 10 mM NaTDC mixtures) as the adsorption of the samples proceeded **(Figure 4.16A and C),** showing a slower deposition and suggesting that the mixed HPC+BS/control samples were interacting with the already adsorbed layer, rather than with the PS surface directly.[209] An initial increase in dissipation was associated with frequency changes and observed for all of the samples, which indicates an increase in the viscoelasticity of the HPC+BS mixed layers and the pure BS and HPC layers **(Figure 4.16B and D)**. During the rinse step, a rapid increase in frequency was observed, followed by a steady slower increase in frequency, which suggests the removal of loosely adsorbed polymer and/or biosurfactant molecules from the surface. None of the mixtures was completely washed off from the hydrophobic surfaces, since the final frequency value did not reach 0 Hz **(Figure 4.16)**. Additionally, a decrease in dissipation was observed, indicating that the films became more elastic during rinsing.

Regarding the concentration of the BSs in the mixtures, at all NaTC concentrations and 2 mM NaTDC, the mixtures attained similar frequency values to the HPC control samples after the adsorption period, compared to the BS control samples. Additionally, the changes in frequency observed in these mixtures continued to decrease during the 15-min adsorption period, suggesting a slow adsorption process of mixed HPC-BS solutions at low BS concentrations, which is also similar to the HPC control sample. On the other hand, when the concentration of NaTDC in the mixtures increased to 5 and 10 mM, the frequency values attained after the adsorption period remained similar to the HPC control sample; however, the adsorption dynamics are more similar to the BS control samples, i.e a fast adsorption attaining a steady state within the adsorption period, compared to a slow adsorption for the HPC control sample. These findings suggest that at all concentrations of NaTC and low NaTDC concentrations (2 mM), the adsorption process of the HPC+BS mixtures was being controlled by HPC and that the adsorbed layer may have been mainly composed of HPC. However, as the concentration of NaTDC increased, the adsorption of the mixed systems may have been controlled by NaTDC.

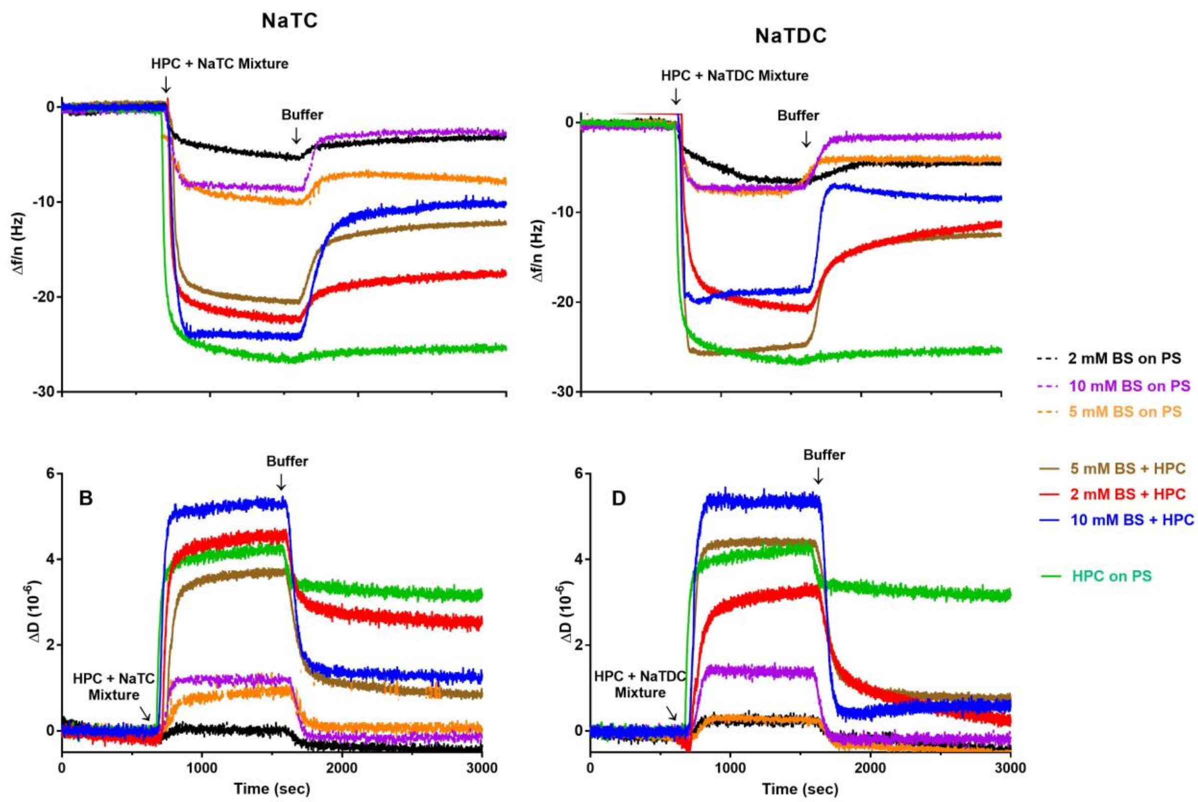

Figure 4.16. Representative QCM-D data of the changes in frequency ($\Delta f/n$) and dissipation (ΔD) versus time at the 5th overtone (25 MHz) for the adsorption of mixed HPC + BS solutions, HPC, and individual BS (2, 5, and 10 mM) onto the PS surface for NaTC (A and B) and NaTDC (C and D). Arrows and labels indicate when solutions were introduced in the flow cell after the initial baselines were set.

After the buffer rinse step, there was most likely a co-existence of both HPC and BSs that remained at the interface since the final frequency values did not reach 0 Hz **(Figure 4.16)**. Previous studies have also indicated that CEs (MC, HPC, HPMC) are able to compete with NaTDC (0.01-100 mM) for the oil-water interface.[11] This finding in the present study is important because even at high BS concentrations (10 mM), HPC was able to compete with the

BSs for the solid interface. The ability for HPC to co-exist on the PS surface might be due to the binding of BSs in the aqueous solution, due to hydrophobic interactions, before the mixture was introduced into flow cell.

Figure 4.17 shows the total adsorbed mass (ng/cm^2) of the HPC+BS mixed systems on the PS surface after the adsorption period and the total mass desorbed (%) during the buffer rinse. Regarding both HPC+BS mixed systems, the total adsorbed mass after the adsorption period was lower than the values obtained for the HPC control sample (0 mM BS) **(Figure 4.17A).** This result suggests that both BSs interacted with HPC in solution, which may have prevented complete adsorption of HPC onto the PS surface. Regarding the 10 mM BS mixtures, the NaTC system had a higher amount of mass adsorbed onto the PS surface **(Figure 4.17A)** as well as a higher % mass desorbed from the PS surface during the buffer **(Figure 4.17B)**, compared to the NaTDC system. These findings suggest that there may have been less interactions between HPC and NaTC, compared to NaTDC, thus resulting in more free NaTC molecules in solution. As a result, this may have given more opportunity for the free NaTC molecules to interact and displace HPC from the PS surface, thus resulting in a higher % mass desorbed during the buffer rinse.

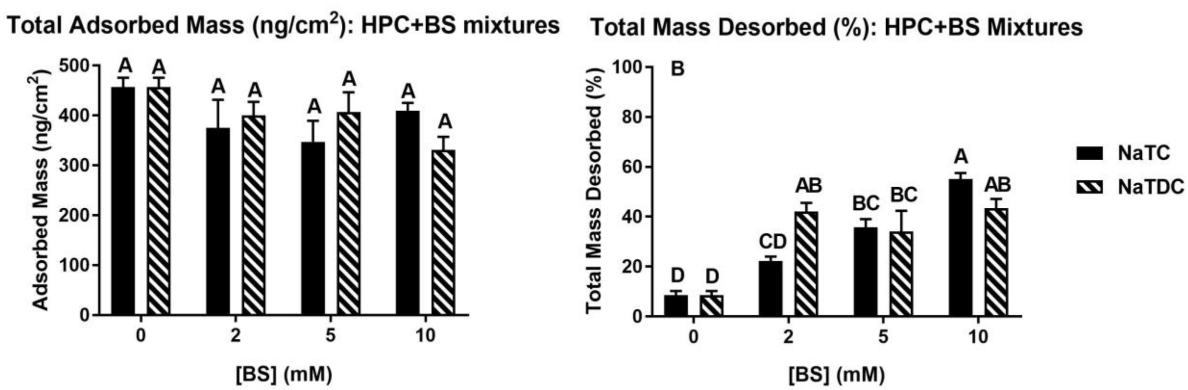

Figure 4.17. Total adsorbed mass (ng/cm^2) (A) and % total mass desorbed of the HPC+BS mixed systems from the PS surface during the buffer rinse (B). Values obtained by the Sauerbrey model and represent mean ± SEM. Values of total adsorbed mass (ng/cm^2) not sharing a common superscript are statistically significantly different (1-way ANOVA with Tukey's post hoc test for all possible comparisons, $p<0.05$). Values of % total mass desorbed not sharing a common superscript are statistically significantly different (1-way ANOVA with Tukey's post hoc test for all possible comparisons, $p<0.05$).

Figure 4.18 represents the changes in dissipation (ΔD) vs frequency ($\Delta f/n$) for the adsorption of mixed HPC+BS solutions, HPC alone, and the individual BS onto the PS surface.

Regarding the NaTC systems, at low NaTC concentrations (2 and 5 mM), the HPC+NaTC mixtures seemed to undergo similar conformational changes at the interface that of the HPC control sample (i.e. a linear adsorption regime). However, in the 10 mM NaTC mixture, an initial linear behavior was observed, followed by gradual increases in dissipation with smaller decreases in frequency as adsorption of the mixture proceeded onto the PS surface **(Figure 4.18A)**. Regarding the mixed HPC+NaTDC solutions **(Figure 4.18B),** while the 2 mM NaTDC mixture showed similar conformational changes at the interface to that of the HPC control sample, when the concentration increased to 5 and 10 mM, the trend lines looked more similar to the BS control samples. These results support the idea that at low NaTDC concentrations and all NaTC concentrations, HPC may have been the main contributor to the changes in dissipation and frequency in the mixtures; however, at higher NaTDC concentrations, it seems like the NaTDC may have controlled the adsorption process. Differences between BS types were also observed. For example, at 10 mM BS, the mixed NaTDC solution showed a sharper increase in dissipation than the mixed NaTC solution, as the frequency increased. This result may indicate that mixed HPC complexes formed by both BSs were starting to be removed/dangling from the surface, which increased the dissipation. However, the complex formed with NaTDC micelles may have been more viscous, compared to the NaTC, as indicated by the sharper increase in dissipation. Previous research on BS-binding ability of CEs[11, 21, 23] have suggested that BSs are bound or "sequestered" by HPMC mainly through hydrophobic interactions, which consequently, may impact the amount of BS that adsorbed to the interface.[21] Previous mechanical spectroscopy studies have also indicated that HPC interacts with NaTDC at a range of concentrations (10-100 mM) in the aqueous phase, which lead to the formation of HPC+NaTDC hydrophobic aggregates regardless of concentration.[23] Therefore, in our study, hydrophobic aggregates might have been formed before the HPC+NaTDC mixture was introduced into the flow cell. As a result, these aggregates may have adsorbed to the PS surface, but the strong desorption property of NaTDC most likely influenced the removal before the buffer rinse. On the other hand, there may have been less interactions HPC and the individual molecules of NaTC in the aqueous solution; therefore, during adsorption it is likely they could not really compete with HPC for the PS surface.

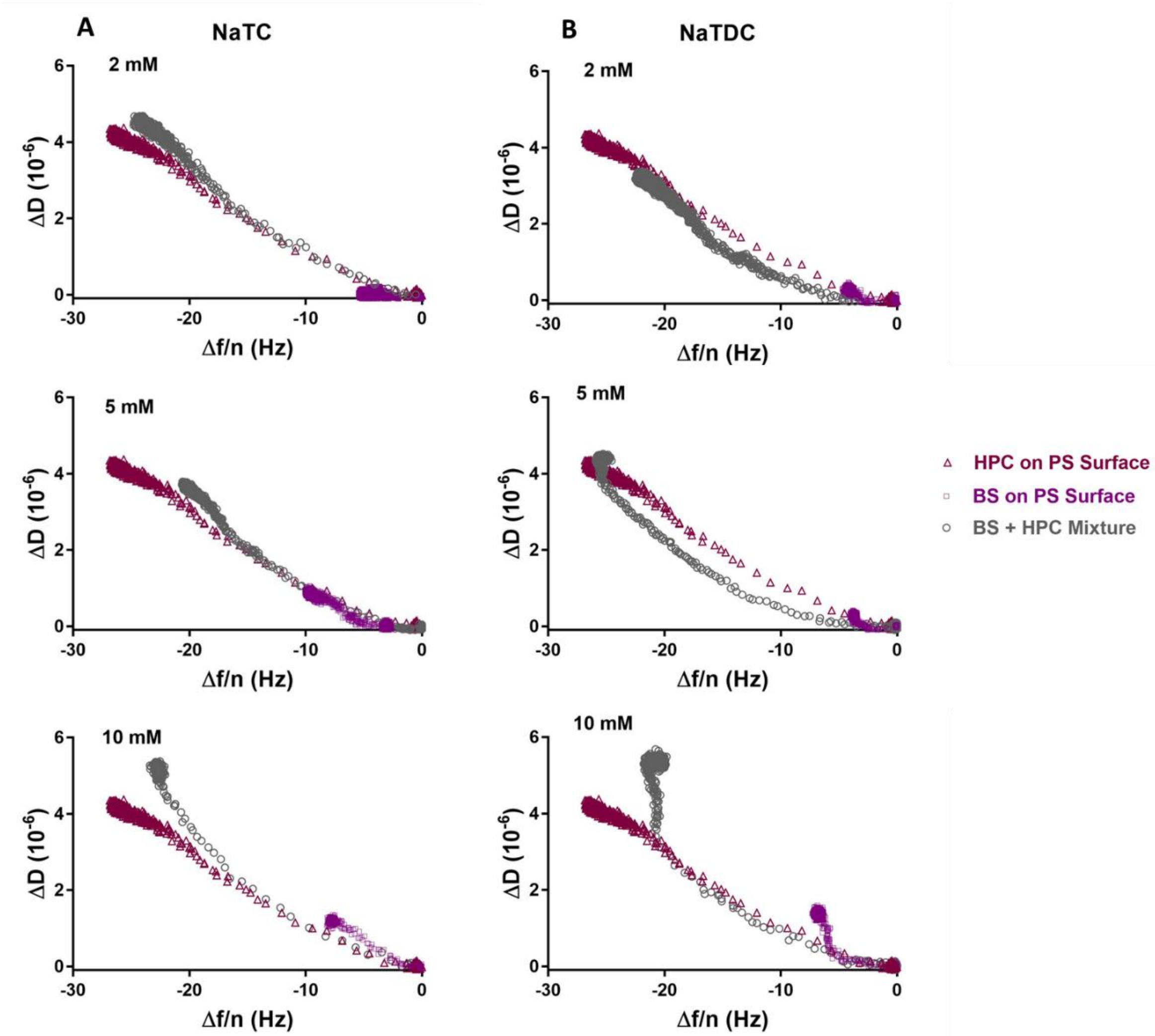

Figure 3.18 Change in dissipation (ΔD) versus frequency (Δf) at the 5th overtone (25 MHz) during the adsorption of mixed HPC + BS solutions, HPC, and individual BS (2, 5 and 10 mM) onto the PS surface for NaTC (A) and NaTDC (B).

Overall, this study has shown that HPC can compete with both BSs for the hydrophobic surface and that HPC-BS complexes are formed at the surface. The type and concentration of BS seem to impact the interactions between HPC and BSs in the bulk, which may impact the adsorption dynamics of the mixed solutions. Specifically, the adsorption of all NaTC mixed solutions is relatively slow and form films that resemble the HPC control sample. On the other hand, 5 and 10 mM NaTDC micelles seem to control the adsorption dynamics of the mixtures through the formation of hydrophobic aggregates and remove some of the complex even before the buffer rinse. Additionally, HPC may interact more with NaTDC in the bulk, compared to NaTC, resulting in less free NaTDC molecules to compete with HPC for the PS surface.

4.3.2 Effect of Cellulose Ether Molecular Properties

The representative profile corresponding to the changes in frequency ($\Delta f/n$) and (ΔD) during the simultaneous adsorption of mixed CE + 10 mM BS onto a hydrophobic PS surface, followed by a buffer rinse step, is shown in **Figure 4.19.** As a general trend, a rapid decrease in frequency was observed after the injection of the mixed CE+BS and control samples into the flow cell, indicating the initial adsorption of mass onto the PS surface. This initial response was followed by a smaller decrease in frequency (except for HPC + NaTDC) as the adsorption of the samples proceeded **(Figure 4.19A and C),** showing a slower deposition and suggesting that the mixed CE+BS systems and control samples were interacting with the already adsorbed layer, rather than with the PS surface directly.[209]

An initial increase in dissipation was associated with frequency changes and observed for all of the samples, which indicates an increase in the viscoelasticity of the CE+BS mixed layer and the pure BS and CE layers **(Figure 4.19B and D)**. However, during the adsorption period, HPC-P+BS mixtures showed a larger change in dissipation, regardless of BS type, compared to the HPC+BS mixtures **(Figure 4.19B and D)**. Specifically, the mixed HPC-P+NaTC had an initial change in dissipation of 11 x 10^{-6}/min, whereas the HPC+NaTC mixture had a change of 3.4 x 10^{-6}/min. A similar dissipation change was observed in the HPC-P+NaTDC system. This larger increase in dissipation during the adsorption of the HPC-P+BS mixtures indicated a more viscous adsorbed layer, compared to the HPC+BS mixtures. It is important to note that the dissipation for both HPC-P+BS mixtures is very similar to the dissipation for the HPC-P control sample. However, the frequency changes are different from one another. This finding indicates that the BSs may impact the amount of HPC-P adsorbed to the PS surface, but viscous film may contain a majority of HPC-P.

After the adsorption period, both HPC-P mixtures attained frequency values more similar to the HPC-P control samples, compared to the BS control samples. Additionally, the changes in frequency observed in these mixtures continued to decrease during the 15-min adsorption period, suggesting a slow adsorption process of mixed HPC-P+BS solutions at low BS concentrations, which is also similar to the HPC-P control sample. Both HPC mixtures attained similar frequency values to the HPC control samples after the adsorption period, compared to the BS control samples; however, the adsorption dynamics for the NaTDC mixture is more similar to the NaTDC control samples, i.e a fast adsorption attaining a steady state within the adsorption period, compared to a slow adsorption for the HPC control sample. These results suggest the adsorption process for the HPC-P mixtures was being controlled by HPC-P and that the adsorbed layer may have been mainly composed of HPC-P, whereas the adsorption for the HPC+NaTDC mixture may have been controlled by the NaTDC and the adsorption for the HPC+NaTC mixture may have been controlled by HPC.

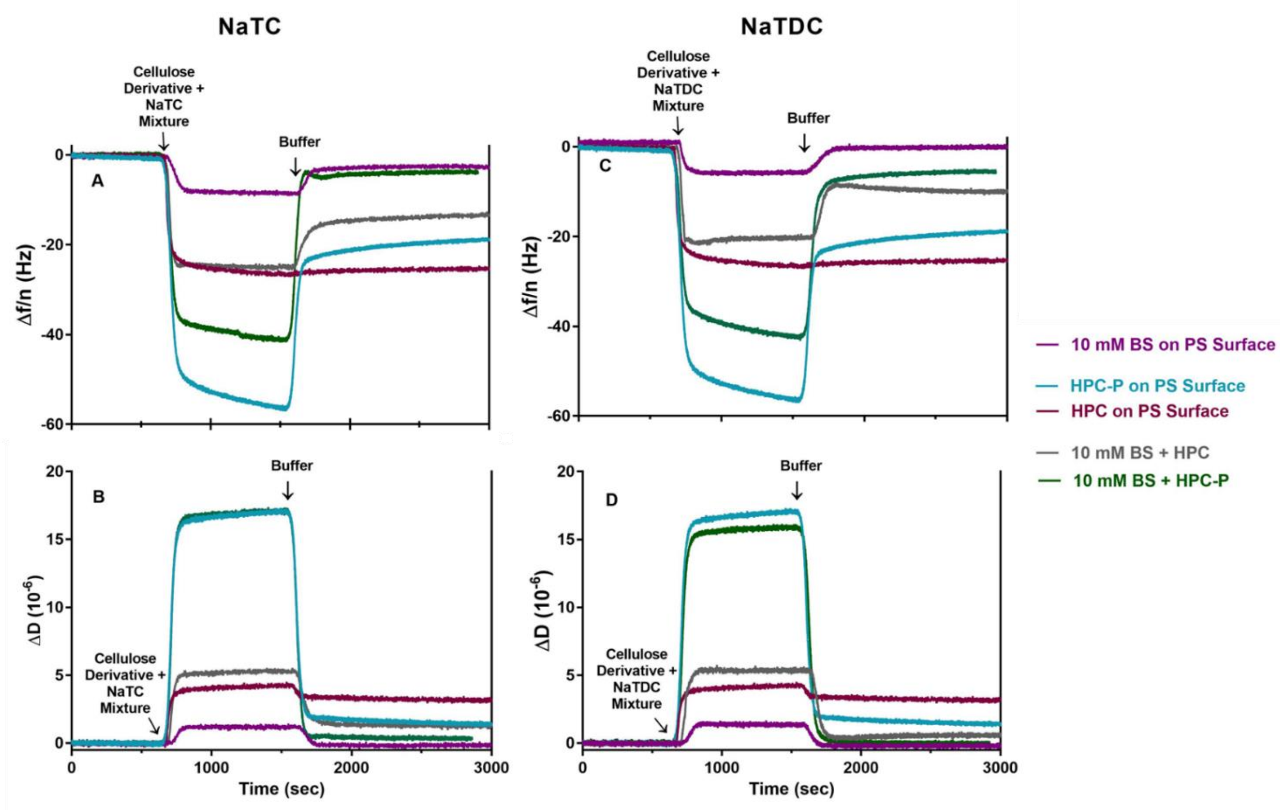

Figure 4.19. Representative QCM-D data of the changes in frequency ($\Delta f/n$) and dissipation (ΔD) versus time at the 5th overtone (25 MHz) for the co-adsorption of mixed CE + BS, HPC, HPC-P, and BS (10 mM) onto the PS surface for NaTC (A and B) and NaTDC (C and D). Arrows and labels indicate when solutions were introduced in the flow cell after the initial baselines were set.

Figure 4.20 represents the changes in dissipation (ΔD) vs frequency ($\Delta f/n$) for the adsorption of mixed CE+BS solutions, HPC alone, and the individual BSs onto the PS surface. During the initial adsorption of both HPC-P and HPC/BS mixtures onto the PS surface, similar conformational changes were observed to that of the CE control samples (i.e a linear adsorption regime). However, the changes in dissipation began to level off for both HPC-P mixtures as the frequency continued to decrease, whereas a sharper increase in dissipation was observed for the HPC/NaTDC mixture (which is similar to the NaTDC control sample) and gradual increases in dissipation were observed for the HPC/NaTC mixture. This result suggests that both of the mixed HPC-P+BS layers became more rigidly attached to the PS surface, whereas the mixed HPC complexes formed by both BSs were starting to be removed/dangling from the surface. These findings support the idea that HPC-P may have controlled the adsorption dynamics of both mixtures, because the trend lines are similar to that of the HPC-P control sample, whereas both BSs may have controlled the adsorption process in the HPC mixtures.

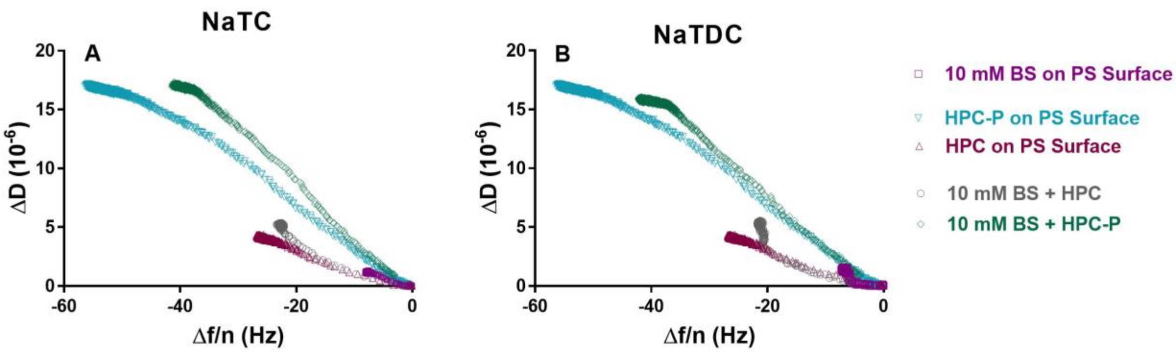

Figure 4.20: Change in dissipation (ΔD) versus frequency (Δf) at the 5th overtone (25 MHz) during the adsorption of mixed CE + BS solutions, CE, and individual BS (10 mM) onto the PS surface for NaTC (A) and NaTDC (B).

Figure 4.21 shows the total adsorbed mass (ng/cm^2) of the CE+BS mixed systems on the PS surface after the adsorption period and the total mass desorbed (%) during the buffer rinse. Regarding both CE+BS mixed systems, the total adsorbed mass (ng/cm^2) was lower compared to the CE control samples. This result suggests that both BSs interacted with both CEs in solution, which prevented complete adsorption of the CEs to the PS surface. However, after the buffer rinse, both HPC-P mixtures had a significantly larger mass desorbed ($p<0.05$) compared to the HPC mixtures. This result suggests that the HPC-P + BS complexes formed in the bulk might be less surface active on the PS surface, compared to the HPC + BS complexes, thus resulting in almost complete desorption.

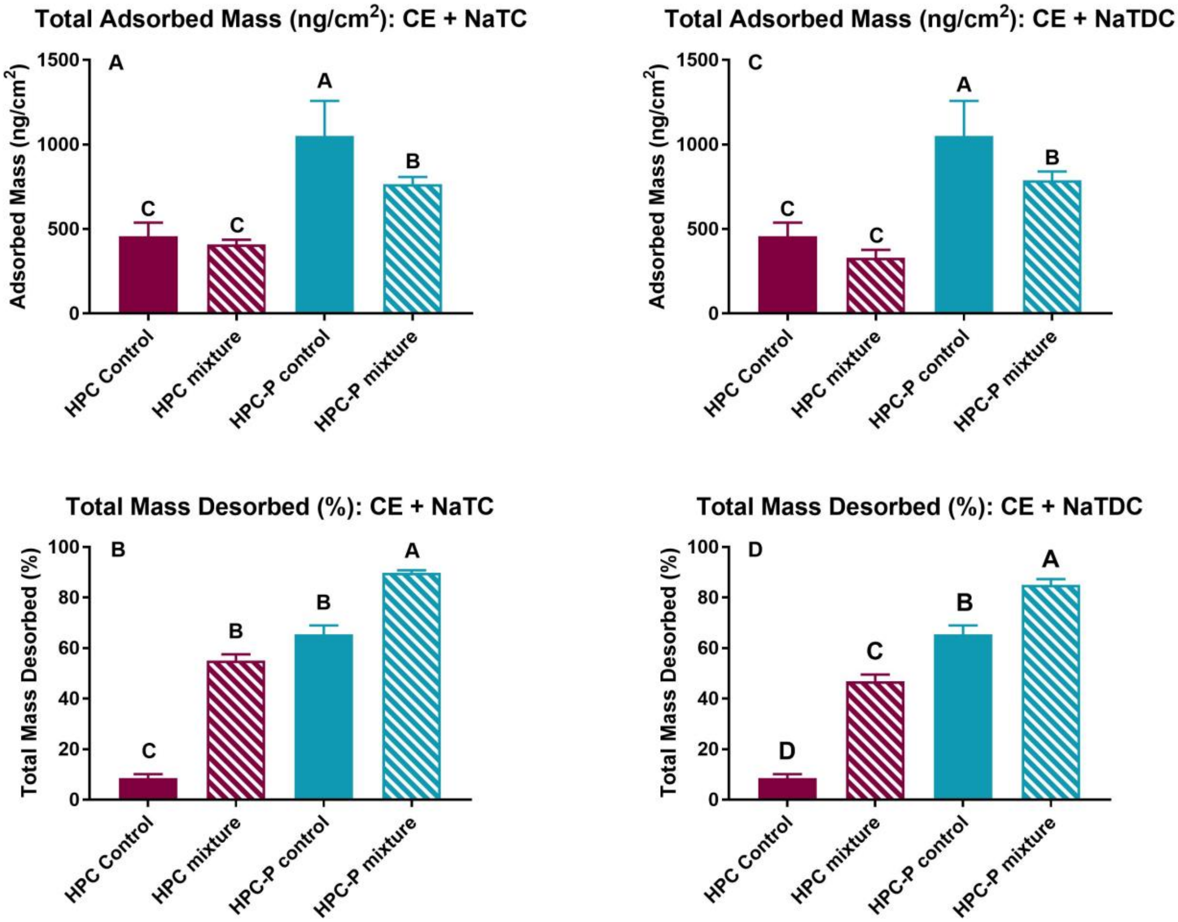

Figure 4.21. Total adsorbed mass (ng/cm^2) and % total mass desorbed of the CE+BS mixed systems from the PS surface during the buffer rinse for NaTC (A and B) and NaTDC (C and D) systems. Values obtained by the Sauerbrey model and represent mean ± SEM. Values of total adsorbed mass (ng/cm^2) not sharing a common superscript are statistically significantly different (1-way ANOVA with Tukey's post hoc test for all possible comparisons, $p<0.05$). Values of % total mass desorbed not sharing a common superscript are statistically significantly different (1-way ANOVA with Tukey's post hoc test for all possible comparisons, $p<0.05$).

As mentioned previously, both HPC-P and NaTC/NaTDC are negatively charged in pH 7, so it is expected for there to be unfavorable electrostatic repulsions resulting in weak or even absent interactions between the molecules.[229] However, since HPC-P is hydrophobically modified, with pendent carboxyl groups, strong interactions might exist between the mixed HPC-P + BS solutions. Hydrophobically modified polymers (hm-polymers) contain hydrophobic groups that are attached either along the backbone or as end groups. Hydrophobic associations can occur between these hydrophobic groups to form micelle-like clusters and cross-links between the chains. When surfactants are introduced into aqueous systems with hm-polymers, the surfactant can associate around the hm-polymer clusters to form mixed micelles.[229, 234-235] Panmai *et al.* investigated the interactions between hydrophobically modified hydroxyethylcellulose (hmHEC) and surfactants using steady-state fluorescence.[234] They found that when surfactants were introduced to the system, mixed hmHEC + surfactant micelles were formed which induced the formation of polymer cross-linking. However, as surfactant concentration increased the cross-linking between the mixed micelles decreased due to repulsive interactions between the micelles.[234]

In this study, a possible mechanism during the adsorption/desorption of the HPC-P mixtures is proposed. Before the injection of the HPC-P+BS mixtures, some BSs may have associated with the attached pendent carboxyl end groups in HPC-P to form mixed micelles in the bulk solution. However, the presence of NaTDC micelles, which have hidden hydrophobic faces, may have caused more electrostatic repulsions between the micelles, therefore decreasing the cross-linking between the mixed micelles. On the other hand, the individual NaTC molecules may have induced more cross-linking between the mixed micelles. During the adsorption of mixed HPC-P + BS solutions a high ΔD was observed (~17×10^{-6}), indicating a viscous film formed on the PS surface **(Figure 4.19).** However, when buffer was introduced into the system, these mixed micelles may have been easily removed from the PS surface, which decreased the ΔD to ~$0 \mathrm{x} 10^{-6}$, indicating a rigid film **(Figure 4.19).** More mass may have been removed from the HPC-P + NaTC mixture due to the increased cross-linking between the mixed micelles, compared to the HPC-P + NaTDC mixture. As mentioned previously, it is possible that the mechanism of action of impacting NaTDC adsorption for the HPC mixtures might include hydrophobic interactions with NaTDC in the bulk solution to form HPC+NaTDC aggregates. On the other hand, it is possible that there were less interactions formed between NaTC and HPC, which allowed more HPC to adsorb to the surface.

Overall, this study showed that polymer charge/hydrophobicity affects the interactions between CEs and BSs in the bulk. Specifically, the surface layers containing HPC-P-BS complexes formed in the bulk might be less resistant to displacement by BSs than layers formed by HPC-BS complexes. Also, HPC-P-BS complexes formed in the bulk might be less surface active than the HPC-BS complexes. The BS structure may also affect the interactions between CEs and BSs in the bulk, which affects adsorption. Specifically, the CE-NaTDC complexes may be more surface active than the CE-NaTC complexes formed on the PS surface.

4.4 Comparison of Sequential and Simultaneous Adsorption Experiments

A comparison of the sequential and simultaneous adsorption experiments was carried out to see if the route of formation of the interfacial had an impact on the displacement of CEs by BSs. We first compared the effect of BS type and concentration as well as the effect of the molecular properties (i.e. charge, molecular weight, substituent type) of the CE.

4.4.1 Effect of Bile Salt Type and Concentration

Figure 4.22 shows relative amount of HPC mass desorbed (ng/cm^2) from the PS surface during the buffer rinse of the sequential and simultaneous adsorption experiments. This graph considers the BS control mass that desorbed from the PS surface. For both BSs, there was a considerably higher amount of HPC mass desorbed from the PS surface when the mixed layer was formed sequentially, compared to simultaneously in the bulk. This may be due to a couple of factors, i) HPC + BS complexes formed simultaneously in the bulk may have been more surface active and strongly adsorbed to the interface, so they were more difficult to displace, and/or ii) HPC might have been more effective at binding to BSs in the bulk, which would have reduced the amount of free BSs available to displace HPC. Additionally, the difference between the amount of HPC that desorbed during the sequential and simultaneous adsorptions was much more pronounced for NaTDC, compared to NaTC. This result may indicate that the HPC-NaTDC complexes were strongly adsorbed to the PS surface and more resistant to displacement by BSs compared to the HPC-NaTC complexes and/or the pre-adsorbed HPC layer was weaker and considerably easier to be displaced by NaTDC.

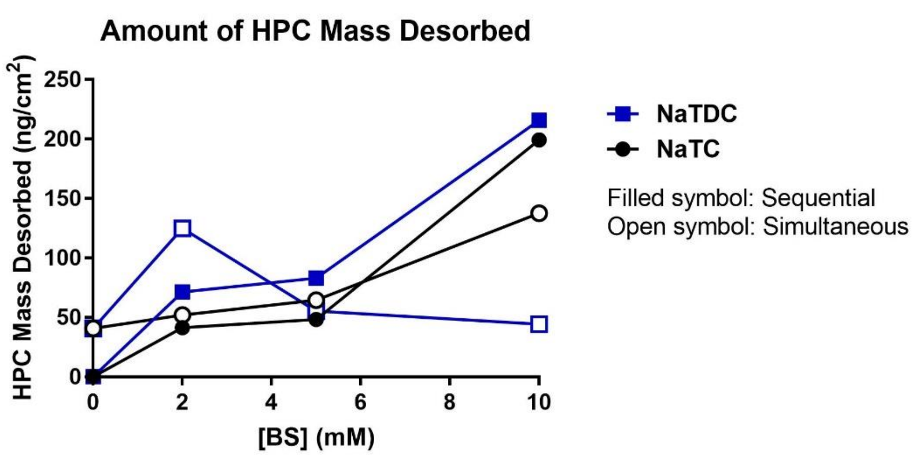

Figure 4.22. The relative amount of HPC mass desorbed (ng/cm^2) from the PS surface during the buffer rinse of the sequential and simultaneous adsorption experiments. These values consider the mass desorbed of the BS control samples from the PS surface.

4.4.2 Effect of Cellulose Ether Molecular Properties

Figure 4.23 shows relative amount of CE mass desorbed (ng/cm^2) from the PS surface during the buffer rinse of the sequential and simultaneous adsorption experiments using 10 mM BS. This graph considers the 10 mM BS control mass that desorbed from the PS surface. Regarding HPC-P, there was a considerably higher amount of mass desorbed when the mixed layers were formed simultaneously, than when they were formed sequentially. This finding may be due to a couple of factors, i) HPC-P was more effective at forming strong pre-adsorbed layers and/or ii) the HPC-P-BS complexes formed simultaneously were less surface active.

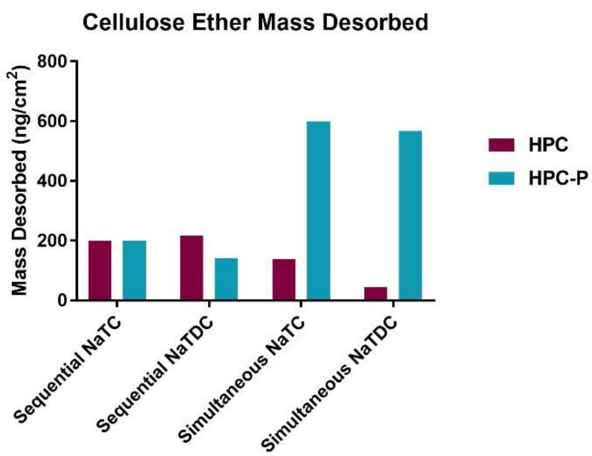

Figure 4.23. The relative amount of CE mass desorbed (ng/cm^2) from the PS surface during the buffer rinse of the sequential and simultaneous adsorption experiments using 10 mM BS. These values consider the mass desorbed of the 10 mM BS control samples from the PS surface.

Overall, these comparisons suggest that the way that mixed CE-BS layers were formed played a decisive role on the surface layer properties and displacement by BSs and it depended on the CE type. The non-ionic, more viscous HPC seemed to be more effective at binding to BSs in the bulk and reducing the amount of free BSs available to interact and displace material from the surface. Additionally, HPC seemed to have also created a stronger layer formed by more surface active mixed complexes. On the other hand, the anionic, HPC-P with more hydrophobic character might have been more effective at forming a pre-adsorbed layer onto the PS surface, that was more resistant to displacement by BSs.

4.5 *In vitro* Digestion of Emulsified Lipids

The purpose of this study was to investigate the influence of the interfacial and bulk properties of CEs as well as BS type on the digestion of emulsified lipids as they passed through an *in vitro* digestion system that simulated conditions occurring within the GIT.[177] In these experiments, we examined the potential of HPC-stabilized emulsions to decrease the rate and extent of intestinal lipolysis and compared it with emulsions stabilized with a non-ionic small molecule surfactant commonly used in the food industry, Tween 20[12, 109]. Our control samples were emulsions stabilized with an individual BS (NaTC or NaTDC) since one major role that BSs play in lipid digestion is to emulsify fats[19-20]. Additionally, previous work revealed that adding just oil to the simulated digestion mixture as the control sample did not mix well with the other components and remained at the top of the mixture. Since the sequential studies suggested that HPC-P was more resistant to the displacement by BSs, compared to HPC, **(Chapter 4.2)** it is possible that this polymer may have more potential to decrease the rate and extent of lipolysis. However, due to the limiting amount of HPC-P that could be synthesized for this project, the *in vitro* digestion experiments were not performed using emulsions stabilized with HPC-P.

We also investigated the impact of the BS hydrophobicity in the *in vitro* digestion of emulsified lipids by employing an individual BS (NaTC or NaTDC) to simulate intestinal conditions. Different interfacial activities of NaTC and NaTDC were observed on the hydrophobic PS surface at various BS concentrations (2, 5, and 10 mM) **(Chapter 4.2)**; it was shown that NaTDC (5 and 10 mM) adsorbed more rapidly and desorbed to a greater extent from the PS surface during a buffer rinse, whereas all concentrations of NaTC adsorbed more slowly and a higher proportion remained on the surface after the buffer rinse. Therefore, it is possible that these different BSs, which differ in one hydroxyl group at the C7 position, may perform different roles during the duodenal digestion process.[89] We performed these experiments using a BS concentration (10 mM) that is within the physiological range found during lipid digestion in the duodenum in the fed state.[48, 189] However, since the bulk concentration of BS affected the amount of NaTC or NaTDC that remained on the PS surface after a buffer rinse (Section 3.2), further experiments should be performed with the other BS concentrations that were tested in the sequential and simultaneous adsorption experiments (2 and 5 mM). The digestion protocol used in this study considers the passage of the o/w emulsions through the small intestine phase and incorporates a gastric pH-conditioning step before the intestinal phase to take into account the effect of the gastric phase.[9, 25] The influence of type of emulsifier (polymeric or small molecule surfactant) and type of BS on the droplet sizes of emulsified lipids before and after *in vitro* digestion is evaluated, followed by an evaluation of the lipid digestion profiles.

4.4.1 Droplet Size Distributions of Fresh O/W Emulsions

Emulsions were left for one hour before determining the particle size or carrying out any further treatment and/or analysis. The droplet size distributions of fresh o/w emulsions are presented in **Figure 4.24**. HPC emulsions showed larger droplet sizes (3.8 ± 0.1 μm) than Tween 20 emulsions (0.5 ± 0.1 μm) and emulsions stabilized with BSs (NaTC = 0.2 ± 0.0 μm; NaTDC = 0.4 ± 0.1 μm). A monomodal, narrower distribution was observed in HPC emulsions compared with the rest of emulsions. Previous studies have also reported that emulsions stabilized with polymeric surfactants, like proteins[236] and HPMC[12], have larger droplet sizes compared to small molecule surfactants, like Tween 20. Polymeric surfactants are large molecules with a more irregular distribution pattern of hydrophobic and hydrophilic sections on the polymer backbone. They slowly diffuse and tend to adsorb to an interface forming “trains,” “loops,” and “tails, typically forming interfacial layers of high viscoelasticy.[44, 237-238] The thickness of the polymeric layer created at the interface has been correlated with emulsion stability against coalescence.[44] For instance, as the thickness of the interfacial layer increases, strong steric repulsion interactions become more significant, which may help prevent droplet aggregation.[44] On the other hand, small molecule surfactants tend to adsorb onto interfaces by arranging their hydrophilic head group in the aqueous phase and the hydrophobic tail within the non-aqueous phase. Since they are smaller in size and do not have conformational constraints (i.e. the hydrophilic and hydrophobic region are at the ends of the molecule) compared to polymeric surfactants, they are very mobile, so they can rapidly adsorb and pack more efficiently at the interface during emulsification forming smaller droplets with compact adsorbed layers. However, small molecule surfactants, do not form highly viscoelastic interfacial films.[12, 44, 237-238].

Tween 20-stabilized emulsions showed a bimodal distribution with a small volume of larger droplet sizes (~4.8 μm). It is possible that 1% Tween 20 was not a high enough concentration to effectively emulsify droplets in emulsions containing 20% oil (w/w). Small molecule surfactants can lower the interfacial tension more than polymeric surfactants; however, they have a lower surface affinity than polymeric surfactants, so a higher concentration of surfactant in the bulk is needed to get a specific adsorption.[44, 239] The same concentration (1%) was chosen for all surfactants tested in order to compare results between samples.

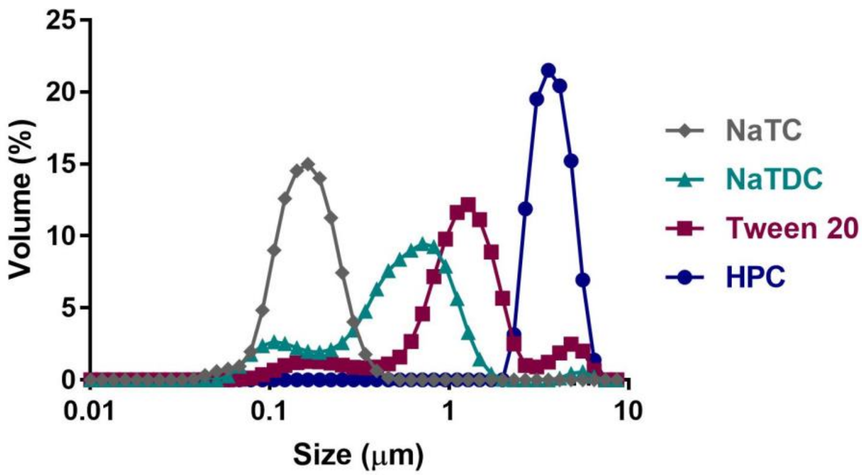

***Figure 4.24. Volume particle size distributions of fresh 20 % olive o/w emulsions stabilized with 1% wt Tween 20* (■), *HPC* (●), *NaTDC (*▲), *and NaTC* (◆).**

The smaller mean particle sizes observed in the emulsions stabilized with NaTC and NaTDC (0.2 ± 0.0 and 0.4 ± 0.1 μm, respectively), compared to Tween 20 (0.5 ± 0.1 μm), are attributed to the unique molecular structure of the BSs. The flat steroidal structure of BS molecules leads to a facial amphilicity, with polar hydroxyl groups on the concave side and methyl groups on the convex side, whereas classical surfactants, like Tween 20, have a distinct hydrophilic head and hydrophobic tail.[20, 228] As a result, this structure of BSs contributes to their extremely fast adsorption, very high surface activity, and lower surface pressures on surfaces compared to classic surfactants.[20] Regarding the type of BS, the smaller particle sizes and monomodal size distribution observed for NaTC, compared to NaTDC with a bimodal distribution, suggests that the hydrophobicity of BSs may impact their adsorption to interfaces.[89] This finding is in agreement with their adsorption behaviors onto the solid hydrophobic interface **(Chapter 4.2, Figure 4.8).** A slower adsorption of NaTC to the solid surface was observed and a higher % of mass remained on the surface after a buffer rinse, compared to NaTDC **(Figure 4.8A).** Therefore, in this context, NaTC may have adsorbed more strongly to the o/w interface during emulsification and remained at the interface to form small droplets, whereas NaTDC may have exchanged readily with the interface, thus have a shorter residence time at the interface.

4.4.2 Droplet Size Distribution/Quantification of FFAs Release during *in vitro* Lipolysis

A pH stat method was employed to determine the rate and extent of lipid digestion of the o/w emulsions (Experimental Section). The *in vitro* digestion experiments were carried out at least 1 h after emulsion preparation in order ensure emulsion stability against creaming. In order to study if BS hydrophobicity has an impact on the digestion of emulsified lipids, NaTC or NaTDC was used as a representative BS in the simulated intestinal fluid. The percentage (%) of titratable FFAs released during lipolysis (which is proportional to the total fatty acid released) was calculated from the volume of NaOH required to maintain a constant pH during 2 hours of lipolysis. **Figure 4.25** shows the lipid digestion profiles (% FFA versus time) of HPC, Tween 20, and BS-stabilized o/w emulsions in the presence of NaTC or NaTDC during lipolysis. The best fit between the experimental digestion data and a mathematical model, described in the Experimental Section**,** was established for each sample. **Figure 4.26** shows the droplet size distributions of the o/w emulsions after being exposed to *in vitro* gastric (pH) and intestinal conditions for 1 h and 2 h, respectively, with either NaTC or NaTDC.

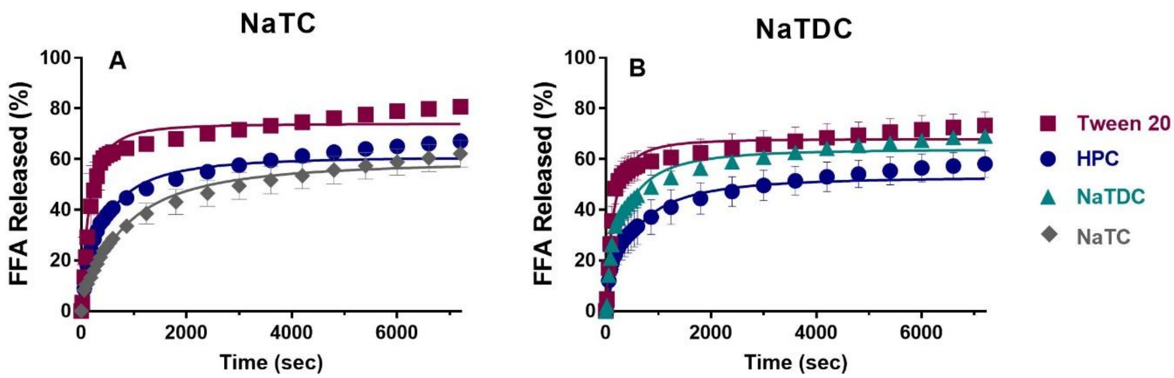

Figure 4.25. The percentage of FFAs released from 20% wt olive o/w emulsions stabilized with 1% wt Tween 20 (■), HPC (●), NaTDC (▲), and NaTC (◆) when NaTC (A) or NaTDC (B) was added during the simulated intestinal step. Values represent mean ± SEM.

In general, there was an initial rapid increase in the release of FFAs from all of the emulsions during the first 10 min of digestion, followed by a more gradual increase as time progressed until a quasi-steady state was reached **(Figure 4.25)**. There may be several factors explaining why the % of FFAs released became gradual after 10 min: 1) the accumulation of surface active FFAs and intermediate products generated during the initial stages of lipolysis at the o/w interface may inhibit lipase activity; at high concentrations, because of their high surface activity, can compete/displace lipase molecules from the interface[47, 240], 2) the formation of a crystalline phase of calcium-complexed fatty acids around the lipid droplets may prevent lipase molecules from gaining access to the undigested lipid droplets[241], and/or 3) the presence of emulsifiers may interfere with the actions of BSs and lipase-colipase, thus impacting the rate and extent of lipolysis.[9, 13, 16, 21] After lipolysis, the mean particle size of all the o/w emulsions decreased, except the NaTC-stabilized emulsion **(Figure 4.26)**. Additionally, a slight decrease in droplet volume (%) was observed for all of the o/w emulsions. Smaller particle diameters and droplet volume may be attributed to the digestion of lipids by pancreatic lipase and the formation of mixed BS micelles containing lipolysis products, like monoglycerides and FFAs.[9, 12-13] The increase in droplet size for the NaTC-stabilized emulsion can be attributed to coalescence of the oil droplets, which may have been caused by a couple of factors: i) depletion and/or bridging flocculation induced by the intestinal components, like BSs, or ii) the displacement of NaTC from the lipid droplet surface by the BS, thus causing poor stability to droplet coalescence.[12-13]

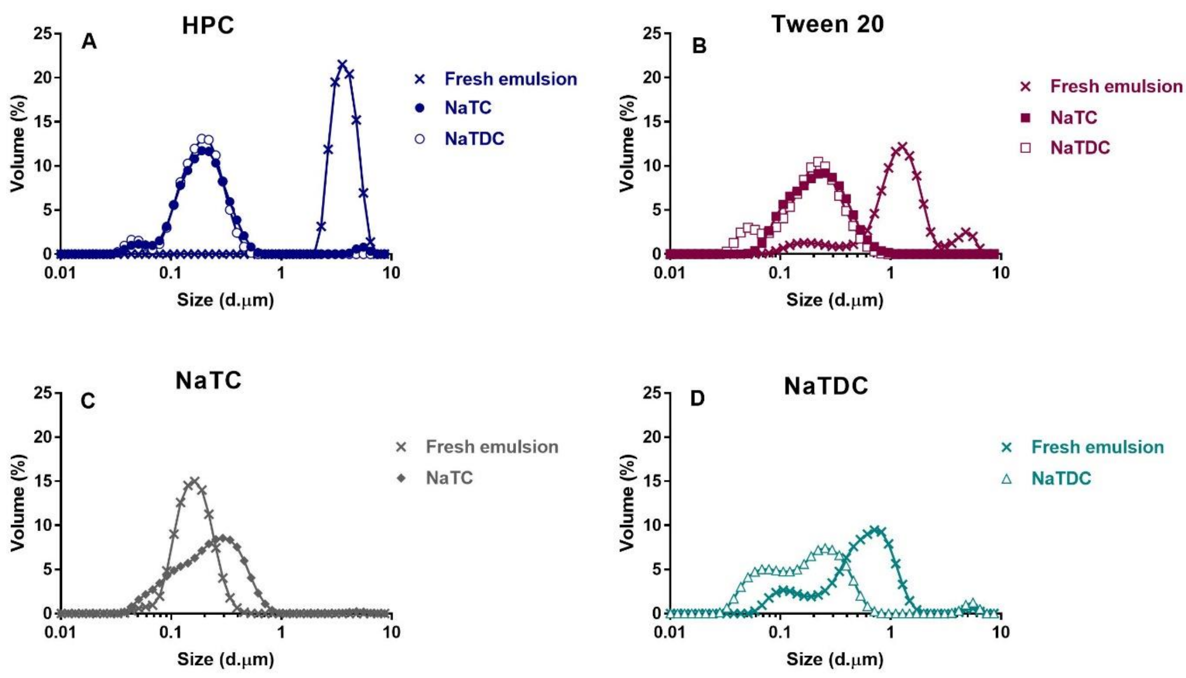

Figure 4.26. Volume particle size distributions of 20 % olive o/w emulsions stabilized with 1% wt HPC (A), Tween 20 (B), NaTC (C), or NaTDC (D) before and after simulated in vitro intestinal digestion. In all cases: fresh emulsion (X) and at the end of the 2 hr in vitro intestinal phase when NaTC (filled symbol) or NaTDC (closed symbol) was added.

Based on the digestion profiles, the type of emulsifier and BS seemed to have an impact on the rate and extent of lipolysis **(Figure 4.25).** When NaTDC was the individual BS used to simulate intestinal conditions, the digestion profile for the HPC-stabilized emulsions showed a slightly lower rate of FFAs released (3.4%/min ± 0.7) during the first 10 min of digestion compared to the Tween 20 (5.8%/min ± 0.6) and NaTDC-stabilized emulsions (4.6%/min ± 0.3). Additionally, the extent of digestion after 2 hours of lipolysis was also lower for the HPC-stabilized emulsions (58% ± 5) than for the Tween 20 (73% ± 5) and NaTDC-stabilized emulsion (69% ± 3). On the other hand, when NaTC was used, a slightly higher initial rate and extent of lipolysis was observed for the HPC-stabilized emulsion (4.1%/min ± 0.1 and 67% ± 4, respectively) compared to the NaTC-stabilized emulsion (2.9%/min ± 0.2 and 62% ± 5, respectively). Nonetheless, the HPC-stabilized emulsion still had a lower initial rate and extent of digestion, compared to the Tween 20-stabilized emulsion (6.3%/min ± 0.1 and 81% ± 1, respectively).

These results suggest that HPC offers a more protective effect against digestion (smaller initial rate and extent of lipolysis) when NaTDC is used in the intestinal phase, compared to NaTC. However, this result was unexpected because the quick and reversible exchange of deoxycholates with the interface may favor the displacement and solubilization of lipolysis products from the interface.[89] Additionally, both BSs (10 mM) were shown to displace a certain amount of HPC from the hydrophobic surface in the sequential adsorption experiments; but NaTDC was shown to be more effective at disrupting the HPC layer and removing some polymer from the solid surface than NaTC **(Chapter 4.2, Figure 4.9B)**. Since a higher % of irreversibly adsorbed NaTC mass remained on the hydrophobic solid surface after a buffer rinse, compared to NaTDC, **(Chapter 4.2, Figure 4.9B)**, this suggests that NaTC adsorbed more strongly to the bare solid surface. Therefore, in the present study, it is possible that both BSs displaced some HPC from the o/w interface, but NaTC may have adsorbed more strongly to the o/w interface and had a longer residence time at the interface than NaTDC. As a result, NaTC may have promoted the adsorption of the co-lipase/lipase complex, thus initiating lipolysis more quickly, compared to NaTDC, which could attribute to its slightly higher extent of lipolysis.

There are possible reasons why the NaTDC and Tween 20-stabilized emulsions showed a higher initial rate and extent of lipolysis than the HPC-stabilized emulsions. Smaller droplet sizes produced by Tween 20 (0.5 μm ± 0.1) and NaTDC (0.4 μm ± 0.1) provides a larger interfacial area for lipase to adsorb and possibly hydrolyzes the lipids at a higher rate and therefore reaches a higher extent of digestion.[12] Also, it is possible that Tween 20 may be more susceptible to displacement by BS at the o/w interface, compared to HPC, which allows the adsorption of lipase.[12, 109] Since HPC was shown to be resistant to displacement by both BSs at 10 mM from the hydrophobic solid surface, it is possible that the remaining adsorbed layer contained a complex of HPC+BS **(Chapter 4.2, Figure 4.16.)**. In the present study, it is possible that a HPC+BS complex was formed on the o/w interface with some BS molecules embedded into the HPC layer that could not reach/adsorb to the interface, thus hindering lipase adsorption. Finally, greater interactions may take place in the bulk between HPC and BSs[12, 21, 23], compared to Tween 20 and NaTDC, which could impact the amount of BSs adsorbed to the interface. Hydrophobic interactions have been postulated to take place between BSs and CEs in the aqueous phase and both methyl and hydroxypropyl groups can bind or "sequester" BSs.[11, 21, 23] Specifically, the hydrophobic face of the BSs may adsorb to the hydrophobic portion of the HPC backbone.[23] HPC was able to compete with both BSs for the hydrophobic surface in the simultaneous adsorption experiments and it is likely that there was a co-existence of both HPC and BS that remained at the interface. The ability for HPC to co-exist with both BSs is likely due to binding of both BSs in the aqueous solution **(Chapter 4.3, Figure 4.16)**. Therefore, in this context, HPC may have bound with the BSs in the aqueous phase through hydrophobic interactions, which may have impacted the amount of free BSs available to adsorb to the o/w interface, thus impacting the adsorption of lipase.

A lower initial lipolysis rate for the NaTC-stabilized emulsion (2.9 ± 0.2%/min), compared to the rest of the o/w emulsions, may suggest that NaTC formed astroner interfacial network that was not easily displaced by the BS. However, it is important to note that the *in vitro* digestion experiments for BS-stabilized emulsions were only performed using their respective BS to simulate intestinal conditions (i.e the digestion of NaTDC-stabilized emulsion was only performed with NaTDC). Therefore, it may be necessary to conduct digestion experiments of NaTDC-stabilized emulsions using NaTC as BS and vice versa, to determine if NaTC formed a stronger interfacial network.

Table 4.4 provides the fitting parameters, digestion extent ($\phi_{\max}$) and rate (k), from the mathematical model which help describe the digestion profiles.[13, 194] Since this model requires the initial droplet diameter of the emulsion (d_0), information can also be obtained to evaluate if the initial droplet size possibly influenced the rate and extent of lipid digestion.[13, 194] Interestingly, the model showed that the normalized digestion rate (k) actually increased with an increasing droplet size **(Table 4.4)**, which is opposite of what was observed in **Figure 4.25.** This indicates that the amount of FFAs released per unit surface area per unit time increased. Similar findings were reported in recent studies that applied this mathematical model to investigate the effect of droplet size on the lipid digestion of β-lactoglobulin[194], Tween 20[104], and lecithin[13] stabilized emulsions. It was suggested that a higher *k* occurred because more lipase molecules adsorbed per unit surface area in emulsions containing larger droplets compared to smaller droplets.[13] Nonetheless, despite no significant differences, HPC was able to reduce the extent of digestion (ϕ_{max}) to a slightly larger degree, compared to Tween 20 and NaTDC **(Table 4.4).** This may indicate that the initial droplet size did not impact the extent of lipolysis. Recent studies that have investigated the effect of CEs on *in vitro* lipolysis have postulated that differences in digestion may be attributed mainly by the interactions that occur between CEs and BS prior to BS adsorption to the o/w interface, rather than the initial size/surface area of the oil droplets and molecular weight of the CEs.[12, 21-22]

Table 4.4. Parameters describing the rate (k) and extent (ϕ_{max}) of digestion in 20% wt olive o/w emulsions stabilized with 1% wt HPC, Tween and a BS (NaTC or NaTDC) during simulated lipid digestion with either NaTC or NaTDC. Values represent mean ± SEM. Values for digestion rate and extent not sharing a common superscript are statistically significant (1-way ANOVA with Tukey's post hoc test for all possible comparisons, p<0.05).

BS added during digestion	Emulsifier type	Initial hydrodynamic diameter (μm)	Mathematical Model	
			Digestion rate *k* ($\mu mol \cdot sec^{-1} \cdot m^{-2}$)	Digestion extent ϕ_{max} (%)
NaTC	Tween 20	0.5 ± 0.1	1.7 ± 0.2[bc]	74 ± 2[a]
	HPC	3.8 ± 0.1	5.2 ± 0.2[a]	61 ± 1[ab]
	NaTC	0.2 ± 0.0	0.2 ± 0.0[c]	60 ± 6[ab]
NaTDC	Tween 20	0.5 ± 0.1	1.8 ± 0.2[bc]	69 ± 6[ab]
	HPC	3.8 ± 0.1	4.5 ± 1.0[ab]	53 ± 5[b]
	NaTDC	0.4 ± 0.1	0.6 ± 0.1[c]	64 ± 2[ab]

Overall, this study demonstrates the impact of the type of emulsifier and BS on the initial droplet sizes and digestibility of emulsified lipids. We have shown that HPC produces o/w emulsions with larger initial droplet sizes, compared to small molecule surfactants (i.e Tween 20 and BSs), which can be attributed to their larger size and slower adsorption onto the o/w interface. Additionally, this study shows that HPC delays lipid digestion of o/w emulsions compared to a conventional food surfactant, Tween 20. This ability does not seem to be ascribed to the initial droplet sizes of the HPC-stabilized emulsions; however, the interactions between

HPC and intestinal components in the aqueous phase and/or the formation of a stronger interfacial layer resistant to displacement by BSs may be the factors responsible for its ability to delay lipid digestion. We have also shown a more protective effect of the HPC-stabilized emulsion against digestion when NaTDC was used to simulate intestinal conditions, compared to NaTC. This suggest the idea that differing adsorption-desorption behaviors between BS types may influence different functions during lipolysis.[89] Specifically, cholates may facilitate the adsorption of the co-lipase/lipase complex, thus initiating lipolysis more quickly than deoxycholates, whereas deoxycholates may favor the displacement and solubilization of lipolysis products from the interface into the micellar phase.[89]

Chapter 5: Overall Conclusions and Future Opportunities

Conclusions

The goal of this research was to better understand the mechanisms by which cellulose ethers (CEs) interact with bile salts (BSs) at the interface and aqueous solution. We investigated the sequential and simultaneous adsorptions of cellulose ethers (CEs) and bile salts (BSs) to solid surfaces using two surface analysis techniques (QCM-D and SPR). We performed these experiments using two types of cellulose ethers (commercial and novel HPC polymers) and BSs (NaTC and NaTDC) at various BS concentrations (2, 5, and 10 mM). To the best of our knowledge, there is no published work that has used QCM-D and SPR to study the interactions between CEs and BSs. Therefore, this was a novel complementary technique that provided us with additional understanding of the dynamic interactions that take place between cellulose ethers and BS in the bulk and the impact that has on the interfacial properties at the oil/water interface. We were able to relate these findings to the ability of CEs to delay lipid digestion *in vitro.* Additionally, this was the first time that the novel HPC derivative (HPC-P) was studied to investigate the interactions with BSs. As a result, we were able to see how the molecular properties of the CEs impacted these interactions which provides further knowledge of how to design rational food matrices to control the rate and extent of lipid digestion.

We found that both CEs show potential in controlling lipid digestion. Using a non-ionic, more viscous CE (like commercial HPC) as a BS binder in the aqueous solution might be a better strategy to control lipid digestion than having a pre-adsorbed layer. On the other hand, using anionic, more hydrophobic CEs (like HPC-P) to create strong interfacial layers that resist complete displacement by BSs might be a better strategy to control lipid digestion than using them as BS sequestrants. Additionally, different BS structures may play key roles at different stages in the lipid digestion process. For instance, cholates (NaTC) may promote the adsorption of co-lipase/lipase onto the droplet interface, thus initiating lipolysis. On the other hand, deoxycholates (NaTDC) may favor the displacement and solubilization of lipolysis products. Finally, the formation of BS micelles is an important factor for controlling adsorption-desorption kinetics and may influence how BSs interact with CEs during lipid digestion.

Overall, this research has increased our understanding of how the structure of CEs and BSs impact the interactions occurring at the interface and in the aqueous solutions. The findings obtained in these studies can be exploited in developing strategies to design novel food and pharmacological matrices with improved functional properties to optimize lipid digestion. Future [242]work could be done with higher concentrations of NaTC (above its CMC) to see if its micelles have any impact on its interfacial behavior or interactions with CEs. Different types of commercially readily available CEs, like hydroxypropylmethyl cellulose acetate succinate (HPMCAS), may be used to obtain a more saturated, continuous CE layer on the sensor surfaces in order to characterize their interactions with BSs. Additionally, different types of BSs and bile acids (BAs) that differ more in charge and conjugated amino acid (like lithocholic acid and chenodeoxycholates) could be used to see if the structure has an impact on their interfacial behaviors and interactions with CEs. *In vivo* studies can also be performed to determine if CEs can control lipid digestion and absorption. For example, animals (like rats or pigs) may be fed a diet consisting of CEs and after the end of the trial, the gastrointestinal tract can be removed to obtain the digesta. Then, pancreatic lipase activity can be analyzed from the digesta to determine if the extent of enzyme activity was altered, compared to the control sample.[242] Additionally, triglycerides and BAs from the digesta samples could be extracted and analyzed using gas chromatography to quantify the individual BAs and determine the apparent fatty acid digestibility.[243] Finally, blood samples may be taken from the jugular vein to analyze for triglycerides, high-density lipoprotein cholesterol, and low-density lipoprotein cholesterol as well as the hepatic portal vein to analyze for total BAs.[243]

Research Limitations

It is important to note that the sequential adsorption studies involving commercial HPC and BSs were performed using QCM-D with both gold and hydrophobic polystyrene (PS) sensor surfaces. However, these experiments were only performed on a gold surface using SPR. Since QCM-D provides the "wet" mass and SPR provides the "dry" adsorbed mass, performing these experiments on a PS surface using SPR could provide qualitative and quantitative complementary information on the ability of HPC to resist displacement by BSs. Unfortunately, this was not possible for our research due to time constraints. For the same reason, the simultaneous adsorption studies were only performed using QCM-D, not SPR

Another limiting factor in this research was the use of a novel HPC polymer (HPC-P). A limited amount of sample was able to be synthesized for this project, due to its difficulty in manufacture. Therefore, a short adsorption period onto the PS surface was used. There is a possibility that a longer adsorption period would create a more saturated layer at the surface which may affect its displacement by BSs. Although we studied the adsorption/desorption behavior of HPC-P and BSs using SPR, it has not been possible to present the results corresponding the sequential adsorption studies. The mixed cellulose ether + BS system and the mixed solvent system (DMSO + buffer) made it difficult to obtain an accurate *dn/dc* value that is necessary to calculate the adsorbed mass using the equation of de Feijter *et. al.* . Additionally, the sequential and simultaneous adsorption experiments with this novel polymer were performed using only 10 mM BS. Therefore, the potential ability of this polymer to resist displacement/interact with BSs in the aqueous phase when micelles were not formed could not be explained. These findings may have helped better explain HPC-P's behavior at higher BS concentrations. Finally, this research could possibly be improved by performing *in vitro* lipid digestions with novel HPC-P since our findings showed that the HPC-P layer formed at the hydrophobic surface was resistant to displacement by BSs. Therefore, it would be interesting to evaluate the impact of HPC-P on the lipolysis of HPC-P-stabilized emulsions under *in vitro* intestinal conditions.

Appendix A

Materials

Hydroxypropyl cellulose (HPC, M_w ~100 kg/mol) and potassium phosphate dibasic (K_2PO_4) were purchased from Acros Organics (Geel, Belgium). Sodium hydride (95% NaH), 5-bromopent-1-ene, anhydrous tetrahydrofuran (THF), acrylic acid (AA), 3,5-di-*tert*-butylhydroxytoluene (BHT), Hoveyda-Grubbs' 2nd generation catalyst, and p-toluenesulfonyl hydrazide (pTSH) were from Sigma-Aldrich. Monopotassium phosphate (KH_2PO_4), isopropanol, and *N,N*-dimethylformamide (DMF) were purchased from Fisher Scientific. Ethyl vinyl ether was purchased from Fluka Analytical. All reagents were used without further purification.

Methods

Synthesis of HPC-Pen106-AA-H

Preparation of hydroxypropyl pent-4-enyl cellulose (HPC-Pen106)

HPC (1.0 g, 2.4 mmol AGU, 7.19 mmol -OH) was dispersed in 15 mL of anhydrous THF using a mechanical stirrer and with a nitrogen purge. Polymer gradually dissolved to form a a clear and transparent solution after overnight stirring. NaH (95%, 0.28 g, 21.6 mmol, 3 equiv./-OH) was added with N_2 protection. The reaction system was cooled to 0°C in an ice bath and then 5-bromopent-1-ene (1.13 g, 7.2 mmol, 1.0 equiv./-OH) was added dropwise under vigorous stirring. The solution was stirred at room temperature for 1 day and then at 50°C for 3 days. After cooling to room temperature, isopropanol was gradually added to deactivate any residual catalyst. The solution was added to 300 mL of pH 7.4 buffer solution (3.54 g KH_2PO_4 and 7.14 g K_2HPO_4 in 1000 mL deionized water) to precipitate the product, which was then recovered by filtration. The precipitate was redissolved in THF, then reprecipitated into hexanes and recovered by filtration, before vacuum drying at 40°C overnight. DS determined by ^{1}H NMR: DS (HP) = 2.2, DS (Pen) = 1.06; yield: 1.03 g, 89%. ^{1}H NMR ($CDCl_3$): 1.12 (br, s, OCH_2CHCH_3OH), 1.63 (br, s, $OCH_2CH_2CH_2CH{=}{=}CH_2$), 2.10 (br, s, $OCH_2CH_2CH_2CH{=}{=}CH_2$), 2.78-4.58 (m, cellulose backbone, OCH_2CHCH_3OH, $OCH_2CH_2CH_2CH{=}{=}CH_2$), 4.88-5.07 (dd, $OCH_2CH_2CH_2CH{=}{=}CH_2$), 5.82 (m, $OCH_2CH_2CH_2CH{=}{=}CH_2$). ^{13}C NMR ($CDCl_3$): 17.6 ($OCH_2CHCH_3OH$), 29.4 ($OCH_2CH_2CH_2CH{=}{=}CH_2$) 30.4 ($OCH_2CH_2CH_2CH{=}{=}CH_2$), 65.8 (C-6), 68.5 ($OCH_2CHCH_3OH$), 73.4-77.4 (C-2, C-3, C-5, OCH_2CHCH_3OH), 83.8 (C-4), 102.6 (C-1), 114.8 ($OCH_2CH_2CH_2CH{=}{=}CH_2$), 138.5 ($OCH_2CH_2CH_2CH{=}{=}CH_2$).

Olefin Cross-Metathesis Reaction with Acrylic Acid

BHT (5 mg) and 3 mL of THF were added to a flask containing HPC-Pen106 (100 mg; 0.20 mmol AGU; 0.22 terminal olefin). The mixture was stirred under N_2 protection at 37°C until all reagents were completely dissolved. Next, acrylic acid (0.82 g; 10.8 mmol; 50 equiv./terminal olefin) was added, followed by the Hoveyda-Grubbs' 2nd generation catalyst (12.8 mg; 8 mol%, dissolved in 4 mL THF). After stirring at 37°C for 2 hours, the reaction was stopped by adding two drops of ethyl vinyl ether. The product solution was concentrated by evaporating the THF solvent with a nitrogen purge and was then added to water to precipitate the product, which was collected by vacuum filtration, then vacuum dried overnight at 40°C. DS by ^1H NMR (500 MHz, DMSO-d_6: DS(HP) 2.2, DS (carboxylic acid) 1.06. Percent conversion by ^1H NMR: 100% yield: 108 mg, 92%.

Hydrogenation of the Cross-Methathesis Product HPC-Pen106-AA by p-toluenesulfonyl hydrazide (pTSH)

BHT (8 mg; 10 wt%) and 4 mL DMF were added to a flask containing HPC-Pen106-AA (80 mg; 0.15 mmol AGU; 0.16 mmol olefin). The mixture was stirred under N_2 protection at room temperature until all reagents were completely dissolved. Next, pTSH (0.18 g; 0.95 mmol; 6 equiv./olefin) was added. After refluxing at 135°C for 5 hours, the product was dialyzed against acetonefor 3 days and then against water for 2 days, with the acetone and water being changed daily, and then freeze dried.

References

1. Fuster, V.; Kelly, B. B.; National Research Council . Committee on Preventing the Global Epidemic of Cardiovascular Disease: Meeting the Challenges in Developing, C.; Institute of Medicine . Committee on Preventing the Global Epidemic of Cardiovascular Disease: Meeting the Challenges in Developing, C., *Promoting cardiovascular health in the developing world: a critical challenge to achieve global health*. National Academies Press: Washington, D.C, 2010.
2. Association, A. H., Cardiovascular disease: A costly burden for America projections through 2035. *Washington DC: American Heart Association* 2017.
3. Cardiovascular Disease. http://www.who.int/cardiovascular_diseases/en/ (accessed 8/20/2018).
4. Nelson, R. H., Hyperlipidemia as a risk factor for cardiovascular disease. *Primary Care: Clinics in Office Practice* 2013, *40* (1), 195-211.
5. Hypercholesterolemia. https://ghr.nlm.nih.gov/condition/hypercholesterolemia#sourcesforpage (accessed 10/1/2018).
6. McClements, D. J.; Decker, E. A.; Park, Y., Controlling Lipid Bioavailability through Physicochemical and Structural Approaches. *Critical Reviews in Food Science and Nutrition* 2008, *49* (1), 48-67.
7. Singh, H.; Ye, A.; Horne, D., Structuring food emulsions in the gastrointestinal tract to modify lipid digestion. *Progress in Lipid Research* 2009, *48* (2), 92-100.
8. Guo, Q.; Ye, A.; Bellissimo, N.; Singh, H.; Rousseau, D., Modulating fat digestion through food structure design. *Progress in Lipid Research* 2017, *68*, 109-118.
9. Bellesi, F. A.; Martinez, M. J.; Pizones Ruiz-Henestrosa, V. M.; Pilosof, A. M. R., Comparative behavior of protein or polysaccharide stabilized emulsion under in vitro gastrointestinal conditions. *Food Hydrocolloids* 2016, *52*, 47-56.
10. Bellesi, F. A.; Ruiz-Henestrosa, V. M. P.; Maldonado-Valderrama, J.; Santaella, T. D. C.; Pilosof, A. M., Comparative interfacial in vitro digestion of protein and polysaccharide oil/water films. *Colloids and Surfaces B: Biointerfaces* 2018, *161*, 547-554.
11. Torcello-Gómez, A.; Foster, T. J., Interactions between cellulose ethers and a bile salt in the control of lipid digestion of lipid-based systems. *Carbohydrate Polymers* 2014, *113*, 53-61.
12. Torcello-Gómez, A.; Foster, T. J., Influence of interfacial and bulk properties of cellulose ethers on lipolysis of oil-in-water emulsions. *Carbohydrate Polymers* 2016, *144*, 495-503.
13. Torcello-Gómez, A.; Maldonado-Valderrama, J.; Martín-Rodríguez, A.; McClements, D. J., Physicochemical properties and digestibility of emulsified lipids in simulated intestinal fluids: influence of interfacial characteristics. *Soft Matter* 2011, *7* (13), 6167-6177.
14. Fernandez Fraguas, C.; Woodward, N. C.; Gunning, A. P.; Wilde, P. J., Interactions Between Hydrocolloids and Bile Salts During Human Digestion of Emulsions. In *Gums and Stabilisers for the Food Industry 17: The Changing Face of Food Manufacture: The Role of Hydrocolloids*, The Royal Society of Chemistry: 2014; pp 342-349.
15. Mun, S.; Decker, E. A.; Park, Y.; Weiss, J.; McClements, D. J., Influence of interfacial composition on in vitro digestibility of emulsified lipids: potential mechanism for chitosan's ability to inhibit fat digestion. *Food Biophysics* 2006, *1* (1), 21-29.

16. Mun, S.; Decker, E. A.; McClements, D. J., Influence of emulsifier type on in vitro digestibility of lipid droplets by pancreatic lipase. *Food Research International* 2007, *40* (6), 770-781.
17. Maldonado-Valderrama, J.; Terriza, J. H.; Torcello-Gomez, A.; Cabrerizo-Vilchez, M., In vitro digestion of interfacial protein structures. *Soft Matter* 2013, *9* (4), 1043-1053.
18. Wilde, P. J.; Chu, B. S., Interfacial & colloidal aspects of lipid digestion. *Advances in Colloid and Interface Science* 2011, *165* (1), 14-22.
19. Sarkar, A.; Ye, A.; Singh, H., On the role of bile salts in the digestion of emulsified lipids. *Food Hydrocolloids* 2016, *60*, 77-84.
20. Maldonado-Valderrama, J.; Wilde, P.; Macierzanka, A.; Mackie, A., The role of bile salts in digestion. *Advances in Colloid and Interface Science* 2011, *165* (1), 36-46.
21. Pizones Ruiz-Henestrosa, V. M.; Bellesi, F. A.; Camino, N. A.; Pilosof, A. M. R., The impact of HPMC structure in the modulation of in vitro lipolysis: The role of bile salts. *Food Hydrocolloids* 2017, *62*, 251-261.
22. Borreani, J.; Espert, M.; Salvador, A.; Sanz, T.; Quiles, A.; Hernando, I., Oil-in-water emulsions stabilised by cellulose ethers: stability, structure and in vitro digestion. *Food & Function* 2017, *8* (4), 1547-1557.
23. Torcello-Gomez, A.; Fernandez Fraguas, C.; Ridout, M. J.; Woodward, N. C.; Wilde, P. J.; Foster, T. J., Effect of substituent pattern and molecular weight of cellulose ethers on interactions with different bile salts. *Food & Function* 2015, *6* (3), 730-739.
24. Stephen, A. M.; Phillips, G. O., *Food polysaccharides and their applications*. CRC press: 2016.
25. Espinal-Ruiz, M.; Parada-Alfonso, F.; Restrepo-Sanchez, L.-P.; Narvaez-Cuenca, C.-E.; McClements, D. J., Impact of dietary fibers [methyl cellulose, chitosan, and pectin] on digestion of lipids under simulated gastrointestinal conditions. *Food & Function* 2014, *5* (12), 3083-3095.
26. Stewart, J.; Manmathan, G.; Wilkinson, P., Primary prevention of cardiovascular disease: A review of contemporary guidance and literature. *JRSM cardiovascular disease* 2017, *6*, 2048004016687211.
27. Ebrahim, S.; Taylor, F. C.; Brindle, P., Statins for the primary prevention of cardiovascular disease. *Bmj* 2014, *348*, g280.
28. Thompson, P. D.; Panza, G.; Zaleski, A.; Taylor, B., Statin-associated side effects. *Journal of the American College of Cardiology* 2016, *67* (20), 2395-2410.
29. Ramkumar, S.; Raghunath, A.; Raghunath, S., Statin therapy: review of safety and potential side effects. *Acta Cardiologica Sinica* 2016, *32* (6), 631.
30. Sinzinger, H.; Wolfram, R.; Peskar, B. A., Muscular side effects of statins. *Journal of cardiovascular pharmacology* 2002, *40* (2), 163-171.
31. Hodel, C., Myopathy and rhabdomyolysis with lipid-lowering drugs. *Toxicology letters* 2002, *128* (1-3), 159-168.
32. Navarese, E. P.; Buffon, A.; Andreotti, F.; Kozinski, M.; Welton, N.; Fabiszak, T.; Caputo, S.; Grzesk, G.; Kubica, A.; Swiatkiewicz, I., Meta-analysis of impact of different types and doses of statins on new-onset diabetes mellitus. *The American journal of cardiology* 2013, *111* (8), 1123-1130.
33. Hofmann, A.; Hagey, L., Bile acids: chemistry, pathochemistry, biology, pathobiology, and therapeutics. *Cellular and Molecular Life Sciences* 2008, *65* (16), 2461-2483.

34. Rifkind, B., The lipid research clinics coronary primary prevention trial results. I. Reduction in incidence of coronary heart disease. *J Am Med Assoc* 1984, *251*, 351-364.
35. Stewart, J.; Manmathan, G.; Wilkinson, P., Primary prevention of cardiovascular disease: A review of contemporary guidance and literature. SAGE Publications: London, England, 2017; Vol. 6, p 204800401668721.
36. Ripsin, C. M.; Keenan, J. M.; Jacobs, D. R.; Elmer, P. J.; Welch, R. R.; Van Horn, L.; Liu, K.; Turnbull, W. H.; Thye, F. W.; Kestin, M., Oat products and lipid lowering: a meta-analysis. *Jama* 1992, *267* (24), 3317-3325.
37. Brown, L.; Rosner, B.; Willett, W. W.; Sacks, F. M., Cholesterol-lowering effects of dietary fiber: a meta-analysis. *The American journal of clinical nutrition* 1999, *69* (1), 30-42.
38. Giese, J., Fats and fat replacers: Balancing the health benefits. *Food technology (USA)* 1996.
39. Grossman, B. M.; Akoh, C. C.; Hobbs, J. K.; Martin, R. J., Effects of a fat substitute, sucrose polyester, on food intake, body composition, and serum factors in lean and obese Zucker rats. *Obesity research* 1994, *2* (3), 271-278.
40. Mattson, F. H.; Jandacek, R. J., The effect of a non-absorbable fat on the turnover of plasma cholesterol in the rat. *Lipids* 1985, *20* (5), 273-277.
41. Flood, M.; Auerbach, M.; Craig, S., A review of the clinical toleration studies of polydextrose in food. *Food and chemical toxicology* 2004, *42* (9), 1531-1542.
42. Tucci, S. A.; Boyland, E. J.; Halford, J. C., The role of lipid and carbohydrate digestive enzyme inhibitors in the management of obesity: a review of current and emerging therapeutic agents. *Diabetes, metabolic syndrome and obesity: targets and therapy* 2010, *3*, 125.
43. Hofmann, A. F., Bile acids: the good, the bad, and the ugly. *Physiology* 1999, *14* (1), 24-29.
44. McClements, D. J., *Food emulsions: principles, practices, and techniques*. CRC press: 2015.
45. Wilde, P. J., Lipid Digestion and Absorption. In *Reference Module in Biomedical Sciences*, Elsevier: 2014.
46. Mu, H.; Høy, C.-E., The digestion of dietary triacylglycerols. *Progress in Lipid Research* 2004, *43* (2), 105-133.
47. Reis, P.; Holmberg, K.; Watzke, H.; Leser, M. E.; Miller, R., Lipases at interfaces: A review. *Advances in Colloid and Interface Science* 2009, *147-148*, 237-250.
48. Lentle, R. G.; Janssen, P. W. M., Colloidal Dynamics and Lipid Digestive Efficiency. In *The Physical Processes of Digestion*, Springer New York: New York, NY, 2011; pp 63-90.
49. Beysseriat, M.; Decker, E. A.; McClements, D. J., Preliminary study of the influence of dietary fiber on the properties of oil-in-water emulsions passing through an in vitro human digestion model. *Food Hydrocolloids* 2006, *20* (6), 800-809.
50. Mu, H.; Høy, C.-E., The digestion of dietary triacylglycerols. Elsevier Ltd: OXFORD, 2004; Vol. 43, pp 105-133.
51. Golding, M.; Wooster, T. J., The influence of emulsion structure and stability on lipid digestion. *Current Opinion in Colloid & Interface Science* 2010, *15* (1), 90-101.
52. Favé, G.; Coste, T.; Armand, M., *Physicochemical properties of lipids: New strategies to manage fatty acid bioavailability*. 2004; Vol. 50, p 815-31.

53. Borel, P.; Grolier, P.; Armand, M.; Partier, A.; Lafont, H.; Lairon, D.; Azais-Braesco, V., Carotenoids in biological emulsions: solubility, surface-to-core distribution, and release from lipid droplets. *Journal of lipid research* 1996, *37* (2), 250-261.
54. Lentle, R. G.; Janssen, P. W. M., Colloidal Dynamics and Lipid Digestive Efficiency. Springer New York: New York, NY, 2011; pp 63-90.
55. Armand, M., Lipases and lipolysis in the human digestive tract: where do we stand? *Current Opinion in Clinical Nutrition & Metabolic Care* 2007, *10* (2), 156-164.
56. Bauer, E.; Jakob, S.; Mosenthin, R., Principles of physiology of lipid digestion. *ASIAN-AUSTRALASIAN JOURNAL OF ANIMAL SCIENCES* 2005, *18* (2), 282-295.
57. O'Connor, C. J.; Wallace, R. G., Physico-chemical behavior of bile salts. *Advances in Colloid and Interface Science* 1985, *22* (1), 1-111.
58. Gunness, P.; Gidley, M. J., Mechanisms underlying the cholesterol-lowering properties of soluble dietary fibre polysaccharides. *Food & Function* 2010, *1* (2), 149-155.
59. Zarras, P.; Vogl, O., Polycationic salts as bile acid sequestering agents. *Progress in Polymer Science* 1999, *24* (4), 485-516.
60. Maldonado-Valderrama, J.; Muros-Cobos, J. L.; Holgado-Terriza, J. A.; Cabrerizo-Vílchez, M. A., Bile salts at the air–water interface: Adsorption and desorption. *Colloids and Surfaces B: Biointerfaces* 2014, *120*, 176-183.
61. Borgström, B.; Erlanson-Albertsson, C.; Wieloch, T., Pancreatic colipase: chemistry and physiology. *Journal of lipid research* 1979, *20* (7), 805-816.
62. Jódar-Reyes, A. B.; Torcello-Gómez, A.; Wulff-Pérez, M.; Gálvez-Ruiz, M. J.; Martín-Rodríguez, A., Different stability regimes of oil-in-water emulsions in the presence of bile salts. *Food Research International* 2010, *43* (6), 1634-1641.
63. Golding, M.; Wooster, T. J., The influence of emulsion structure and stability on lipid digestion. *Current Opinion in Colloid & Interface Science* 2010, *15* (1-2), 90-101.
64. Wickham, M.; Garrood, M.; Leney, J.; Wilson, P. D.; Fillery-Travis, A., Modification of a phospholipid stabilized emulsion interface by bile salt: effect on pancreatic lipase activity. *Journal of Lipid Research* 1998, *39* (3), 623-632.
65. Russell, D. W., Cholesterol biosynthesis and metabolism. *Cardiovascular drugs and therapy* 1992, *6* (2), 103-110.
66. Dietschy, J. M., Regulation of cholesterol metabolism in man and in other species. *Klinische Wochenschrift* 1984, *62* (8), 338-345.
67. Moghimipour, E.; Ameri, A.; Handali, S., Absorption-Enhancing Effects of Bile Salts. MDPI AG: Basel, 2015; Vol. 20, pp 14451-14473.
68. Hofmann, A. F.; Hagey, L. R., Bile Acids: Chemistry, Pathochemistry, Biology, Pathobiology, and Therapeutics. *Cellular and Molecular Life Sciences* 2008, *65* (16), 2461-2483.
69. Hofmann, A. F.; Mysels, K. J., Bile salts as biological surfactants. *Colloids and Surfaces* 1987, *30* (1), 145-173.
70. Dawson, P. A., Bile formation and the enterohepatic circulation. In *Physiology of the Gastrointestinal Tract (Sixth Edition)*, Elsevier: 2018; pp 931-956.
71. Wiest, R.; Albillos, A.; Trauner, M.; Bajaj, J. S.; Jalan, R., Targeting the gut-liver axis in liver disease. *Journal of Hepatology* 2017, *67* (5), 1084-1103.
72. Li, T.; Chiang, J. Y., Bile acid signaling in metabolic disease and drug therapy. *Pharmacological reviews* 2014, *66* (4), 948-983.

73. Teo, A.; Dimartino, S.; Lee, S. J.; Goh, K. K. T.; Wen, J.; Oey, I.; Ko, S.; Kwak, H.-S., Interfacial structures of whey protein isolate (WPI) and lactoferrin on hydrophobic surfaces in a model system monitored by quartz crystal microbalance with dissipation (QCM-D) and their formation on nanoemulsions. *Food Hydrocolloids* 2016, *56*, 150-160.
74. Bishop-Bailey, D.; Walsh, D. T.; Warner, T. D., Expression and activation of the farnesoid X receptor in the vasculature. *Proceedings of the National Academy of Sciences* 2004, *101* (10), 3668-3673.
75. Madenci, D.; Egelhaaf, S. U., Self-assembly in aqueous bile salt solutions. *Current Opinion in Colloid & Interface Science* 2010, *15* (1–2), 109-115.
76. Malik, N. A., Solubilization and Interaction Studies of Bile Salts with Surfactants and Drugs: a Review. *Applied Biochemistry and Biotechnology* 2016, *179* (2), 179-201.
77. Anderson, S. L.; Rovnyak, D.; Strein, T. G., Direct Measurement of the Thermodynamics of Chiral Recognition in Bile Salt Micelles. *Chirality* 2016, *28* (4), 290-298.
78. Kawamura, H.; Murata, Y.; Yamaguchi, T.; Igimi, H.; Tanaka, M.; Sugihara, G.; Kratohvil, J. P., Spin-label studies of bile salt micelles. *The Journal of Physical Chemistry* 1989, *93* (8), 3321-3326.
79. Giglio, E.; Loreti, S.; Pavel, N. V., EXAFS: a new approach to the structure of micellar aggregates. *The Journal of Physical Chemistry* 1988, *92* (10), 2858-2862.
80. Carey, M. C.; Small, D. M., Micelle formation by bile salts: Physical-chemical and thermodynamic considerations. *Archives of Internal Medicine* 1972, *130* (4), 506-527.
81. Warren, D. B.; Chalmers, D. K.; Hutchison, K.; Dang, W.; Pouton, C. W., Molecular dynamics simulations of spontaneous bile salt aggregation. *Colloids and Surfaces A: Physicochemical and Engineering Aspects* 2006, *280* (1), 182-193.
82. Garidel, P.; Hildebrand, A.; Neubert, R.; Blume, A., Thermodynamic Characterization of Bile Salt Aggregation as a Function of Temperature and Ionic Strength Using Isothermal Titration Calorimetry. *Langmuir* 2000, *16* (12), 5267-5275.
83. Mithani, S. D.; Bakatselou, V.; TenHoor, C. N.; Dressman, J. B., Estimation of the increase in solubility of drugs as a function of bile salt concentration. *Pharmaceutical research* 1996, *13* (1), 163-167.
84. Matsuoka, K.; Suzuki, M.; Honda, C.; Endo, K.; Moroi, Y., Micellization of conjugated chenodeoxy- and ursodeoxycholates and solubilization of cholesterol into their micelles: comparison with other four conjugated bile salts species. *Chemistry and Physics of Lipids* 2006, *139* (1), 1-10.
85. Matsuoka, K.; Maeda, M.; Moroi, Y., Micelle formation of sodium glyco- and taurocholates and sodium glyco- and taurodeoxycholates and solubilization of cholesterol into their micelles. *Colloids and Surfaces B: Biointerfaces* 2003, *32* (2), 87-95.
86. Tiss, A.; Ransac, S.; Lengsfeld, H.; Hadvàry, P.; Cagna, A.; Verger, R., Surface behaviour of bile salts and tetrahydrolipstatin at air/water and oil/water interfaces. *Chemistry and Physics of Lipids* 2001, *111* (1), 73-85.
87. Matubayasi, N.; Kanzaki, M.; Sugiyama, S.; Matuzawa, A., Thermodynamic Study of Gaseous Adsorbed Films of Sodium Taurocholate at the Air/Water Interface. *Langmuir* 1996, *12* (7), 1860-1862.

88. O'Connor, J.; Wallace, R. G., Studies in bile salt solutions. The effect of pH on the cholate and taurocholate stimulation of human milk lipase catalyzed hydrolysis of p-nitrophenylacetate. *European journal of biochemistry / FEBS* 1984, *141* (2), 379-383.
89. Parker, R.; Rigby, N. M.; Ridout, M. J.; Gunning, A. P.; Wilde, P. J., The adsorption–desorption behaviour and structure function relationships of bile salts. *Soft matter* 2014, *10* (34), 6457-6466.
90. Klemm, D.; Heublein, B.; Fink, H. P.; Bohn, A., Cellulose: fascinating biopolymer and sustainable raw material. *Angewandte Chemie International Edition* 2005, *44* (22), 3358-3393.
91. Brown, R., Cellulose structure and biosynthesis. *Pure and Applied Chemistry* 1999, *71* (5), 767-775.
92. Klemm, D.; Heublein, B.; Fink, h. H.-P.; Bohn, A., Cellulose: Fascinating Biopolymer and Sustainable Raw Material. *Angewandte Chemie (International Edition)* 2005, *44* (22), 3358-3393.
93. Cellulose. In *Cellulose and Cellulose Derivatives in the Food Industry*, Wüstenberg, T., Ed. Wiley-VCH Verlag GmbH & Co. KGaA: 2014; pp 91-142.
94. Stephen, A. M.; Phillips, G. O.; Williams, P. A., *Food polysaccharides and their applications*. 2nd ed.; CRC/Taylor & Francis: Boca Raton, FL, 2006; Vol. 160.;160;.
95. Majewicz, T. G.; Erazo-Majewicz, P. E.; Podlas, T. J., Cellulose Ethers. In *Encyclopedia of Polymer Science and Technology*, John Wiley & Sons, Inc.: 2002.
96. Phillips, G. O.; Williams, P. A., *Handbook of Hydrocolloids*. 2nd;2; ed.; Woodhead Publishing Limited: Sawston, 2009.
97. Setser, C. S.; Racette, W. L., Macromolecule replacers in food products. *Critical Reviews in Food Science and Nutrition* 1992, *32* (3), 275-297.
98. Silva, S. M. C.; Pinto, F. V.; Antunes, F. E.; Miguel, M. G.; Sousa, J. J. S.; Pais, A. A. C. C., Aggregation and gelation in hydroxypropylmethyl cellulose aqueous solutions. *Journal of Colloid and Interface Science* 2008, *327* (2), 333-340.
99. Sekiguchi, Y.; Sawatari, C.; Kondo, T., A gelation mechanism depending on hydrogen bond formation in regioselectively substituted O-methylcelluloses. *Carbohydrate Polymers* 2003, *53* (2), 145-153.
100. Camino, N. A.; Pérez, O. E.; Pilosof, A. M. R., Molecular and functional modification of hydroxypropylmethylcellulose by high-intensity ultrasound. *Food Hydrocolloids* 2009, *23* (4), 1089-1095.
101. Wollenweber, C.; Makievski, A. V.; Miller, R.; Daniels, R., Adsorption of hydroxypropyl methylcellulose at the liquid/liquid interface and the effect on emulsion stability. *Colloids and Surfaces A: Physicochemical and Engineering Aspects* 2000, *172* (1), 91-101.
102. Mezdour, S.; Lepine, A.; Erazo-Majewicz, P.; Ducept, F.; Michon, C., Oil/water surface rheological properties of hydroxypropyl cellulose (HPC) alone and mixed with lecithin: Contribution to emulsion stability. *Colloids and Surfaces A: Physicochemical and Engineering Aspects* 2008, *331* (1), 76-83.
103. Lesmes, U.; Baudot, P.; McClements, D. J., Impact of interfacial composition on physical stability and in vitro lipase digestibility of triacylglycerol oil droplets coated with lactoferrin and/or caseinate. *Journal of agricultural and food chemistry* 2010, *58* (13), 7962-7969.

104. Salvia-Trujillo, L.; Qian, C.; Martín-Belloso, O.; McClements, D. J., Influence of particle size on lipid digestion and β-carotene bioaccessibility in emulsions and nanoemulsions. *Food Chemistry* 2013, *141* (2), 1472-1480.
105. Pilosof, A. M., Potential impact of interfacial composition of proteins and polysaccharides stabilized emulsions on the modulation of lipolysis. The role of bile salts. *Food Hydrocolloids* 2017, *68*, 178-185.
106. Sandra, S.; Decker, E. A.; McClements, D. J., Effect of interfacial protein cross-linking on the in vitro digestibility of emulsified corn oil by pancreatic lipase. *Journal of agricultural and food chemistry* 2008, *56* (16), 7488-7494.
107. Maldonado-Valderrama, J.; Woodward, N. C.; Gunning, A. P.; Ridout, M. J.; Husband, F. A.; Mackie, A. R.; Morris, V. J.; Wilde, P. J., Interfacial characterization of beta-lactoglobulin networks: displacement by bile salts. *Langmuir : the ACS journal of surfaces and colloids* 2008, *24* (13), 6759-6767.
108. Sarkar, A.; Horne, D. S.; Singh, H., Interactions of milk protein-stabilized oil-in-water emulsions with bile salts in a simulated upper intestinal model. *Food Hydrocolloids* 2010, *24* (2), 142-151.
109. Bellesi, F. A.; Pizones Ruiz-Henestrosa, V. M.; Pilosof, A. M. R., Behavior of protein interfacial films upon bile salts addition. *Food Hydrocolloids* 2014, *36*, 115-122.
110. Thongngam, M.; McClements, D. J., Isothermal titration calorimetry study of the interactions between chitosan and a bile salt (sodium taurocholate). *Food Hydrocolloids* 2005, *19* (5), 813-819.
111. Singh, H.; Ye, A., Structural and biochemical factors affecting the digestion of protein-stabilized emulsions. *Current Opinion in Colloid & Interface Science* 2013, *18* (4), 360-370.
112. Dickinson, E., Milk protein interfacial layers and the relationship to emulsion stability and rheology. *Colloids and Surfaces B: Biointerfaces* 2001, *20* (3), 197-210.
113. Wolever, T. M. S.; Tosh, S. M.; Gibbs, A. L.; Brand-Miller, J.; Duncan, A. M.; Hart, V.; Lamarche, B.; Thomson, B. A.; Duss, R.; Wood, P. J., Physicochemical properties of oat β-glucan influence its ability to reduce serum LDL cholesterol in humans: a randomized clinical trial. *The American journal of clinical nutrition* 2010, *92* (4), 723.
114. Olson, B. H.; Anderson, S. M.; Becker, M. P.; Anderson, J. W.; Hunninghake, D. B.; Jenkins, D. J.; LaRosa, J. C.; Rippe, J. M.; Roberts, D. C.; Stoy, D. B.; Summerbell, C. D.; Truswell, A. S.; Wolever, T. M.; Morris, D. H.; Fulgoni, r. V. L., Psyllium-enriched cereals lower blood total cholesterol and LDL cholesterol, but not HDL cholesterol, in hypercholesterolemic adults: results of a meta-analysis. *The Journal of nutrition* 1997, *127* (10), 1973.
115. Truswell, A. S., Cereal grains and coronary heart disease. *European journal of clinical nutrition* 2002, *56* (1), 1-14.
116. Dongowski, G., Interactions between dietary fibre-rich preparations and glycoconjugated bile acids in vitro. *Food Chemistry* 2007, *104* (1), 390-397.
117. Sayar, S.; Jannink, J.-L.; White, P. J., In vitro bile acid binding activity within flour fractions from oat lines with typical and high β-glucan amounts. *Journal of agricultural and food chemistry* 2006, *54* (14), 5142-5148.
118. Lia, A.; Hallmans, G.; Sandberg, A.-S.; Sundberg, B.; Aman, P.; Andersson, H., Oat beta-glucan increases bile acid excretion and a fiber-rich barley fraction increases cholesterol

excretion in ileostomy subjects. *The American journal of clinical nutrition* 1995, *62* (6), 1245-1251.
119. Ellegård, L.; Andersson, H., Oat bran rapidly increases bile acid excretion and bile acid synthesis: an ileostomy study. *European journal of clinical nutrition* 2007, *61* (8), 938.
120. Theuwissen, E.; Mensink, R. P., Water-soluble dietary fibers and cardiovascular disease. *Physiology & behavior* 2008, *94* (2), 285-292.
121. Marlett, J. A., Sites and mechanisms for the hypocholesterolemic actions of soluble dietary fiber sources. In *Dietary fiber in health and disease*, Springer: 1997; pp 109-121.
122. Naumann, S.; Schweiggert-Weisz, U.; Bader-Mittermaier, S.; Haller, D.; Eisner, P., Differentiation of Adsorptive and Viscous Effects of Dietary Fibres on Bile Acid Release by Means of In Vitro Digestion and Dialysis. *International Journal of Molecular Sciences* 2018, *19* (8), 2193.
123. Vickerman, J. C.; Gilmore, I. S., *Surface analysis: the principal techniques*. John Wiley & Sons: 2011.
124. Konradi, R.; Textor, M.; Reimhult, E., Using Complementary Acoustic and Optical Techniques for Quantitative Monitoring of Biomolecular Adsorption at Interfaces. *Biosensors* 2012.
125. Zhang, B.; Wang, Q., Quartz Crystal Microbalance with Dissipation. In *Nanotechnology Research Methods for Foods and Bioproducts*, Wiley-Blackwell: 2012; pp 181-194.
126. Cooper, M. A.; Singleton, V. T., A survey of the 2001 to 2005 quartz crystal microbalance biosensor literature: applications of acoustic physics to the analysis of biomolecular interactions. *Journal of Molecular Recognition* 2007, *20* (3), 154-184.
127. Ali, Z.; Pavey, K.; Robens, E., Survey on mass determination with oscillating systems: Part III. Acoustic wave mass sensors for chemical and biological sensing. *Journal of Thermal Analysis and Calorimetry* 2003, *71* (1), 31-35.
128. O'Sullivan, C. K.; Guilbault, G. G., Commercial quartz crystal microbalances – theory and applications. *Biosensors and Bioelectronics* 1999, *14* (8), 663-670.
129. Ferreira, G. N.; Da-Silva, A.-C.; Tomé, B., Acoustic wave biosensors: physical models and biological applications of quartz crystal microbalance. *Trends in biotechnology* 2009, *27* (12), 689-697.
130. Marx, K. A., Quartz Crystal Microbalance: A Useful Tool for Studying Thin Polymer Films and Complex Biomolecular Systems at the Solution−Surface Interface. *Biomacromolecules* 2003, *4* (5), 1099-1120.
131. Dixon, M. C., Quartz Crystal Microbalance with Dissipation Monitoring: Enabling Real-Time Characterization of Biological Materials and Their Interactions. *Journal of Biomolecular Techniques : JBT* 2008, *19* (3), 151-158.
132. Sauerbrey, G., The Use of Quartz Crystal Oscillators for Weighing Thin Layers and for Microweighing Applications. *The European physical journal* 1959, *155* (2), 206-222.
133. Guilbault, G. G., Determination of formaldehyde with an enzyme-coated piezoelectric crystal detector. *Analytical Chemistry* 1983, *55* (11), 1682-1684.
134. Guilbault, G. G.; Jordan, J. M.; Scheide, E., Analytical Uses of Piezoelectric Crystals: A Review. *C R C Critical Reviews in Analytical Chemistry* 1988, *19* (1), 1-28.
135. Konash, P.; Bastiaans, G., A SAW device for immunoreactions. *Anal. Chem* 1980, *52*, 1929-1935.

136. Höök, F.; Rodahl, M.; Brzezinski, P.; Kasemo, B., Energy Dissipation Kinetics for Protein and Antibody−Antigen Adsorption under Shear Oscillation on a Quartz Crystal Microbalance. *Langmuir* 1998, *14* (4), 729-734.
137. Voinova, M. V.; Rodahl, M.; Jonson, M.; Kasemo, B., Viscoelastic acoustic response of layered polymer films at fluid-solid interfaces: continuum mechanics approach. *Physica Scripta* 1999, *59* (5), 391.
138. Liu, Z.; Choi, H.; Gatenholm, P.; Esker, A. R., Quartz crystal microbalance with dissipation monitoring and surface plasmon resonance studies of carboxymethyl cellulose adsorption onto regenerated cellulose surfaces. *Langmuir : the ACS journal of surfaces and colloids* 2011, *27* (14), 8718.
139. Amirkhani, M.; Volden, S.; Zhu, K.; Glomm, W. R.; Nyström, B., Adsorption of cellulose derivatives on flat gold surfaces and on spherical gold particles. *Journal of Colloid and Interface Science* 2008, *328* (1), 20-28.
140. Richert, L.; Lavalle, P.; Payan, E.; Shu, X. Z.; Prestwich, G. D.; Stoltz, J.-F.; Schaaf, P.; Voegel, J.-C.; Picart, C., Layer by Layer Buildup of Polysaccharide Films: Physical Chemistry and Cellular Adhesion Aspects. *Langmuir* 2004, *20* (2), 448-458.
141. Wang, X.; Ruengruglikit, C.; Wang, Y.-W.; Huang, Q., Interfacial Interactions of Pectin with Bovine Serum Albumin Studied by Quartz Crystal Microbalance with Dissipation Monitoring: Effect of Ionic Strength. *Journal of Agricultural and Food Chemistry* 2007, *55* (25), 10425-10431.
142. Höök, F.; Kasemo, B.; Nylander, T.; Fant, C.; Sott, K.; Elwing, H., Variations in Coupled Water, Viscoelastic Properties, and Film Thickness of a Mefp-1 Protein Film during Adsorption and Cross-Linking: A Quartz Crystal Microbalance with Dissipation Monitoring, Ellipsometry, and Surface Plasmon Resonance Study. *Analytical Chemistry* 2001, *73* (24), 5796-5804.
143. Green, R. J.; Frazier, R. A.; Shakesheff, K. M.; Davies, M. C.; Roberts, C. J.; Tendler, S. J. B., Surface plasmon resonance analysis of dynamic biological interactions with biomaterials. Elsevier Ltd: ENGLAND, 2000; Vol. 21, pp 1823-1835.
144. Piliarik, M.; Homola, J., SPR Sensor Instrumentation. In *Surface Plasmon Resonance Based Sensors*, Homola, J., Ed. Springer Berlin Heidelberg: Berlin, Heidelberg, 2006; pp 95-116.
145. Homola, J.; Yee, S. S.; Gauglitz, G., Surface plasmon resonance sensors: review. *Sensors and Actuators B: Chemical* 1999, *54* (1), 3-15.
146. Achen, M. G.; Roufail, S.; Domagala, T.; Catimel, B.; Nice, E. C.; Geleick, D. M.; Murphy, R.; Scott, A. M.; Caesar, C.; Makinen, T.; Alitalo, K.; Stacker, S. A., Monoclonal antibodies to vascular endothelial growth factor-D block its interactions with both VEGF receptor-2 and VEGF receptor-3. *European Journal of Biochemistry* 2000, *267* (9), 2505-2515.
147. Vogel, M.; Miescher, S.; Kuhn, S.; Zürcher, A. W.; Stadler, M. B.; Ruf, C.; Effenberger, F.; Kricek, F.; Stadler, B. M., Mimicry of human IgE epitopes by anti-idiotypic antibodies11Edited by I. A. Wilson. *Journal of Molecular Biology* 2000, *298* (5), 729-735.
148. Pattnaik, P., Surface plasmon resonance. *Applied Biochemistry and Biotechnology* 2005, *126* (2), 79-92.
149. Homola, J., Surface Plasmon Resonance Sensors for Detection of Chemical and Biological Species. *Chemical Reviews* 2008, *108* (2), 462-493.
150. Kretschmann, E.; Raether, H., Notizen: Radiative Decay of Non Radiative Surface Plasmons Excited by Light. In *Zeitschrift für Naturforschung A*, 1968; Vol. 23, p 2135.

151. Ritchie, R. H., Plasma Losses by Fast Electrons in Thin Films. *Physical Review* 1957, *106* (5), 874-881.
152. Tang, Y.; Zeng, X.; Liang, J., Surface Plasmon Resonance: An Introduction to a Surface Spectroscopy Technique. *Journal of chemical education* 2010, *87* (7), 742-746.
153. De Feijter, J. A.; Benjamins, J.; Veer, F. A., Ellipsometry as a tool to study the adsorption behavior of synthetic and biopolymers at the air–water interface. *Biopolymers* 1978, *17* (7), 1759-1772.
154. Norman, L. L.; Badia, A., Electrochemical Surface Plasmon Resonance Investigation of Dodecyl Sulfate Adsorption to Electroactive Self-Assembled Monolayers via Ion-Pairing Interactions. *Langmuir* 2007, *23* (20), 10198-10208.
155. Tulpar, A.; Ducker, W. A., Surfactant Adsorption at Solid−Aqueous Interfaces Containing Fixed Charges: Experiments Revealing the Role of Surface Charge Density and Surface Charge Regulation. *The Journal of Physical Chemistry B* 2004, *108* (5), 1667-1676.
156. Konradi, R.; Textor, M.; Reimhult, E., Using Complementary Acoustic and Optical Techniques for Quantitative Monitoring of Biomolecular Adsorption at Interfaces. *Biosensors* 2012, *2* (4), 341.
157. Tehrani-Bagha, A. R.; Holmberg, K., Cationic Ester-Containing Gemini Surfactants: Adsorption at Tailor-Made Surfaces Monitored by SPR and QCM. *Langmuir* 2008, *24* (12), 6140-6145.
158. Bordes, R.; Tropsch, J.; Holmberg, K., Adsorption of Dianionic Surfactants Based on Amino Acids at Different Surfaces Studied by QCM-D and SPR. *Langmuir* 2010, *26* (13), 10935-10942.
159. Hedin, J.; Löfroth, J.-E.; Nydén, M., Adsorption Behavior and Cross-Linking of EHEC and HM-EHEC at Hydrophilic and Hydrophobic Modified Surfaces Monitored by SPR and QCM-D. *Langmuir* 2007, *23* (11), 6148-6155.
160. Pilosof, A. M. R., Potential impact of interfacial composition of proteins and polysaccharides stabilized emulsions on the modulation of lipolysis. The role of bile salts. *Food Hydrocolloids* 2017, *68*, 178-185.
161. Hur, S. J.; Lim, B. O.; Decker, E. A.; McClements, D. J., In vitro human digestion models for food applications. *Food Chemistry* 2011, *125* (1), 1-12.
162. Minekus, M.; Alminger, M.; Alvito, P.; Ballance, S.; Bohn, T.; Bourlieu, C.; Carriere, F.; Boutrou, R.; Corredig, M.; Dupont, D., A standardised static in vitro digestion method suitable for food–an international consensus. *Food & function* 2014, *5* (6), 1113-1124.
163. Alminger, M.; Aura, A. M.; Bohn, T.; Dufour, C.; El, S. N.; Gomes, A.; Karakaya, S.; Martínez-Cuesta, M. C.; McDougall, G. J.; Requena, T.; Santos, C. N., In Vitro Models for Studying Secondary Plant Metabolite Digestion and Bioaccessibility. *Comprehensive Reviews in Food Science and Food Safety* 2014, *13* (4), 413-436.
164. Wolf, B. W.; Bauer, L. L.; Fahey, G. C., Effects of Chemical Modification on in Vitro Rate and Extent of Food Starch Digestion: An Attempt To Discover a Slowly Digested Starch. *Journal of Agricultural and Food Chemistry* 1999, *47* (10), 4178-4183.
165. Bravo, L.; Siddhuraju, P.; Saura-Calixto, F., Effect of Various Processing Methods on the in Vitro Starch Digestibility and Resistant Starch Content of Indian Pulses. *Journal of Agricultural and Food Chemistry* 1998, *46* (11), 4667-4674.

166. Chatterton, D. E. W.; Rasmussen, J. T.; Heegaard, C. W.; Sørensen, E. S.; Petersen, T. E., In vitro digestion of novel milk protein ingredients for use in infant formulas: Research on biological functions. *Trends in Food Science & Technology* 2004, *15* (7), 373-383.
167. Bermúdez-Soto, M. J.; Larrosa, M.; García-Cantalejo, J.; Espín, J. C.; Tomás-Barberan, F. A.; García-Conesa, M. T., Transcriptional changes in human Caco-2 colon cancer cells following exposure to a recurrent non-toxic dose of polyphenol-rich chokeberry juice. *Genes & Nutrition* 2007, *2* (1), 111-113.
168. Garrett, D. A.; Failla, M. L.; Sarama, R. J., Development of an in Vitro Digestion Method To Assess Carotenoid Bioavailability from Meals. *Journal of Agricultural and Food Chemistry* 1999, *47* (10), 4301-4309.
169. Bering, S.; Bukhave, K.; Henriksen, M.; Sandström, B.; Pariagh, S.; Fairweather-Tait, S. J.; Lund, E. K., Development of a three-tier in vitro system, using Caco-2 cells, to assess the effects of lactate on iron uptake and transport from rye bread following in vitro digestion. *Journal of the Science of Food and Agriculture* 2006, *86* (14), 2438-2444.
170. Alminger, M.; Aura, A. M.; Bohn, T.; Dufour, C.; El, S.; Gomes, A.; Karakaya, S.; Martínez-Cuesta, M.; McDougall, G.; Requena, T., In vitro models for studying secondary plant metabolite digestion and bioaccessibility. *Comprehensive Reviews in Food Science and Food Safety* 2014, *13* (4), 413-436.
171. Vardakou, M.; Mercuri, A.; Barker, S. A.; Craig, D. Q.; Faulks, R. M.; Wickham, M. S., Achieving antral grinding forces in biorelevant in vitro models: comparing the USP dissolution apparatus II and the dynamic gastric model with human in vivo data. *Aaps Pharmscitech* 2011, *12* (2), 620-626.
172. Kong, F.; Singh, R. P., A human gastric simulator (HGS) to study food digestion in human stomach. *Journal of food science* 2010, *75* (9), E627-E635.
173. Minekus, M.; Marteau, P.; Havenaar, R., Multicompartmental dynamic computer-controlled model simulating the stomach and small intestine. *Alternatives to laboratory animals: ATLA* 1995.
174. Hemery, Y. M.; Anson, N. M.; Havenaar, R.; Haenen, G. R.; Noort, M. W.; Rouau, X., Dry-fractionation of wheat bran increases the bioaccessibility of phenolic acids in breads made from processed bran fractions. *Food Research International* 2010, *43* (5), 1429-1438.
175. Öhrvik, V.; Witthöft, C., Orange juice is a good folate source in respect to folate content and stability during storage and simulated digestion. *European journal of nutrition* 2008, *47* (2), 92-98.
176. Blanquet-Diot, S.; Soufi, M.; Rambeau, M.; Rock, E.; Alric, M., Digestive stability of xanthophylls exceeds that of carotenes as studied in a dynamic in vitro gastrointestinal system. *The Journal of nutrition* 2009, *139* (5), 876-883.
177. McClements, D. J.; Li, Y., Review of in vitro digestion models for rapid screening of emulsion-based systems. *Food & Function* 2010, *1* (1), 32-59.
178. Reis, P. M.; Raab, T. W.; Chuat, J. Y.; Leser, M. E.; Miller, R.; Watzke, H. J.; Holmberg, K., Influence of surfactants on lipase fat digestion in a model gastro-intestinal system. *Food biophysics* 2008, *3* (4), 370.
179. Hu, M.; Li, Y.; Decker, E. A.; Xiao, H.; McClements, D. J., Influence of tripolyphosphate cross-linking on the physical stability and lipase digestibility of chitosan-coated lipid droplets. *Journal of agricultural and food chemistry* 2009, *58* (2), 1283-1289.

180. Juhel, C.; Armand, M.; Pafumi, Y.; Rosier, C.; Vandermander, J.; Lairon, D., Green tea extract (AR25®) inhibits lipolysis of triglycerides in gastric and duodenal medium in vitro. *The Journal of nutritional biochemistry* 2000, *11* (1), 45-51.
181. Brogård, M.; Troedsson, E.; Thuresson, K.; Ljusberg-Wahren, H., A new standardized lipolysis approach for characterization of emulsions and dispersions. *Journal of colloid and interface science* 2007, *308* (2), 500-507.
182. Schmelz, T.; Lesmes, U.; Weiss, J.; McClements, D. J., Modulation of physicochemical properties of lipid droplets using β-lactoglobulin and/or lactoferrin interfacial coatings. *Food Hydrocolloids* 2011, *25* (5), 1181-1189.
183. Dong, Y.; Mosquera-Giraldo, L. I.; Troutman, J.; Skogstad, B.; Taylor, L. S.; Edgar, K. J., Amphiphilic hydroxyalkyl cellulose derivatives for amorphous solid dispersion prepared by olefin cross-metathesis. *Polymer Chemistry* 2016, *7* (30), 4953-4963.
184. Bermúdez, B.; Pacheco, Y. M.; López, S.; Abia, R.; Muriana, F. J., Digestion and absorption of olive oil. 2004.
185. Zhang, R.; Zhang, Z.; Zhang, H.; Decker, E. A.; McClements, D. J., Influence of lipid type on gastrointestinal fate of oil-in-water emulsions: In vitro digestion study. *Food Research International* 2015, *75*, 71-78.
186. Madenci, D.; Egelhaaf, S., Self-assembly in aqueous bile salt solutions. *Current Opinion in Colloid & Interface Science* 2010, *15* (1-2), 109-115.
187. Kaya, A.; Du, X.; Liu, Z.; Lu, J. W.; Morris, J. R.; Glasser, W. G.; Heinze, T.; Esker, A. R., Surface Plasmon Resonance Studies of Pullulan and Pullulan Cinnamate Adsorption onto Cellulose. *Biomacromolecules* 2009, *10* (9), 2451-2459.
188. Benito-Gallo, P.; Franceschetto, A.; Wong, J. C.; Marlow, M.; Zann, V.; Scholes, P.; Gershkovich, P., Chain length affects pancreatic lipase activity and the extent and pH–time profile of triglyceride lipolysis. *European Journal of Pharmaceutics and Biopharmaceutics* 2015, *93*, 353-362.
189. Charman, W. N.; Porter, C. J. H.; Mithani, S.; Dressman, J. B., Physicochemical and physiological mechanisms for the effects of food on drug absorption: The role of lipids and pH. *Journal of Pharmaceutical Sciences* 1997, *86* (3), 269-282.
190. Krämer, S. D.; Jakits-Deiser, C.; Wunderli-Allenspach, H., Free Fatty Acids Cause pH-Dependent Changes in Drug-Lipid Membrane Interactions Around Physiological pH. *Pharmaceutical Research* 1997, *14* (6), 827-832.
191. Heider, M.; Hause, G.; Mäder, K., Does the commonly used pH-stat method with back titration really quantify the enzymatic digestibility of lipid drug delivery systems? A case study on solid lipid nanoparticles (SLN). *European Journal of Pharmaceutics and Biopharmaceutics* 2016, *109*, 194-205.
192. Christensen, J. Ø.; Schultz, K.; Mollgaard, B.; Kristensen, H. G.; Mullertz, A., Solubilisation of poorly water-soluble drugs during in vitro lipolysis of medium- and long-chain triacylglycerols. *European Journal of Pharmaceutical Sciences* 2004, *23* (3), 287-296.
193. Desnuelle, P.; Savary, P., Specificities of lipases. *Journal of Lipid Research* 1963, *4* (4), 369-384.
194. Li, Y.; McClements, D. J., New mathematical model for interpreting pH-stat digestion profiles: Impact of lipid droplet characteristics on in vitro digestibility. *Journal of Agricultural and Food Chemistry* 2010, *58* (13), 8085-8092.

195. Ayela, C.; Roquet, F.; Valera, L.; Granier, C.; Nicu, L.; Pugnière, M., Antibody–antigenic peptide interactions monitored by SPR and QCM-D: A model for SPR detection of IA-2 autoantibodies in human serum. *Biosensors and Bioelectronics* 2007, *22* (12), 3113-3119.
196. Campagnolo, C.; Meyers, K. J.; Ryan, T.; Atkinson, R. C.; Chen, Y.-T.; Scanlan, M. J.; Ritter, G.; Old, L. J.; Batt, C. A., Real-Time, label-free monitoring of tumor antigen and serum antibody interactions. *Journal of Biochemical and Biophysical Methods* 2004, *61* (3), 283-298.
197. Vikinge, T. P.; Hansson, K. M.; Sandström, P.; Liedberg, B.; Lindahl, T. L.; Lundström, I.; Tengvall, P.; Höök, F., Comparison of surface plasmon resonance and quartz crystal microbalance in the study of whole blood and plasma coagulation. *Biosensors and Bioelectronics* 2000, *15* (11), 605-613.
198. Yilmaz, E.; Majidi, D.; Ozgur, E.; Denizli, A., Whole cell imprinting based Escherichia coli sensors: A study for SPR and QCM. *Sensors and Actuators B: Chemical* 2015, *209*, 714-721.
199. Wilczewski, M.; Van der Heyden, A.; Renaudet, O.; Dumy, P.; Coche-Guérente, L.; Labbé, P., Promotion of sugar–lectin recognition through the multiple sugar presentation offered by regioselectively addressable functionalized templates (RAFT): a QCM-D and SPR study. *Organic & Biomolecular Chemistry* 2008, *6* (6), 1114-1122.
200. Winslow, C. J.; Nichols, B. L. B.; Novo, D. C.; Mosquera-Giraldo, L. I.; Taylor, L. S.; Edgar, K. J.; Neilson, A. P., Cellulose-based amorphous solid dispersions enhance rifapentine delivery characteristics in vitro. *Carbohydrate Polymers* 2018, *182*, 149-158.
201. Volden, S.; Zhu, K.; Nyström, B.; Glomm, W. R., Use of cellulose derivatives on gold surfaces for reduced nonspecific adsorption of immunoglobulin G. *Colloids and Surfaces B: Biointerfaces* 2009, *72* (2), 266-271.
202. Sundman, O., Adsorption of four non-ionic cellulose derivatives on cellulose model surfaces. *Cellulose* 2014, *21* (1), 115-124.
203. Camino, N. A.; Pérez, O. E.; Sanchez, C. C.; Rodriguez Patino, J. M.; Pilosof, A. M. R., Hydroxypropylmethylcellulose surface activity at equilibrium and adsorption dynamics at the air–water and oil–water interfaces. *Food Hydrocolloids* 2009, *23* (8), 2359-2368.
204. Mezdour, S.; Cuvelier, G.; Cash, M. J.; Michon, C., Surface rheological properties of hydroxypropyl cellulose at air–water interface. *Food Hydrocolloids* 2007, *21* (5), 776-781.
205. Floury, J.; Desrumaux, A.; Axelos, M. A. V.; Legrand, J., Effect of high pressure homogenisation on methylcellulose as food emulsifier. *Journal of Food Engineering* 2003, *58* (3), 227-238.
206. Pérez, O. E.; Sánchez, C. C.; Pilosof, A. M. R.; Rodríguez Patino, J. M., Dynamics of adsorption of hydroxypropyl methylcellulose at the air–water interface. *Food Hydrocolloids* 2008, *22* (3), 387-402.
207. Quartz Crystal Microbalance with Dissipation. In *Nanotechnology Research Methods for Foods and Bioproducts*.
208. Liu, Z.; Choi, H.; Gatenholm, P.; Esker, A. R., Quartz crystal microbalance with dissipation monitoring and surface plasmon resonance studies of carboxymethyl cellulose adsorption onto regenerated cellulose surfaces. *Langmuir* 2011, *27* (14), 8718-8728.
209. Lin, D.; Lopez-Sanchez, P.; Selway, N.; Gidley, M. J., Viscoelastic properties of pectin/cellulose composites studied by QCM-D and oscillatory shear rheology. *Food Hydrocolloids* 2018, *79*, 13-19.

210. Ash, A.; Ridout, M. J.; Parker, R.; Mackie, A. R.; Burnett, G. R.; Wilde, P. J., Effect of calcium ions on in vitro pellicle formation from parotid and whole saliva. *Colloids and Surfaces B: Biointerfaces* 2013, *102*, 546-553.
211. Scheutjens, J. M. H. M.; Fleer, G. J., Statistical theory of the adsorption of interacting chain molecules. 2. Train, loop, and tail size distribution. *The Journal of Physical Chemistry* 1980, *84* (2), 178-190.
212. Park, E. J.; Draper, D. D.; Flynn, N. T., Adsorption and Thermoresponsive Behavior of Poly(N-isopropylacrylamide-co-N,N'-cystaminebisacrylamide) Thin Films on Gold. *Langmuir* 2007, *23* (13), 7083-7089.
213. Malmsten, M.; Lindman, B., Ellipsometry studies of the adsorption of cellulose ethers. *Langmuir* 1990, *6* (2), 357-364.
214. Ash, A.; Burnett, G. R.; Parker, R.; Ridout, M. J.; Rigby, N. M.; Wilde, P. J., Structural characterisation of parotid and whole mouth salivary pellicles adsorbed onto DPI and QCMD hydroxyapatite sensors. *Colloids and Surfaces B: Biointerfaces* 2014, *116*, 603-611.
215. Bodratti, A. M.; Sarkar, B.; Alexandridis, P., Adsorption of poly (ethylene oxide)-containing amphiphilic polymers on solid-liquid interfaces: Fundamentals and applications. *Advances in colloid and interface science* 2017, *244*, 132-163.
216. Millet, F.; Benattar, J.-J.; Perrin, P., Structures of Free-Standing Vertical Thin Films of Hydrophobically Modified Poly(sodium acrylate)s. *Macromolecules* 2001, *34* (20), 7076-7083.
217. Muñoz, M. G.; Monroy, F.; Ortega, F.; Rubio, R. G.; Langevin, D., Monolayers of Symmetric Triblock Copolymers at the Air−Water Interface. 1. Equilibrium Properties. *Langmuir* 2000, *16* (3), 1083-1093.
218. Diaconu, G.; Schäfer, T., Study of the interactions of proteins with a solid surface using complementary acoustic and optical techniques. *Biointerphases* 2014, *9* (2), 029015.
219. Pérez, O. E.; Carrera Sánchez, C.; Pilosof, A. M. R.; Rodríguez Patino, J. M., Impact of hydroxypropylmethylcellulose on whey protein concentrate spread film at the air–water interface: Structural and surface dilatational characteristics. *Colloids and Surfaces A: Physicochemical and Engineering Aspects* 2015, *465*, 1-10.
220. Göbel, J.; Besseling, N.; Stuart, M. C.; Poncet, C., Adsorption of hydrophobically modified polyacrylic acid on a hydrophobic surface: Hysteresis caused by an electrostatic adsorption barrier. *Journal of colloid and interface science* 1999, *209* (1), 129-135.
221. Dobrynin, A. V.; Rubinstein, M., Theory of polyelectrolytes in solutions and at surfaces. *Progress in Polymer Science* 2005, *30* (11), 1049-1118.
222. Woods, D. A.; Petkov, J.; Bain, C. D., Surfactant adsorption kinetics by total internal reflection Raman spectroscopy. 2. CTAB and Triton X-100 mixtures on silica. *The Journal of Physical Chemistry B* 2011, *115* (22), 7353-7363.
223. Fainerman, V.; Leser, M.; Michel, M.; Lucassen-Reynders, E.; Miller, R., Kinetics of the desorption of surfactants and proteins from adsorption layers at the solution/air interface. *The Journal of Physical Chemistry B* 2005, *109* (19), 9672-9677.
224. Maldonado-Valderrama, J.; Woodward, N. C.; Gunning, A. P.; Ridout, M. J.; Husband, F. A.; Mackie, A. R.; Morris, V. J.; Wilde, P. J., Interfacial Characterization of β-Lactoglobulin Networks: Displacement by Bile Salts. *Langmuir* 2008, *24* (13), 6759-6767.

225. Feiler, A. A.; Sahlholm, A.; Sandberg, T.; Caldwell, K. D., Adsorption and viscoelastic properties of fractionated mucin (BSM) and bovine serum albumin (BSA) studied with quartz crystal microbalance (QCM-D). *Journal of Colloid and Interface Science* 2007, *315* (2), 475-481.
226. Plunkett, M. A.; Claesson, P. M.; Ernstsson, M.; Rutland, M. W., Comparison of the Adsorption of Different Charge Density Polyelectrolytes: A Quartz Crystal Microbalance and X-ray Photoelectron Spectroscopy Study. *Langmuir* 2003, *19* (11), 4673-4681.
227. Belegrinou, S.; Mannelli, I.; Lisboa, P.; Bretagnol, F.; Valsesia, A.; Ceccone, G.; Colpo, P.; Rauscher, H.; Rossi, F., pH-dependent immobilization of proteins on surfaces functionalized by plasma-enhanced chemical vapor deposition of poly (acrylic acid)-and poly (ethylene oxide)-like films. *Langmuir* 2008, *24* (14), 7251-7261.
228. Euston, S. R.; Baird, W. G.; Campbell, L.; Kuhns, M., Competitive Adsorption of Dihydroxy and Trihydroxy Bile Salts with Whey Protein and Casein in Oil-in-Water Emulsions. *Biomacromolecules* 2013, *14* (6), 1850-1858.
229. Magny, B.; Iliopoulos, I.; Audebert, R.; Piculell, L.; Lindman, B., Interactions between hydrophobically modified polymers and surfactants. In *Trends in Colloid and Interface Science Vi*, Springer: 1992; pp 118-121.
230. Lopez-Pena, C.; Arroyo-Maya, I. J.; McClements, D. J., Interaction of a bile salt (sodium taurocholate) with cationic (ε-polylysine) and anionic (pectin) biopolymers under simulated gastrointestinal conditions. *Food Hydrocolloids* 2019, *87*, 352-359.
231. Dongowski, G., Effect of pH on the in vitro interactions between bile acids and pectin. *Zeitschrift für Lebensmitteluntersuchung und-Forschung A* 1997, *205* (3), 185-192.
232. Cervantes-Paz, B.; Ornelas-Paz, J. d. J.; Pérez-Martínez, J. D.; Reyes-Hernández, J.; Zamudio-Flores, P. B.; Rios-Velasco, C.; Ibarra-Junquera, V.; Ruiz-Cruz, S., Effect of pectin concentration and properties on digestive events involved on micellarization of free and esterified carotenoids. *Food Hydrocolloids* 2016, *60*, 580-588.
233. Espinal-Ruiz, M.; Parada-Alfonso, F.; Restrepo-Sánchez, L.-P.; Narváez-Cuenca, C.-E.; McClements, D. J., Interaction of a Dietary Fiber (Pectin) with Gastrointestinal Components (Bile Salts, Calcium, and Lipase): A Calorimetry, Electrophoresis, and Turbidity Study. *Journal of Agricultural and Food Chemistry* 2014, *62* (52), 12620-12630.
234. Panmai, S.; Prud'homme, R. K.; Peiffer, D. G.; Jockusch, S.; Turro, N. J., Interactions between Hydrophobically Modified Polymers and Surfactants: A Fluorescence Study. *Langmuir* 2002, *18* (10), 3860-3864.
235. Biggs, S.; Selb, J.; Candau, F., Effect of surfactant on the solution properties of hydrophobically modified polyacrylamide. *Langmuir* 1992, *8* (3), 838-847.
236. Qian, C.; McClements, D. J., Formation of nanoemulsions stabilized by model food-grade emulsifiers using high-pressure homogenization: Factors affecting particle size. *Food Hydrocolloids* 2011, *25* (5), 1000-1008.
237. Wilde, P. J., Interfaces: their role in foam and emulsion behaviour. *Current Opinion in Colloid & Interface Science* 2000, *5* (3), 176-181.
238. Coupland, J. N., *An introduction to the physical chemistry of food*. Springer: 2014.
239. Mun, S.; Kim, Y.-R.; Shin, M.; McClements, D. J., Control of lipid digestion and nutraceutical bioaccessibility using starch-based filled hydrogels: Influence of starch and surfactant type. *Food Hydrocolloids* 2015, *44*, 380-389.

240. Reis, P.; Holmberg, K.; Miller, R.; Krägel, J.; Grigoriev, D. O.; Leser, M. E.; Watzke, H. J., Competition between Lipases and Monoglycerides at Interfaces. *Langmuir* 2008, *24* (14), 7400-7407.

241. Patton, J. S.; Carey, M. C., Watching fat digestion. *Science* 1979, *204* (4389), 145-148.

242. Pluschke, A. M.; Williams, B. A.; Zhang, D.; Gidley, M. J., Dietary pectin and mango pulp effects on small intestinal enzyme activity levels and macronutrient digestion in grower pigs. *Food & function* 2018, *9* (2), 991-999.

243. Gunness, P.; Williams, B. A.; Gerrits, W. J.; Bird, A. R.; Kravchuk, O.; Gidley, M. J., Circulating triglycerides and bile acids are reduced by a soluble wheat arabinoxylan via modulation of bile concentration and lipid digestion rates in a pig model. *Molecular nutrition & food research* 2016, *60* (3), 642-651.